Università degli Studi di Napoli Federico II
Facoltà di Ingegneria

Manuela Brescia

ROTATION CAPACITY AND OVERSTRENGTH OF STEEL MEMBERS FOR SEISMIC DESIGN

Tesi di Dottorato
XXI ciclo

Il Coordinatore
Prof. Ing. Federico M. MAZZOLANI

Dottorato di Ricerca in Ingegneria delle Costruzioni

CONTENTS

INTRODUCTION

MOTIVATION AND SCOPE OF THE STUDY

<< Structural engineering is the science and the art of designing and making, with elegance and economy, buildings, bridges, frameworks and other similar structures so that they can safely resist the forces to which they may be subjected>>

Petroski 1985

Earthquake is generally considered the most destructive and frightening of all forces of nature. It consists in sudden slippages or movements in a portion of the earth's crust accompanied by a series of vibrations. After shocks with similar or minor intensity can follow the main quake. Earthquakes can occur at any time of the day, of the week, of the month and of the year. Every day small ground motions are registered in some parts of the world, but they have generally small intensities and do not cause great damages, while every year two or three strong earthquakes fill the mass media with dramatic accounts of human losses. Geologists have identified regions where earthquakes are likely to occur. With the increasing population of the world and urban migration trends, higher death tolls and greater property losses are more likely in many areas prone to earthquakes. At least 70 million people face significant risk of death or injury from earthquakes because they live in the 39 states that are seismically active. Deaths and injuries derived form earthquakes, vary according to a lot of factors, one of the most important is safety of structure in which people live. Often the real tragedy is that human losses are due not to the earthquakes themselves but to the failure of the constructions.

Actually, seismic design has brought a lot of progress into the engineering practice. The current work has the purpose to furnish a small contribute to the difficult topic of the structural behaviour under seismic actions. The attention is focused on Steel Moment Resisting Frames and in particular on the Member behaviour. Starting form the assumption that in modern design practice it is generally accepted that steel is an excellent material for seismic-resistant

structures because of its strength, ductility and capability to withstanding substantial inelastic deformations, an experimental campaign on steel beams has been made. The principal scope of the work has been the revision of the classification criteria of steel members actually adopted by seismic codes and the introduction of a new criterion which takes into account the principal factors that influence the structural response.

FRAMING OF THE ACTIVITY

The first part of the work, as visible in **Chapter 1**, has regarded the state of art concerning the Ultimate Limit State (ULS) design of dissipative steel Moment Resisting Frames (MRF) in seismic areas. Subsequently the attention has focused on the classification criteria of steel members and steel sections adopted by principal seismic codes like Eurocode 3 [60], OPCM 3274 [68] and Technical Codes for Constructions '08 [69]. This preliminary work has allowed the understanding that the main factors that influence the classification are Rotation Capacity and Overstrength, so in **Chapter 2 and 3** these parameters are defined and studied through theoretical, semi-empirical and empirical approaches. In this way it has been possible to underline the necessity of a classification criterion which subdivides, at the same time, members into ductility and overstrength classes. In fact, the subdivision of members into ductility classes is necessary because the rotation capacity influences the behavioural factor of the structure. At the same time, the subdivision of the members into overstrength classes is necessary in order to apply the capacity design criteria both to local level (connections among dissipative and not dissipative zones), and to global level (overstrength of non-dissipative members). The twice classification of the steel members in ductility and overstrength classes, based on relevant criteria, should be the most appropriate approach for the seismic applications.
Unfortunately, as illustrated in **Chapter 4** current seismic codes adopt only one classification criterion, from which both the consequences in terms of global ductility (behavioural factor) and in terms of capacity design are dependent.
In **Chapter 5** the principal results of the experimental campaign carried out in the Laboratory of Civil Engineer at the University of Salerno are illustrated. The main scope of the experimental campaign is the study of the behaviour of steel members under monotonic and cyclic loads. The adopted scheme is the cantilever beam which reproduces the behaviour of a beam in a frame subject

to seismic actions. Rotation capacity and overstrength play a key role in the design of dissipative structures, so the principal purpose has been the investigation of parameters that influences these factors, as material strength, ratios of slenderness between flange and web of plates in the section, moment gradient and cyclic loads. Three different typologies of cross-section have been investigated: 1) I sections, 2) Rectangular hollow sections, 3) Square hollow sections. The experimental activity has been constituted by two parts:

a) the identification of the material mechanical properties through the tensile tests on specimens taken from flange and web of the beams
b) tests on members performed through an equipment that applies predetermined strengths or displacements checking their values through a control device during monotonic and cyclic tests

The considerations regarding the obtained results confirm the necessity of a classification criterion which takes into account the characteristics of the whole member and not only of cross-section and takes into account simultaneously rotation capacity and overstrength parameters. Subsequently, to evaluate the influence of cyclic loads on rotation capacity and overstrength factors, comparisons between energy dissipated by monotonic and cyclic tests have been performed. The dissipated energies by monotonic (E1) and cyclic (E2) tests have been calculated as areas subtended by curves.

In **Chapter 6** the finite element analyses on I, RHS, SHS members, to simulate the experimental tests of Chapter 5 are described. The proposed numerical models are finalized to reproduce the observed monotonic and cyclic behaviour of tested members. Starting from experimental results, two numerical models have been realized to obtain a reliable predictive model. Numerical or finite element analysis provides a relatively inexpensive, and time efficient alternative to physical experiments. It is vital to have a sound set of experimental data upon which to calibrate a finite element model. In this way, it is possible to investigate a wide range of parameters within the model. In order to model the plastic bending tests, the finite element program should include the effects of material like geometric and mechanical non-linearity, imperfections, and local buckling. The program ABAQUS (Version 6.7-1), has been used to perform the numerical analyses [79].

In **Chapter 7** the first objective has been to propose a new expression of the overstrength factor "s" for "I" profiles starting from the interpolation of a greater number of experimental results including the ones obtained by technical literature and the ones made by the experimental campaign. For the

validation of the obtained expressions of the overstrength factor the percentage errors EP[%] have been plotted for the considered tests. These errors have been calculated by the introduction of the factor MSE (Mean Square Error) to evaluate the differences between the experimental and numerical values. The second objective of the current research has to propose new expressions of the overstrength factor "s" for members with different cross-sections as RHS and SHS, for which, till today, OPCM 3274 does not provide expressions. With the same procedures already illustrated, new expressions of the ductility factor R for I, RHS, SHS profiles are provided for considered member, validated quantifying the MSE.

ACKNOWLEDGEMENTS

CHAPTER 1: THE SEISMIC DESIGN OF STEEL FRAMES

1.1 NATURE OF THE PROBLEM

The occurrence of earthquakes, their consequent impact on people and on the facilities they live and work in, the evaluation and interpretation of damage caused by severe ground motions, are the principal items for structural engineers designing buildings in seismic areas. The attempts to find the answer to the question: "why does damage occur, after a wide amount of research work?" is an ethical duty of the specialists. The paradox of Structural engineering is that while engineers can learn from the structural mistakes of what not to do, they do not necessarily learn from successes how to do [1]. The failure of a structure contributes more to the evolution of design concepts than Structures standing without accidents, on the condition that the engineers have the capability to understand what happened. So, the damage of a structure during an earthquake represents a challenge for structural engineers to improve the design methods.

This aspect can be very well illustrated with the example of steel structures. For a long time it was accepted in design practice that steel is an excellent material for seismic-resistant structures, thanks to its performance in terms of material strength and ductility. To exemplify this good behaviour, in many papers the excellent performance of the Torre Latino-Americana building in Mexico City was mentioned, without showing that the fundamental period of this building is much larger than the predominant period of the Michoachan ground motion and the structure has piles supported by rock. Therefore, the seismic demand was relatively low [2], [3]. Contrary to this, the last severe earthquakes of Michoacan (1985), Northridge (1994) and Kobe (1995) have seriously compromised this image of steel as the most suitable material for seismic resistant structures. It was a providential sign that in the same place, Mexico City, where the case of Torre Latino-Americana building was assumed as example of good performance of steel structures, the first overall collapse of a

steel structure occurred: the Pino Suarez building. The bad performance of joints in steel structures, both in Northridge and Kobe earthquakes, having the same characteristics of damage, shows that there are some general mistakes in design concept. And the fact that in both cases damage arises also when the design and detailing were performed in perfect accordance with the design philosophy and code provisions, amplifies the challenge addressed to structural engineers.

Generally, when such failures occur, the observed damage depends on following factors [4]:

- General characteristics of the earthquake;

- Local soil behaviour;

- Seismic vulnerability of buildings;

- Incomplete knowledge in seismic behaviour of structures;

- Inadequacy of code provisions;

- Wrong design, in opposition with code provisions;

- Bad construction;

- Lack of maintenance.

On the other side, the main characteristics of earthquakes are as follows:

Pulse characteristic. The analysis of records reveals that the aspect of the time-history variation of ground motions is qualitatively different from the other well known records, for instance the famous El Centro records. Figure 1 shows the 1979 Imperial Valley records, which are typical for a near-field earthquake record. The feature of these records is the low frequency pulses in the acceleration time-history, which translate into the pronounced coherent pulses in velocity and displacement histories.
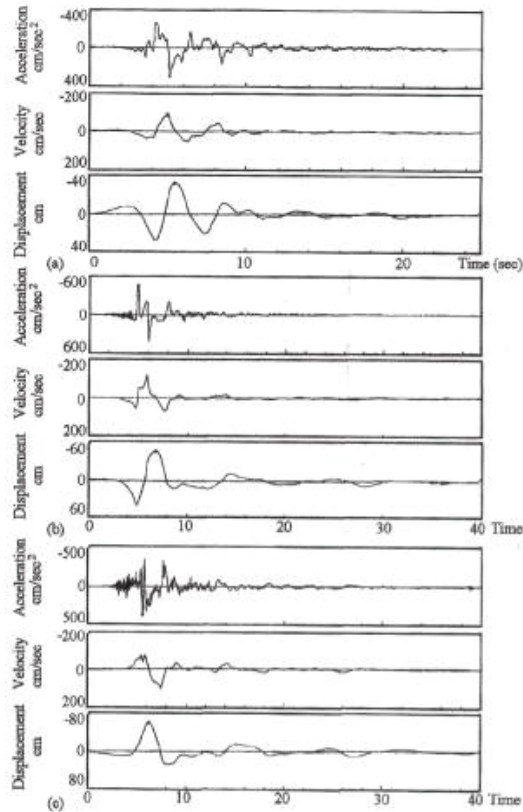
Fig. 1.   Pulse characteristic- Imperial Valley, 1979: (a) Meloland Overpass; (b) Array No. 7; (c) Array No. 5

(ii) *Vertical components of ground motions.* For a long time, the study of earthquake ground motions has been limited to the examination of the horizontal components. The vertical ground motions have been largely ignored, because until last time the recorded earthquakes were far from the source. But during the recent recorded earthquakes near the source, it has been observed that the vertical ground motions are sometimes greater in amplitude than the horizontal components. This remark was very evident in the strong ground motions which were recorded during the 1979 Imperial Valley earthquake [5], [6]. From Figure 2, it can be observed that the largest maximum vertical accelerations generally occur close to the fault rupture zone. In addition, the vertical movements are associated with frequencies higher than the horizontal ones, showing that different design spectra must be considered.

Ratio of peak vertical to horizontal acceleration
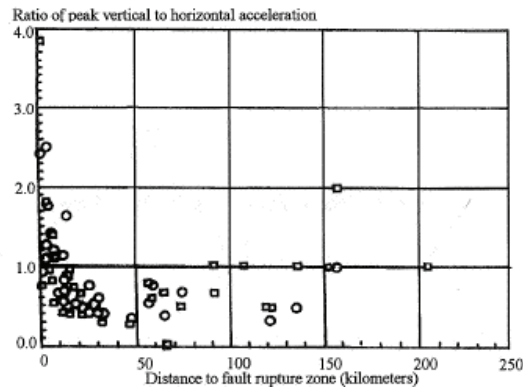
Fig. 2.   *Ratio of vertical to horizontal peak ground acceleration for Imperial Valley earthquake, 1979*

(iii) *Combination of horizontal and vertical components.* It is generally accepted that the first waves which arrive to the structure are the vertical ones, as shown in the Figure 3a for the Imperial Valley earthquake. But in other cases, as Morgan Hill earthquake, the vertical and horizontal motions are almost exactly coincident in time as visible in Figure 3b. Both cases must be considered in structure analysis, because it is not sure which situation will arise.
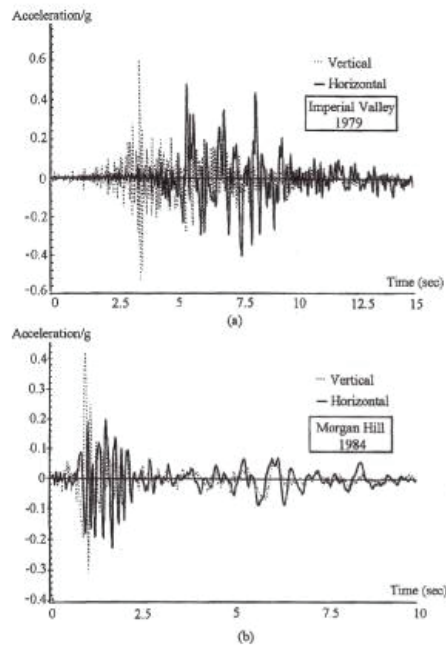
Fig. 3.   *Combination of horizontal and vertical components: (a) Imperial Valley, 1979; (b) Morgan Hill, 1984 (after Elnashai and Papazoglu, 1997)*

(iv) *Velocity.* An increase of velocity near-field is marked. Velocities often exceed 150 to 200 cm/sec in areas surrounding the source [7]. The velocity histories of several Californian records are shown in Figure 4. The ground motion has in the near source field a pronounced coherent pulse in velocity and displacement.
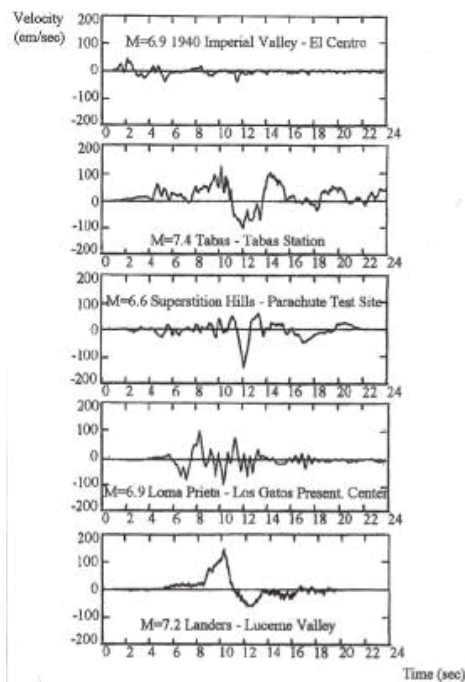
Fig. 4.   Ground velocity of Californian earthquakes (after Hall et al, 1995)

From the structural engineers point of view the most important aspects of post-earthquake analysis are the lessons to be learned after each event, having the conviction that the best teacher is the full-scale laboratory of nature. No theory or mathematical model can be accepted, unless they correctly explain what happens in nature [8].

1.2 BASIC DESIGN PHILOSOPY

The accurate knowledge of the performances of a structure in the occasion of violent earthquakes needs sophisticated numerical procedures, because the quantitative evaluation of the structural damage requires non linear dynamic

analyses. Nevertheless such analyses are not used in the common practical design, so simplified procedures have to be adopted to evaluate the inelastic seismic response of a structure, also preserving a satisfactory level of approximation.

The modern approach to the seismic design, for the great part of the buildings, is based on the strength required by the earthquake (represented by base shear) from an elastic system of a simple degree of freedom, equivalent in terms of strength and damping to the real structural system, inelastic and with more degrees of freedom. The required strength is evaluated through the linear elastic damping spectrum correspondent to a seismic event whose potential of damage is associated to the return period.

In accord with such philosophy of design, steel structures must be designed to satisfy the verification to the ultimate limit state, under the action of a destructive earthquake characterized by a return period of 475 years respecting of one of the following structural behaviours:

a) Dissipative behaviour;

b) Non dissipative behaviour

In the case a) the structures are designed considering that a part of the input energy of the earthquake is dissipated through cycles of inelastic deformations of specific structural elements or parts of structural elements, called respectively dissipative elements or zones. They have to be designed to withstand the actions due to the destructive earthquake assuring wide deformations in plastic field, while the other structural parts to withstand the solicitations transmitted from the elements or from dissipative zones having an elastic behaviour. Because of the dissipation of energy due to the plastic deformation of the ductile parts, and therefore considering the ductility of the structures, all the modern seismic codes introduce a factor of reduction of the required elastic strength, called behavioural factor q from the Eurocode 8 [9], response modification factor R from the recommendations of the NEHRP [10], or structural System factor R_w from the SEAOC [11]. The value of this factor, related to the ductility of the structural system, allows the definition of the design spectrum and provide the possibility to have a very simple design procedure. Linear elastic analyses are made, such as the method of equivalent horizontal static forces and the method of linear dynamic response spectrum considering valid the principle of superimposition of the effects. The evaluation of the behavioural factor q representative of structural ductility, is

the critical aspect of the procedure. Generally, in the actual codes this factor is assigned in function of the structural typology, keeping into account other parameters of influence, as the fundamental period of the structure, the conditions of the ground in-site and also the dynamic characteristics of the earthquake [12]. The direct correlation between behavioural factor and ductility is possible only for the simple degree of freedom systems, while for the systems with more degrees of freedom the problem is already existent [13], [14], [15]. In relationship to the global seismic performances, the design procedure is based on the control of the collapse mechanism to optimize the exploitation of the plastic resources of the structure [16]. For these reasons in the practice the capacity design criterion is applied, according to which the structural element more ductile must be also the more "weak", while the other parts of structure connected to it have to remain elastic field [17], [18]. In relationship to the different structural typologies, and therefore to the different dissipative elements or zones, such objective can be achieved with different methods, characterized by different levels of complexity [19], [20], [21].

Adequate requirement of local ductility and capacity of dissipation must be assigned through an appropriate design of the constructive details, preventing the formation of local instabilities before the development of wide excursions in plastic field [22]. Only in this case the redistribution of the solicitations is possible in the whole structure, exploiting the benefits that the structural static redundancy can offer. To allow this condition, the codes already mentioned propose, for the material, the use of ductile steels, characterized by high level of hardening and plastic deformation. In the same way, for the structural element, the use of ductile transversal cross-sections and members is foreseen, according to a classification in categories of ductility that takes into account their geometric characteristics, influence forces of compression and the strength of the material. Finally, the connections among the structures have to fully restore the resistance that is they have a resistance at least equal to the one of the more weak connected structure, to allow the development of plastic deformations in the zones or in the dissipative elements, rather than in the connection.

The structures with a dissipative structural behaviour are instead planned to withstand seismic actions through an elastic behaviour. As a result, the design spectrum of the accelerations is the elastic damped, this means that the behavioural factor q is assumed equal to one. This is the case of structures characterized by small ductility, do not able to dissipate energy, so that, for the verification at the ultimate limit states, only the strength of the structural

elements must be controlled, while it is not necessary to satisfy requirements of local or global ductility.

1.3 MULTI-LEVEL SEISMIC DESIGN CRITERIA

A building can be subjected to low, moderate, or severe earthquakes. It may overcome these events undamaged, can undergo slight, moderate or heavy damage, may be partially destroyed or can collapse. These levels of damage depend On the earthquake intensities. The low intensity earthquakes occur frequently, the moderate earthquakes more rarely, while the strong earthquakes may occur once or maximum two times during the structure life. It is also possible that a devastating earthquake will not affect the structure during its life.

In these conditions, the checks, required to assure a good behaviour of a structure during a seismic attack, must be examined in the light of a multi-level design approach. Thus, it is very rational to establish some limit states, as a function on the probability of damage occurrence, both for structure and non-structural elements [23], [24], [25], [26]. These limit states are presented in Figure 5, in function of both structure and non-structural elements.
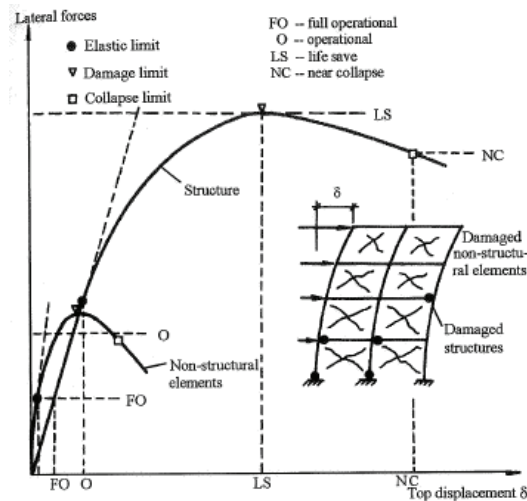
Fig. 5.   Performance Levels

Three categories of damage may occur during the structure behaviour [27]:

- damage of contents, which depends on the accelerations of each storey and on the integrity of the non-structural and structural components of the building;
- damage of non-structural components as a result of earthquake induced deformations, the inter-storey drifts being the most important characteristic for this damage type;
- damage of structural elements produced by local and/or overall budding of members, brittle fracture of members or joints. The damage index is proposed to be a criterion for the damage level.

In the seismic load-top-sway displacement curve, there are three very important points: limit of elastic behaviour without any damage, limit of damage with major damage and limit of collapse, for which the structure is at the threshold of breakdown. In function of taking different limit states for structure and non-structural elements, some multi-level approaches are possible:

(i) *Four levels design approach.* The performance-based seismic engineering, elaborated by the Vision 2000 [84], Committee of SEAOC [11] and ATC [83], consists of a selection of appropriate systems, layout and detailing of a structure and non-structural components and contents, so that at specified levels of ground motion and defined levels of reliability, the structure will not be damaged, beyond certain limit states. The performance levels have been defined for different levels as a combination of damage of structure and non-structural elements, building facilities and required repairs (Table 1). To the goals of the planning, NTC '08 [69] and EC8 [9] require, for the verification, only two limit states implicitly admitting the satisfaction of the other ones.
A classification of performances in five levels is proposed by Yamawaki [81]. The relation between the four limit states and the four probabilities of occurrence are presented in Figure 6, as a performance objective matrix. The minimum objectives of an earthquake design are illustrated in the figure as the diagonal line. The unacceptable performance is values under these minimum objectives. In the same way, there are enhanced objectives, if the owner consents to a supplementary payment for providing better performance, or lower risk than the one corresponding to the minimum objectives [28].

(ii) *Three level design approach.* Verification at the three levels has been proposed by [29], [30], [31]:

- Serviceability limit state (SLS), for the frequent earthquake; the corresponding design earthquake is called a service earthquake. This limit state imposes that the structure, together with non structural elements, should suffer minimum damage and the discomfort for inhabitants should be reduced to the minimum. So, for this level, the structure must remain within the elastic range or it may suffer unimportant plastic deformations;

Table 1.   Seismic performance levels according to 1.EC8[9]; 2.ATC[83]; 3.SEAOC[11]; 4. NTC'08[69]; 5.Yamawaki [81]

	Designation	Overall	Structure	Repairs
1	2.Operational 3.Fully operational 4.Operational 5.Keep function	• No damage to almost all functions • Facilities continue in operation	• No damage in structure • No visible residual deformations	Without repairs
2	1.Damage limitation 2.Immediate occupancy 3.Functional 4.Damage limitation 5.Keep major functions	• Light damage to non-structural components • Main facilities continue in operation. non-essential facilities are interrupted, but can resume immediately	• Very minor structural damage • No residual deformation • Structure retains all its original stiffness and strength	• Slight repairs for non-structural components • Without repairs for structure
3	1. Significant damage 2.Life safety 3.Life safe 4.Life safety 5.Life safety	• Significant non-structural component damage • Activity is interrupted • Building remains accessible to emergency activity	• Significant structural damage • Structure loses its original stiffness and strength, but retains some lateral strength against collapse	• Repairs of non-structural components • Immediate repairs for structural elements
4	1.Near collapse 2.Collapse prevention 3.Near collapse 4.Near collapse 5.No guarantee for life safety	• Non-structural components are completely damaged and present a falling hazard • No entry into building is permitted	• Serious damage in structural members • Substantial loss of structural strength • Structure supports only the gravity loads • Partial collapse is probable, but not overall collapse	• Experts decide if the building should be demolished or can be repaired • Repair is probably not practical

-damageability limit state (DLS), for occasional earthquake; this limit state considers an earthquake intensity which produces damage in non-structural elements and moderate damage in the structure, which can be repaired without great technical difficulties.

-survivability-ultimate limit state (ULS), for earthquakes which may rarely occur, represents the strongest possible ground shaking. For these earthquakes, both structural and non-structural damage are expected, but the safety of inhabitants has to be assured. In many cases damage is so substantial that structures are not repaired and demolition is the recommended solution.

(iii) *Two levels of design approach.* Although it is recognized that the ideal methodology would use four or three levels for design, today current code

methodologies and seismic design philosophy may be based on just two levels (Eurocode 8)[9]:

-*serviceability limit state*, for which structures are designed to remain elastic, or with minor plastic deformations and the non structural elements remain undamaged or have minor damage;

-*ultimate limit state,* for which structures exploit their capability to deform beyond the elastic range, the non-structural elements being partially or totally damaged.
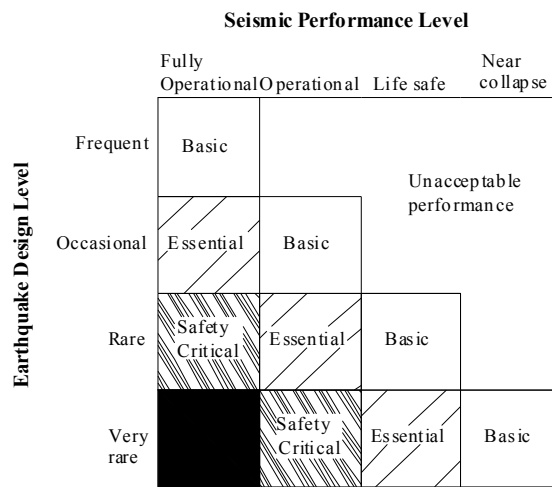
Fig. 6.   Earthquake occurrence versus seismic performance levels

In the Eurocode 8, the accelerations corresponding to the serviceability limit state are given as a fraction of the corresponding ones for the ultimate limit state. Generally, this methodology cannot assure a controlled damage, also because the determination of this relationship is not clearly assigned in code [9].

1.4 PERFORMANCE BASED DESIGN

A fundamental question in performance-based design is to validate the reliability of the selected performance levels, the specific parameters used to define their minimum performance, and the seismic hazard definitions. For the case of three performance levels (serviceability, damage control and life safety or collapse prevention), three corresponding structural characteristics

(stiffness, strength and deformation capacity) dominate the performance as illustrated in Figure 7. If more intermediate performance levels are selected, then it becomes difficult to define which structural characteristics dominate the performance. It can be argued that different performance objectives may impose conflicting demands on strength and stiffness [32]. Much research is needed to associate the displacement or drift limits with the damage states and the stated general performance objectives. The displacements or drift limits are also functions of the structural system and its ability to deform (ductility). Design criteria may be established on the basis of observation and experimental data of deformation capacity. For example, near the collapse point, the drift limits of structural walls are different from a moment-resisting frame, which suggest that different structural systems will undergo unequal displacements. Other issues related to the damage evaluation are the quantification of the relationship between building restoration time/costs and earthquake hazard level. It is of interest to identify the damage level at which building restoration becomes impractical, which represents the state of irreparable damage.
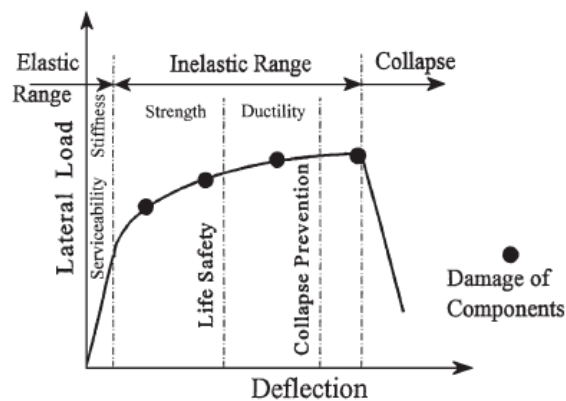
Fig. 7.   Typical performance curve for the structure

A major challenge to performance-based design is to develop an efficient and effective general methodology for the design of structures at multiple performance and hazard levels. Improved procedures are needed for the assessment of strength and deformation capacities of structural elements, components and systems at all performance levels. Addressing multiple performance objectives will require more complex and time-consuming analytical techniques to evaluate the building performance to more than one earthquake demand level. This is expected to increase building development

and design cost. These analysis procedures need to be calibrated and their adequacy verified [33]. Eventually, consideration needs to be given to the complete soil-foundation-structure system, all non-structural systems and components and the building contents. Appropriate acceptance criteria for site performance in terms of permissible foundation settlements, lateral spreading, liquefaction and faulting will need to be established for each performance objective.

The most suitable approach to achieve the objectives of performance-based seismic design with displacement-based performance objectives appears to be the deformation-controlled design approach. It is anticipated that deformation-controlled design will be implemented in future codes, both by enhancing force-based design through verification of deformation targets and by the development of direct deformation-based design procedures.

Computer tools are needed to predict the inelastic dynamic response of complex structures. Extensive efforts are believed to be necessary to develop versatile and robust, yet efficient, numerical standard programs to simulate seismic response of three-dimensional structures taking into account various nonlinearities. It is necessary that these tools be design-oriented rather than research-oriented.

The general design methodology may have to go beyond the methods that assume a single-degree-of-freedom representation of the structure. This assumption results in severe restrictions on the reliability of the estimated performance. At the risk of sacrificing simplicity, it is important to obtain a good estimate of the local displacements within the structure, take higher-mode effects into consideration, and account for the sequence of element damage. Nonlinear static pushover analysis coupled with new methods (other than SDOF-based spectra) to determine demand, or nonlinear inelastic dynamic analysis, may provide a more reliable prediction of the performance [34].

1.5 CONCLUSIONS

There is general agreement that future seismic design needs to be based on defined multiple performance objectives and associated earthquake hazard levels. The advantage of performance-based design is the possibility of achieving predictable seismic performance with uniform risk. However, the reliability of the approach may ultimately depend on the development of explicit and quantifiable performance criteria that can be related to the

response parameters (which can be calculated) such as stresses, strains, displacements, accelerations and their derivatives.

The developments in performance-based design in seismic engineering will be directed towards a general design methodology that permits performance-based design at multiple performance and hazard levels, and with consideration given to the complete soil-foundation-structure system, non-structural systems and components and the building contents.

The framework for a unified seismic design approach could be based on performance-based design concepts for multiple performance levels. However, much research and development remain to be done before such a design methodology can be implemented.

CHAPTER 2: THE ROTATION CAPACITY OF STEEL MEMBERS

2.1 INTRODUCTION

The plastic behaviour of a structure depends upon the amount of moment redistribution. The attainment of the predicted collapse load is strictly related not only to the hinge position where sections reach the full plastic moment, but also to the inelastic rotation which other hinges can have elsewhere. Hence, plastic hinges require a certain amount of ductility in addition to their strength requirement. In the practice of plastic design of structures, ductility defines the capacity of a structure to undergo deformations after its initial yield, without any significant reduction in ultimate strength. The ductility of a structure allows us to predict the ultimate capacity of a structure, which is the most important criteria for designing structures under conventional loads. The following ductility types are widely used in literature (Fig.8)[22]:

- material ductility, or deformation ductility, which characterizes the material plastic deformations for different loading type;
- cross-section ductility, or curvature ductility, which refers to the plastic deformations of the cross-section, considering the interaction between the parts composing the cross-section itself;
- member ductility, or rotation capacity, when the properties of members are considered;
- structure ductility, or displacement ductility, which considers the overall behaviour of the structure;
- energy ductility, when the ductility is considered at the level of dissipated energy;
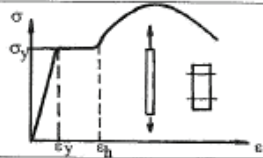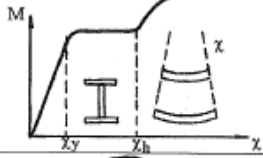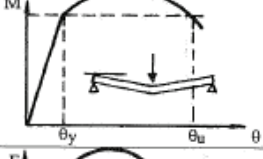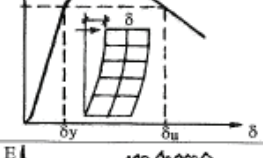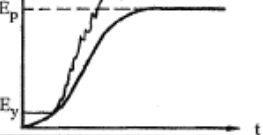
DUCTILITY TYPE	SCHEME	DEFINITION
MATERIAL DUCTILITY (deformation ductility)		$\mu_\varepsilon = \dfrac{\varepsilon_h - \varepsilon_y}{\varepsilon_y}$
CROSS-SECTION DUCTILITY (curvature ductility)		$\mu_\chi = \dfrac{\chi_h - \chi_y}{\chi_y}$
MEMBER DUCTILITY (rotation ductility)		$\mu_\theta = \dfrac{\theta_u - \theta_y}{\theta_y}$
STRUCTURE DUCTILITY (displacement ductility, kinematic ductility)		$\mu_\delta = \dfrac{\delta_u - \delta_y}{\delta_y}$
ENERGY DUCTILITY (hysteretic ductility)		$\mu_E = \dfrac{E_p - E_y}{E_y}$

Fig. 8.   Ductility types

To obtain a globally ductile behaviour of the structure, members must show a locally ductile behaviour, the rotation capacity is a measure of local ductility. Rotation capacity usually is considered connected to the deformation which a given cross-sectional shape can accept at the plastic moment without premature failure occurring.

In limit design of structures, it is postulated that plastic hinges have a sufficient rotation capacity. Therefore, it is clear that the cross-section of members must satisfy precise geometrical requisites in order to allow plastic deformations until the collapse mechanism of the structure is reached without loosing its load carrying capacity. The rotation capacity of steel members is damaged by the occurrence of local buckling in the plate elements which constitute the member cross-section and, if torsional restraints are not provided, by the occurrence of lateral torsional buckling.

Regarding the local ductility, the modern codes define the concept of cross-section behavioural classes which depends only on the width-to-thickness ratios of flanges and of web. These proposals contain some shortcomings [29]:

a) Independent limitations of these ratios are unreasonable, because, obviously, the flange is restrained by the web and the web is restrained by the flange.

b) The local ductility depends not only on the width-to-thickness ratios, but also on the ratio between width of flange and web, member length, moment gradient, level of axial load, eccentricity of axial load, steel quality, flexural-torsional buckling, etc. As a consequence of such additional factors, it seems that the concept of cross-section behavioural classes should be substituted by the concept of member behavioural classes [30].

c) As far as the values of b/t ratios in the different ductility classes are concerned, we can observe that this subdivision does not correspond to the actual behaviour of beam and beam-columns which are a continuous one and the given discrete values of b/t ratio seem to be very arbitrary. The local ductility is also influenced by the low-cycle fatigue, which reduces the ductility, causing premature failure.

2.2 DEFINITIONS OF ROTATION CAPACITY

In the plastic classical theory it is assumed that in correspondence of the plastic hinge of a bent member the plastic moment remains constant as far the rotation increases. This assumption neglects two important aspects:

a) The additional moment capacity due to the strain-hardening effects;
b) The possibility of moment reduction due to the local buckling of flanges and/or web.

Neglecting the first aspect is on the safe side, but the omission of the second aspect can produce an uncontrolled plastic redistribution, followed by an important increasing of lateral displacement.
Because this situation must be avoided, a method for eliminating the achievement of the strong degradation is required. The codes use the concept of cross-section behavioural classes to provide a sufficient plastic rotation capacity for a well controlled redistribution. This is a qualitative method, in

which the actual behaviour is not able to be determined. A more accurate method to determine the rotation capacity is based on the actual behavioural M-θ curve. On this base, two different approaches can be followed (Fig.9):
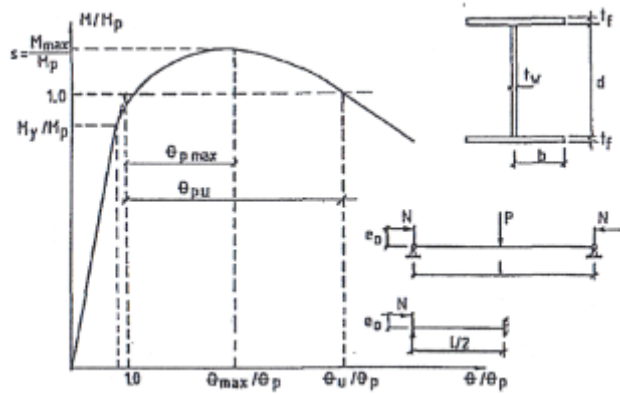
Fig. 9.   Moment-rotation curve

- The rotation capacity is defined by considering the stable part of the M-θ curve:

$$R_{max} = \frac{\vartheta_{p,max}}{\vartheta_p} = \frac{\vartheta_{max} - \vartheta_p}{\vartheta_p} = \frac{\vartheta_{max}}{\vartheta_p} - 1 \qquad (2.1)$$

being θ_p the rotation corresponding to the full plastic moment M_p and θ_{max} the plastic rotation corresponding to the maximum value of the moment M_{max}. This approach has been followed by [35], [36], [37], [30].

- The rotation capacity is defined by considering also the unstable branch of the M-θ curve up to the value θ_u, which corresponds to the plastic moment M_p in the lowering curve:

$$R_u = \frac{\vartheta_{p,u}}{\vartheta_p} = \frac{\vartheta_u - \vartheta_p}{\vartheta_p} = \frac{\vartheta_u}{\vartheta_p} - 1 \qquad (2.2)$$

This way has been followed by [38], [39], [40], [41], [42], [43], [44], [45] and [46]. Figure 10 shows a comparison of R_{raax} and R_u [41].
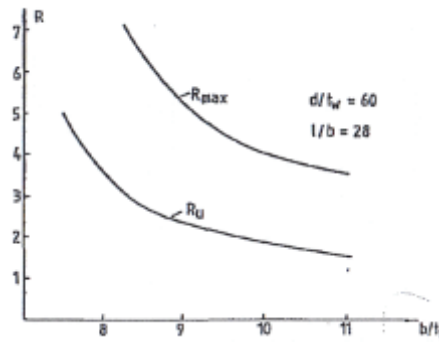
Fig. 10. Comparison between R_{max} and R_u

Two types of beams are used for determining the rotation capacity of a member:

i) *3-point loaded beam* (Fig. 11a), used in the case of gradient moment. Due to behaviour with hardening-stresses, the increase of plastic moment over the full theoretical plastic moment is produced. If a plastic buckling occurs in the compression flange, a maximum value for bending moment is reached and a slump in moment capacity is produced. In this case the formulation to calculate this rotation capacity is the number (2.2).

ii) *4-points loaded beam* (Fig. 11b), used for member with uniform moment. For this beam, at the collapse, the central part remains in the plastic range, without excursion in strain-hardening range, the plastic moment being the maximum one. Because in many cases during the experimental tests the yielding plateau occurs bellow the reference values M_p, the above mentioned definition of rotation capacity can not be used. Thus, for this case, the rotation capacity is determined for a reduced plastic moment $0.95\,M_p$:

$$R_{0.95} = \frac{\vartheta_{u0.95}}{\vartheta_p} - 1 \tag{2.3}$$

Fig. 11.   Different definitions of rotation capacity
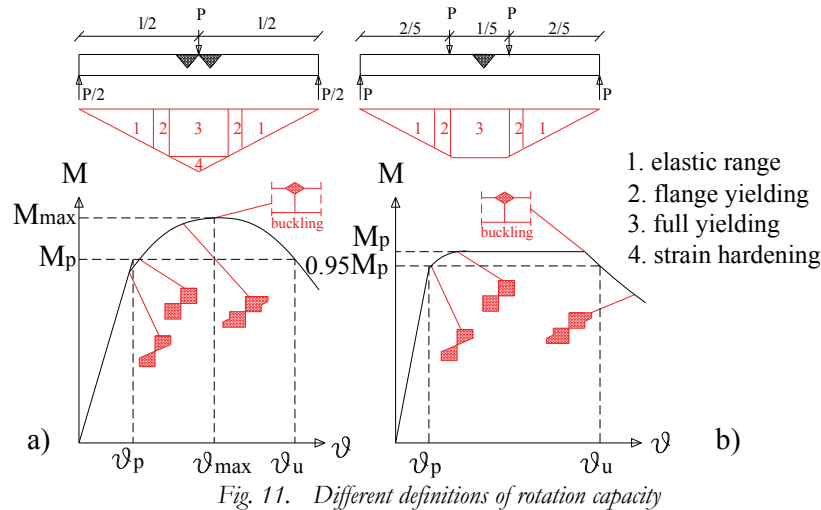
2.3 PREDICTIVE METHODS OF THE ROTATION CAPACITY

From the operative point of view, the calculation of the rotation capacity of steel members can be obtained by different methods [47]:

- *Theoretical methods* based on the use of FEM for evaluation of the moment versus rotation relationship [41].

- *Semi-empirical methods* in which the theoretical method is based on the experimental evidence. These methods are developed by integrating the moment-curvature relationship until the maximum value of the moment experimentally determined; in this way expressions for practical calculations of rotation capacity are provided [47].
A second way is based on the interpretation of the collapse mechanism coming from the experimental evidence. This methodology provides values of the maximum plastic rotation θ_u [45]. The use of the effective width method can be also followed [46].

 - *Empirical methods* are based upon the statistical analysis of experimental data of full-scale member tests and provide practical relationships for determining the rotation capacity [48], [44].

2.3.1 Theoretical methods

Theoretical methods required the evaluation of the relationship Moment - Curvature. For I sections such relationship depends by the thickness of the flanges and webs and it is influenced by the distribution of the residual stresses. Considering these factors negligible, the theoretical investigation of the relationship Moment - Curvature has been carried making reference to an ideal I section constituted by two concentrated masses. This approach, generally approved in the technical literature, has been employed by B. Kato [36], [37], [49] also in the analysis of the capacity of deformation of tubular square and circular sections. In any case, the equivalent ideal section of two concentrated masses has the same area of the actual section, while its height is calculated imposing the equivalence of the two sections in terms of plastic moment. Besides, in the theory developed by the author B. Kato the rotation due to the part of the member that remains in elastic field is neglected assuming, as stress-strain curve (σ,ε), a rigid-perfectly plastic-hardening behaviour. The Moment-Curvature relationship is determined, in presence of an axial force, of an ideal I section constituted by two concentrated masses, assuming as stress-strain curve an elastic-perfectly plastic-hardening behaviour (Fig. 12).
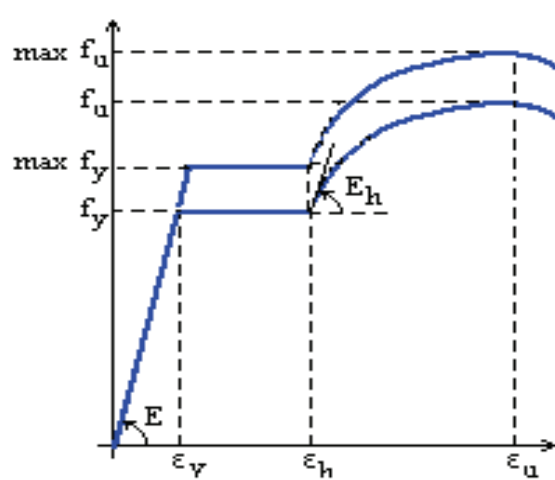
Fig. 12.   *Elastic - perfectly plastic – hardening behaviour*

being:

N_0 the external axial force;

N_{up} the axial force corresponding to upper flange;

N_{lo} the axial force corresponding to lower flange;

M external bending moment;

ε_{up} deformation of upper flange;

ε_{lo} deformation of lower flange;

ε_y deformation corresponding to yielding limit;

ε_h deformation corresponding to hardening limit;

E Young modulus;

E_h hardening modulus;

σ_y yielding stress;

$\sigma_u = s \cdot \sigma_y$ critical stress of compressed flange that causes the flexural-torsional instability;

$\sigma_0 = \rho \cdot \sigma_y$ stress due to the external axial force;

A area of the section;

h_e the height of two flanges;

Subsequently the stresses, the deformations and the forces are assumed positive when they correspond to the compression.

The equation of equilibrium to the translation in the longitudinal direction is the following:

$$N_{up} + N_{lo} = N_o \qquad (2.4)$$

while the equation of equilibrium to the rotation can be written as:

$$M = \frac{N_{up} - N_{lo}}{2} \cdot h_e \qquad (2.5)$$

The general expression of the curvature is following given:

$$\chi = \frac{\varepsilon_{up} - \varepsilon_{lo}}{h_e} \qquad (2.6)$$

Different steps of behaviour can considered according to deformation of the flanges: elastic, plastic or hardening.

CASE 1: Both flanges in elastic field
The expression of bending moment is the following

$$M = \chi \cdot E \cdot I_e \qquad (2.7)$$

being:

$$I_e = \frac{A \cdot h_e^2}{4} \qquad (2.8)$$

the moment of inertia of the ideal section.
The equation (2.7) can be used until it does not occur the compression of flange and the bending moment reaches the value:

$$M = (1 - \rho)M_p \qquad (2.9)$$

being:

$$M_{pl} = \frac{A \cdot \sigma_y}{2} \cdot h_e \qquad (2.10)$$

the plastic moment of the ideal section.
The limit value of the curvature corresponding to the attainment of the bending moment (2.9) is given from:

$$\chi = (1 - \rho) \cdot \frac{M_p}{E \cdot I_e} = 2 \cdot (1 - \rho) \cdot \chi_y \qquad (2.11)$$

being

$$\chi_y = \frac{\varepsilon_y}{h_e} \qquad (2.12)$$

CASE 2: The upper flange is in plastic field. In this case the bending moment assumes a constant value and equal to the one of equation (2.9), while the plastic deformation provides an increase of the curvature. This equation is used untill the attainment of the following value of the curvature:

$$\chi_2 = 2 \cdot (1 - \rho) \cdot \chi_y + \chi_h - \chi_y \qquad (2.13)$$

In which:

$$\chi_h = \frac{\varepsilon_h}{h_e} \qquad (2.14)$$

CASE 3: The upper flange is in hardening field
The efforts of upper (N_{up}) and lower flanges (N_{lo}) are:

$$N_{up} = \frac{A \cdot \sigma_y}{2} + E_h \cdot \frac{A}{2} (\varepsilon_{up} - \varepsilon_h) \qquad (2.15)$$

$$N_{lo} = \rho \cdot \sigma_y \cdot A - \frac{A \cdot \sigma_y}{2} - E_h \cdot \frac{A}{2} (\varepsilon_{up} - \varepsilon_h) \qquad (2.16)$$

Combining the equations (2.4), (2.5), (2.15) and (2.16) the following expression of bending moment is obtained:

$$M = (1 - \rho) \cdot M_p + E_h \cdot \frac{A}{2} \cdot (\varepsilon_{up} - \varepsilon_h) \cdot h_e \qquad (2.17)$$

At this point it is necessary to consider two different situations:

1) The critical bending moment $(s - \rho) \cdot M_p$ is reached when the lower flange is already in elastic field;
2) The critical bending moment $(s - \rho) \cdot M_p$ is reached when the lower flange is in hardening field.

The first condition is verified in the following case:

$$N_{lo} > -\sigma_y \cdot \frac{A}{2} \qquad (2.18)$$

Combining the equations (2.16) and (2.18), the following relationship can be satisfied:

$$\varepsilon_{up} - \varepsilon_h < \frac{2 \cdot \rho \cdot \sigma_y}{E_h} \qquad (2.19)$$

The attainment of the critical moment can be express through the following relationship:

$$(s - \rho) \cdot M_p = (1 - \rho) \cdot M_p + E_h \cdot \frac{A}{2} \cdot (\varepsilon_{up} - \varepsilon_h) \cdot h_e \qquad (2.20)$$

which provides:

$$\varepsilon_{up} - \varepsilon_h = (s - 1) \cdot \frac{\sigma_y}{E_h} \qquad (2.21)$$

Combining the relationships (2.19) and (2.21) it can be concluded that the critical moment is reached when the lower flange is in elastic field if the following condition is satisfied

$$\rho > \frac{s - 1}{2} \qquad (2.22)$$

in the other case the lower flange results in plastic or in hardening field when the critical moment is attained.

Analyzing therefore the two cases:

Case 1 $\qquad \Rightarrow \qquad \rho > \dfrac{s - 1}{2}$

The force in the lower flange can be written in the following way:

$$N_{lo} = \varepsilon_{lo} \cdot E \cdot \frac{A}{2} \qquad (2.23)$$

Comparing the relationship (2.23) and (2.16) the following relationship is obtained between ε_{lo} and ε_{up}.

$$\varepsilon_{lo} = (2 \cdot \rho - 1) \cdot \varepsilon_y - \frac{E_h}{E} \cdot (\varepsilon_{up} - \varepsilon_h) \qquad (2.24)$$

Combining the equations (2.6), (2.24) and (2.14) it can be shown that:

$$\varepsilon_{up} - \varepsilon_h = \frac{E}{E + E_h} \cdot h_e \cdot \left[\chi + (2 \cdot \rho - 1) \cdot \chi_y - \chi_h \right] \qquad (2.24)$$

Combining the equations (2.17), (2.25) and (2.8) the following relationship moment-curvature is obtained

$$M = (1 - \rho) \cdot M_p + \frac{2 \cdot E \cdot E_r}{E + E_h} \cdot I_e \cdot \left[\chi - (1 - 2 \cdot \rho) \cdot \chi_y - \chi_h \right] \quad (2.26)$$

and introducing the Reduced Elastic Modulus E$_r$.

$$E_r = \frac{2 \cdot E \cdot E_h}{E + E_h} \qquad (2.27)$$

The relationship Moment-Curvature can be simplified as following illustrated:

$$M = (1 - \rho) \cdot M_p + E_r \cdot I_e \cdot \left[\chi - (1 - 2 \cdot \rho) \cdot \chi_y - \chi_h \right] \qquad (2.28)$$

The critical value of curvature χ_{cr} corresponding to the attainment of critical moment $(s - \rho) \cdot M_p$ is obtained through the following equation:

$$(s - \rho) \cdot M_p = (1 - \rho) M_p + E_r I_e \left[\chi_{cr} - (1 - 2\rho) \chi_y - \chi_h \right] \qquad (2.29)$$

The critical curvature is:

$$\chi_{cr} = \frac{(s-1)\cdot M_p}{E_r \cdot I_e} + (1-2\rho)\chi_y + \chi_h \tag{2.30}$$

Case 2 $\Rightarrow$ $\rho \leq \dfrac{s-1}{2}$

In this case, the equation (2.28) is valid until the condition $\varepsilon_{lo} = -\varepsilon_y$ is reached. For such condition, the equation (2.24) gives:

$$-\varepsilon_y = (2\cdot\rho-1)\cdot\varepsilon_y - \frac{E_h}{E}\cdot(\varepsilon_{up} - \varepsilon_h) \tag{2.31}$$

or:

$$2\cdot\rho\cdot\varepsilon_y = \frac{E_h}{E}\cdot(\varepsilon_{up} - \varepsilon_h) \tag{2.32}$$

so, from the (2.25) it results:

$$2\cdot\rho\cdot\chi_y = \frac{E_h}{E+E_h}\cdot[\chi_3 - (1-2\rho)\cdot\chi_y - \chi_h] \tag{2.33}$$

Taking into account that:

$$2\cdot\chi_y = \frac{M_p}{E\cdot I_e} \tag{2.34}$$

and introducing the Reduced Elasticity Modulus, the following value of the curvature is obtained

$$\chi_3 = \frac{2\rho\cdot M_p}{E_r \cdot I_e} + (1-2\rho)\chi_y + \chi_h \tag{2.35}$$

When this value of curvature is reached, a plastic flow and therefore a plastic increase of the curvature occur $\Delta\chi = \chi_h - \chi_y$.

Insofar, the bending moment reaches a constant value that can be obtained introducing the limit curvature (2.35) in the (2.28).

This value

$$M = (1 + \rho) \cdot M_p \qquad (2.36)$$

is constant until a new limit curvature is reached:

$$\chi_4 = \frac{2\rho \cdot M_p}{E_r \cdot I_e} + (1 - 2\rho)\chi_y + 2\chi_h - \chi_y \qquad (2.37)$$

When the value of the curvature is greater than the one obtained by the relationship (2.37), the lower flange is in the hardening range too. The equations (2.15) (2.16) (2.17) are still valid. Besides the effort in the lower flange, can be express through the following relationship:

$$N_{lo} = -\sigma_y \cdot \frac{A}{2} + \frac{E_h \cdot A}{2} \cdot (\varepsilon_{lo} + \varepsilon_h) \qquad (2.38)$$

Comparing the (2.16) and the (2.38), the relationship that ties the deformation of lower and upper flanges is obtained:

$$\varepsilon_{lo} + \varepsilon_{up} = \frac{2\rho \cdot \sigma_y}{E_h} \qquad (2.39)$$

Combining the equations (2.6) and (2.39) the deformation of the upper flange can be correlated to the curvature as follows:

$$\varepsilon_{up} = \frac{\rho \cdot \sigma_y}{E_h} + \chi \cdot \frac{h_e}{2} \qquad (2.40)$$

Finally, through the equations (2.10), (2.14), (2.17) and (2.40), the expression of the bending moment is obtained

$$M = M_p + E_h \cdot I_e \cdot (\chi - 2\chi_h) \qquad (2.41)$$

The critical value of the curvature is provided by the condition:

$$(s - \rho) \cdot M_p = M_p + E_h \cdot I_e \cdot (\chi_{cr} - 2\chi_h) \qquad (2.42)$$

its value is:

$$\chi_{cr} = \frac{(s - \rho - 1) \cdot M_p}{E_h \cdot I_e} + 2 \cdot \chi_h \qquad (2.43)$$

In Figure 13 the relationship between Moment and Curvature in the case $\rho \geq (s-1)/2$ is reported:
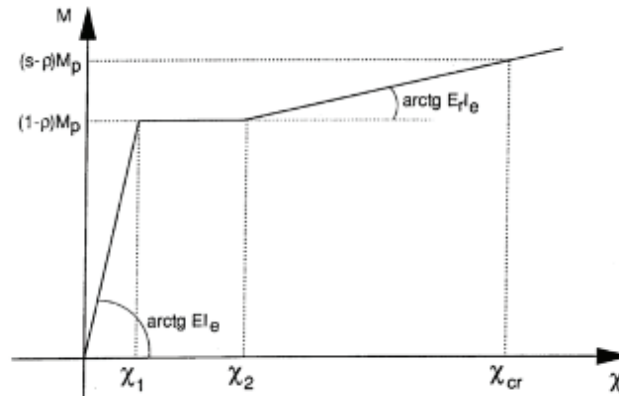
Fig. 13.   Relationship Moment-Curvature for $\rho \geq (s-1)/2$

In Figure 14 the relationship between Moment and Curvature in the case $\rho < (s-1)/2$ is reported:
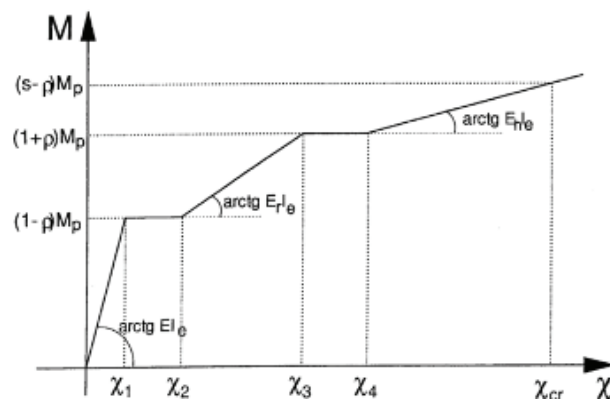
Fig. 14.   Relationship Moment-Curvature for $\rho < (s-1)/2$

Through the relationships Moment - Curvature previously obtained and assuming the attainment of the critical moment as ultimate condition, it is possible to calculate the ultimate rotation of a cantilever beam or of a simple supported beam through the integration of the diagram of the curvature.

Case 1 $\Rightarrow$ $\rho > \dfrac{s-1}{2}$
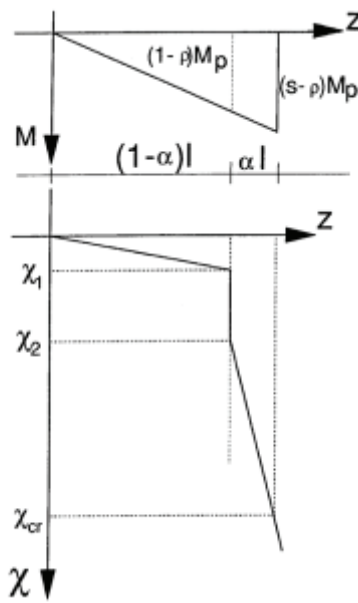
Fig. 15.   Ultimate rotation for $\rho \geq (s-l)/2$

$$\vartheta_m = \frac{L}{s-\rho}\left\{(1-\rho)^2\,\chi_y + (s-1)\left[(1-2\rho)\chi_y + \chi_h + \frac{(s-1)M_p}{2E_r I_r}\right]\right\} \qquad (2.44)$$

Case 2 $\Rightarrow$ $\rho \leq \dfrac{s-1}{2}$

this is the final expression of the ultimate rotation:

$$\vartheta_m = \frac{L}{s-\rho}\left\{ \begin{array}{l} \left[\left(1-\rho^2\right)-2\rho\left(s-1\right)\right]\chi_y + 2\chi_h\left(s-\rho-1\right)+ \\ +\frac{M_p}{E_r I_e}2\rho\left(s-\rho-1\right)+\frac{\left(s-2\rho-1\right)^2 M_p}{2E_h I_e} \end{array} \right\} \tag{2.45}$$
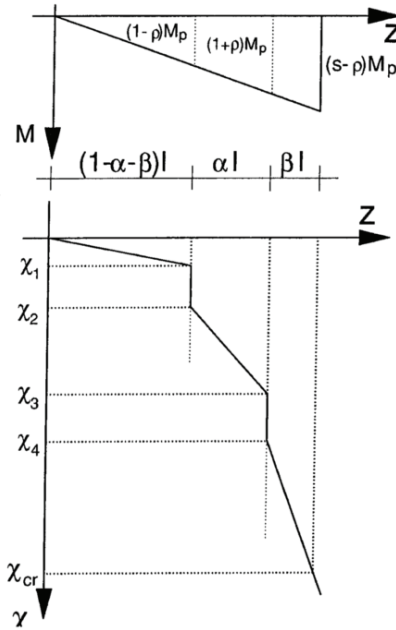
Fig. 16. *Ultimate rotation for* $\rho<(s-l)/2$

Case 3 $\Rightarrow$ $\rho = 0$

Through the condition $\rho = 0$ the following expression is obtained:

$$\vartheta_m = \frac{L}{s}\left\{ \chi_h + 2\chi_h\left(s-1\right)+\frac{\left(s-1\right)^2 M_p}{2E_h I_e} \right\} \tag{2.46}$$

At this point it is possible to define the rotation at the first yielding of the actual beam through the following formulations:

$$\vartheta_y = (1-\rho)L\frac{\varepsilon_y}{h} \tag{2.47}$$

and

$$\vartheta_y = (1-\rho)\frac{M_p L}{2EI} \tag{2.48}$$

being h and I the height and the moment of inertia of the actual section.
The expression of the rotation capacity is the following

$$R_{st} = \frac{\vartheta_m}{\vartheta_y} - 1 = \frac{\vartheta_p}{\vartheta_y} \tag{2.49}$$

which assumes particular expressions in different cases:

For $\rho > (s-1)/2$

$$R_{st} = \frac{1}{s-\rho}\left\{(1-\rho)\frac{h}{h_e} + \frac{s-1}{1-\rho}\left[(1-2\rho)\frac{h}{h_e} + \frac{\varepsilon_h}{\varepsilon_y}\frac{h}{h_e} + (s-1)\frac{E}{E_r}\frac{I}{I_e}\right]\right\} - 1 \tag{2.50}$$

h and I represent, respectively, the height and the moment of inertia of the actual section, while h_e and I_e are respectively the height and the moment of inertia of the ideal section with two flanges and with a plastic modulus equal to the actual section.

Case for $\rho \le (s-1)/2$

The following expression is obtained:

$$R_{st} = \frac{1}{(s-\rho)(1-\rho)}\left\{\begin{array}{l}\left[1+\rho^2 - 2\rho(s-1)\right]\frac{h}{h_e} + 2\frac{\varepsilon_h}{\varepsilon_y}\frac{h}{h_e}(s-\rho-1) + \\ + \frac{E}{E_r}\frac{I}{I_e}4\rho(s-\rho-1) + (s-2\rho-1^2)\frac{E}{E_h}\frac{I}{I_e}\end{array}\right\} - 1 \tag{2.51}$$

The procedure developed by Kemp [35] is based on an elastic-perfectly-plastic-hardening constitutive low and on the determination of the moment-curvature relationship for an ideal I section. The theoretical analysis developed by Kemp with reference to the beams ($\rho = 0$), conducts to the following relationship:

$$R = \gamma \cdot \left(2 \cdot \frac{\varepsilon_h}{\varepsilon_y} - 1 + \frac{E}{E_h} \cdot \frac{\gamma}{1 - \gamma} \right) \tag{2.52}$$

being:

$$\gamma \cdot l = \frac{s - 1}{s} \cdot l \tag{2.53}$$

the extension of plastic zone.

The expression (2.52) is a particular case of (2.51) for $\rho = 0$ and $\dfrac{h}{h_e} = \dfrac{I}{I_e} = 1$ (ideal I section).

Using the expression (2.52), the conditions of local instabilities of compressed flange are required. Very interesting is the interpretation of Lay and Galambos [50] according to which local instability is developed when the extension of the plastic zone is equal to the length of the wave corresponding to the attainment of instability of compressed flange. The critical condition is:

$$l_f = \gamma \cdot l \tag{2.54}$$

The hypothesis introduced by Kemp is that the critical deformation, provided by the relationship of Southward, is obtained in the middle of the plastic zone, so:

$$\frac{\sigma_{cr}}{\sigma_y} = 1 + \frac{0.5 \cdot \gamma}{1 - \gamma} \tag{2.55}$$

Combining the (2.55) the Southward expression and taking into account the assumptions of Southward [51] $G_h / E_h = 1/3$:

$$\frac{4}{3}\cdot\left(\frac{t_f}{b_f}\right)^2 + \frac{2}{3}\cdot\pi^2\cdot\left(\frac{t_f}{\gamma\cdot L}\right)^2 = \varepsilon_h + \frac{\sigma_y}{E_h}\cdot\frac{0.5\cdot\gamma}{1-\gamma} \qquad (2.56)$$

it results to be a third degree equation in the unknown quantity γ.

The value of γ, resulting from (2.56), provides the expression (2.52) which represents the value of rotation capacity.

For columns, in which $\rho \neq 0$ the equation (2.52) assumes the following approximate expression:

$$R = \frac{h'_w}{2h'_c}\cdot\left(2\cdot\frac{\varepsilon_h}{\varepsilon_y} - 1 + \frac{E}{E_h}\cdot\frac{\gamma}{1-\gamma}\right) \qquad (2.57)$$

in which:

- h'_w is the distance between the centre of masses of the two flanges

- h'_c is the distance between the centre of mass of compressed flange and the plastic neutral axis.

So, the ratio $h'_w/2h'_c$ is a function of the non-dimensional axial load ρ.

2.3.2 Semi-empirical methods

In the theoretical methods the evaluation of the rotational capacity is based on the approximate theoretical evaluation (neglecting both the effects derived from the geometric configuration of the section and the mechanical imperfections) of the relationship moment-curvature of the section and on the theoretical analysis of the instability phenomena (particularly the local instability of the compressed flange). Semi-empirical methods are instead procedures in which the theoretical evaluation of the relationship moment-curvature of the section is connected with the determination, on experimental bases, of the conditions that conduct to the local instability of the compressed flange.

Le procedure proposed by B. Kato [36], [37], [49] is based on the employment of a rigid-perfectly plastic-hardening constitutive low of the material and on the use of an equivalent I section. The evaluation of the rotation capacity is made through the equations (2.50) and (2.51). In these relationships the

parameter s, that defines the conditions corresponding to the local instability of the compressed flange, is calculated through the following experimental relationships:

- for I sections

$$\frac{1}{s} = 0.6003 + \frac{1.600}{\alpha_f} + \frac{0.1535}{\alpha_w}$$

(2.58)

- for welded square hollow sections (SHS)

$$\frac{1}{s} = 0.710 + \frac{0.167}{\alpha}$$

(2.59)

- for cold formed square hollow sections (SHS)

$$\frac{1}{s} = 0.778 + \frac{0.13}{\alpha}$$

(2.60)

- for cold formed circular hollow sections (cold-formed CHS)

$$\frac{1}{s} = 0.777 + \frac{1.18}{\alpha}$$

(2.61)

being:

$\alpha_f = \frac{E}{\sigma_y} \cdot \left(\frac{t_f}{b_f/2} \right)^2$ the slenderness factor for the flange;

$\alpha_w = \frac{E}{\sigma_y} \left(\frac{t_w}{d_w} \right)^2$ the slenderness factor of the web (d_w is the height of the

web); $\alpha = \frac{E}{\sigma_y} \left(\frac{t}{B} \right)^2$ and $\alpha = \frac{E}{\sigma_y} \left(\frac{t}{D} \right)^2$ the slenderness factor for SHS and

CHS (B is the side of SHS, D is the diameter of the CHS and t is the thickness).

The greatest problem in the theoretical evaluation of the rotational capacity is the determination of the critical tension that brings to the local instability of the compressed flange. This value is influenced by the degree of constraint that the web offers towards the flange and, they depend on the stress condition (in elastic or plastic field) of the same web. Besides, the theoretical analyses in technical literature don't include the effects derived from the stress gradient, in the plastic zone, due to the longitudinal variation of the bending moment. The dependence of the critical tension from the stress gradient, underlined particularly by the experimental results of U. Kuhlmann [43], is not considered by empirical formulations proposed by B. Kato [36], [37], [49]. On the base of the experimental results, the length of the instabilized part of the beam is about equal to 1.20 b_f [43]. The influence of the stress gradient on the critical tension, that causes the local instability of the compressed flange, depends on the ratio b_f/L (being, generally, L the distance among the zero point of the diagram of the moment and the section of maximum moment). The analysis of experimental results illustrated in [37], [35] and [43] has provided, through a multiple regression, the following empirical relationship:

$$\frac{1}{s} = 0.546321 + 1.632533 \cdot \lambda_f^2 + 0.062124 \cdot \lambda_w^2 - 0.602125 \frac{b_f}{L} +$$
$$+0.001471 \frac{E}{E_h} + 0.007766 \frac{\varepsilon_h}{\varepsilon_y} \tag{2.62}$$

being:

$$\lambda_f = \frac{b_f}{2 \cdot t_f} \cdot \sqrt{\frac{f_y}{E}}$$

$$\tag{2.63}$$

$$\lambda_w = \frac{d_{w,e}}{t_w} \cdot \sqrt{\frac{f_y}{E}}$$

the slenderness parameters of flange and web.

The relationship of Mazzolani-Piluso (2.62), differently from the one proposed by Kato, includes not only the influence of the slenderness of the flange and the web but also the consequential effects of the stress gradient and of the mechanical properties of the material. The model of the ideal I section assumed for the evaluation of the ultimate rotation is already used, the rotation

capacity R is calculated through the equations (2.50) and (2.51) with the condition $h/h_e = l/l_e = 1$ (the rotation corresponding to the yield limit is evaluated with reference an ideal I section too). The parameter s, that defines the conditions corresponding to the local instability of the compressed flange, is calculated through the followings experimental relationships:

$$\frac{1}{s} = 0.546321 + 1.632533 \cdot \lambda_f^2 + 0.062124 \cdot \lambda_w^2 - 0.602125 \frac{b_f}{L} +$$
$$+0.001471 \frac{E}{E_h} + 0.007766 \frac{\varepsilon_h}{\varepsilon_y} \tag{2.64}$$

The analyzed procedures have to be integrated with the control of the conditions that determines the flexural-torsional instability.

2.3.3 Empirical methods

Different empirical relationships for the evaluation of the rotation capacity of the beams and the columns, based on the analysis of the experimental results, have been proposed by Japanese researchers (Kato e Akiyama, [48], [52] – Mitani e Makino, [53] – Nakamura, [54] - Sedlacek e Spangemacher, [44], [55]). In the following all the complete formulations are illustrated.

Kato and Akiyama have proposed, for members subjected to a bi-triangular distribution of the bending moment and therefore with inversion of the sign of the curvature, the employment of a simplified relationship moment-rotation constituted by three linear parts;

The non-dimensional curve moment-rotation, proposed by the Authors, has shown in Figure 17.
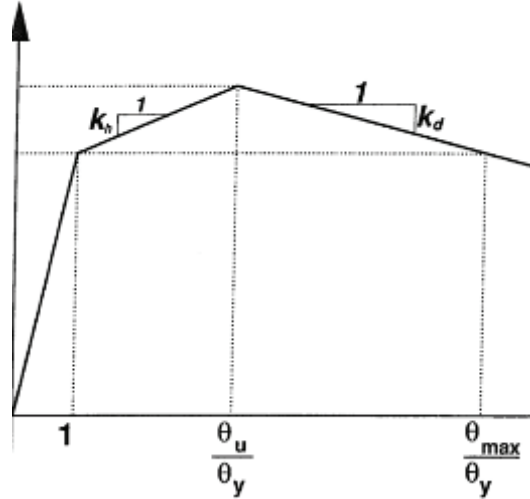
Fig. 17.   Non-dimensional simplified curve Moment-Curvature of Kato and Akiyama

The first increasing line represents the elastic behaviour while the second line is the plastic one characterized by the parameter k_h, the non-dimensional stiffness, which is the ratio between the stiffness of hardening and of elastic ranges. At the attainment of the maximum strength, because of the instability phenomena, a progressive reduction of the load carrying capacity occurs. The decreasing line is characterized by non-dimensional stiffness k_d that represents the ratio between the stiffness of the decreasing and of the elastic ranges. Finally, the ratio between the maximum bending strength and the yielding one is pointed out with m and represents the non-dimensional ultimate moment called by the authors "Stress - increasing ratio." The relationships illustrated in the current section are specific for I sections that satisfy the following limitations:

$$\frac{b_f}{2 \cdot t_f} \le \frac{0.52}{\sqrt{\varepsilon_y}} \qquad \text{and} \qquad \frac{d_w}{t_w} \le \frac{2.40}{\sqrt{\varepsilon_y}} \qquad\qquad (2.65)$$

For beams ($\rho = 0$), the non-dimensional ultimate moment can be calculated as the maximum value provided by the following relationships:

$$m = m_0 = 1 + \left[\left(0.043 - 0.0744 \cdot \lambda_f\right)^2 - \left(0.00024 \cdot \lambda_w - 0.00025\right) \right] \cdot \frac{1}{\varepsilon_y} \qquad (2.66)$$

and for $\lambda_y \leq 200$,

$$m = m_0 = 1.46 - \left[0.63 \cdot \lambda_y + 0.053 \cdot \lambda_w + 0.02 \cdot \left(\lambda_y - 50 \right) \cdot \sqrt{\varepsilon_y} \right] \qquad (2.67)$$

or, in case of $\lambda_y \geq 200$

$$m = m_0 = 1.46 - \left(0.63 \cdot \lambda_f + 0.053 \cdot \lambda_w + 3 \cdot \sqrt{\varepsilon_y} \right) \qquad (2.68)$$

being:

- $\lambda_f = \dfrac{b_f}{2 \cdot t_f} \cdot \sqrt{\varepsilon_y}$ the slenderness parameter of the flange;

- $\lambda_w = \dfrac{d_w}{t_w} \cdot \sqrt{\varepsilon_y}$ the slenderness parameter of the web;

- λ_y the slenderness parameter of the member in comparison to the weak axle of the section.

In any case, the limitation $1 \leq m_o \leq \sigma_u / \sigma_y$ must be respected, being σ_u the collapse stress of the material.

For columns ($\rho \neq 0$), the non-dimensional ultimate moment is provided by the relationship:

$$m = \frac{Z_\rho'}{Z_\rho} \cdot m_o \qquad (2.69)$$

being:
- Z_ρ' the plastic moment of the section correspondent to the non-dimensional axial force ρ / m_o ;
- Z_ρ the plastic modulus of the section correspondent to the non-dimensional axial force ρ .

For $\rho > 2A_w/3A$ the slenderness parameter λ_w in equations (2.66) and (2.67) must be doubled for $\lambda_y > 100$ and $\rho < 2A_w/3A$, the parameter λ_w in the equation (2.66) must be multiplied for 1.5.

The proposed relationships are valid when the ultimate bending capacity is regulated by the local instability phenomena. For flexural-torsional instability, the non-dimensional ultimate moment must be calculate through the following relationship:

$$m = \left(\frac{6.82}{\lambda_e^{1.7}} + 0.9 \right)^{\!\!\frac{1}{2}} \qquad (2.70)$$

being:

- $\lambda_e = \lambda_y \cdot \sqrt{\varepsilon_y}$ for $\rho = 0$ (beams);
- $\lambda_e = 1.28 \cdot \lambda_y \cdot \sqrt{\varepsilon_y}$ for $\rho \neq 0$ (columns)

The maximum bending strength is not influenced from the coupling of the flexural-torsional and local instabilities, so it can be assumed equal to the minimum of the values provided by the equations (2.66-2.68) or (2.69) and (2.70).

The non-dimensional stiffness of the hardening range can be calculated through the following relationship:

$$k_h = 0.03 + 0.04 \cdot \rho \qquad (2.71)$$

If there is only local instability, the non-dimensional stiffness of the decreasing range can be assumed equal to the minimum of the values provided by the following relationships:

$$k_d = -0.355 \cdot \lambda_w \cdot \sqrt{\varepsilon_y} \qquad (2.72)$$

and

$$k_d = -\left[-1.33 + \left(10.6 \cdot \lambda_f - 2\right) \cdot \left(0.63 + 0.33 \cdot \lambda_w\right)\right] \cdot \sqrt{\varepsilon_y} \qquad (2.73)$$

In the equations (2.72) and (2.73) λ_w must be doubled if $\rho > 2A_w/3A$.

To evaluate the possibility of coupling of the two instability phenomena, it is necessary to calculate another parameter:

$$m^* = \left(\frac{2.36}{\lambda_e^{1.7}} + 0.9\right)^{1/2} \qquad (2.74)$$

If the value of the non-dimensional ultimate moment is greater of m^*, there is the coupling of the flexural-torsional and local instabilities; consequently, a strong increase of the slope of the decreasing line occurs, so the value of equation (2.72) or of (2.73) must be tripled.

Using these equations the definition of the simplified curve moment-rotation has been possible. At this point the value of the rotation capacity is:

$$R = \frac{\vartheta_u - \vartheta_y}{\vartheta_y} = \frac{m - 1}{k_h} \qquad (2.75)$$

Taking into account the capacity of deformation due to the decreasing line, the rotational capacity assumes the following expression:

$$R' = \frac{\vartheta_{max} - \vartheta_y}{\vartheta_y} = (m - 1) \cdot \left(\frac{1}{k_h} + \frac{1}{|k_d|}\right) \qquad (2.76)$$

The authors have studied some relationships for the definition of the simplified moment - rotation curve also for the case of the circular and square sections (CHS and SHS) [48], [52].

Empirical formulations for the determination of the rotation capacity of beams and of columns are also obtained by Mitani and Makino [53] starting from experimental results. The authors produced the followings relationships:

$$R = \left(\frac{500}{K \cdot \dfrac{l_x}{i_x} \cdot \dfrac{l_b}{i_y}} \cdot \frac{235}{\sigma_y} \right)^{1/2} \cdot \left[80 \cdot \left(\lambda_f - 0.65 \right)^2 - 4.0 \cdot \lambda_w + 6 \right] \qquad (2.77)$$

valid for $\rho < \dfrac{A_w}{2A}$ and

$$R = \left(\frac{500}{K \cdot \dfrac{l_x}{i_x} \cdot \dfrac{l_b}{i_y}} \cdot \frac{235}{\sigma_y} \right)^{1/2} \cdot \left[50 \cdot \left(\lambda_f - 0.65 \right)^2 - 5.5 \cdot \lambda_w + 7 \right] \qquad (2.78)$$

valid in the opposite case.

Both the relationships are been obtained for $\lambda_f < 0.65$.

In the equations (2.77) and (2.78) the following symbolisms have been used:

- l_x is the distance between the plastic hinge and the zero point of the bending moment;
- l_b is the distance between two consecutive torsional restraints;
- l_x is the inertia radius according to the strong axis;
- i_x is the inertia radius according to the weak axis;
- i_y is the distance between two consecutive torsional restraints;
- K is the numerical coefficient, dependent on the lateral restraints, that defines the length of free bending for flexural-torsional instability as Kl_b

These relationships have been derived by the analysis of results of experimental tests carried on cantilever beams with K=0.60 in relationship with the test conditions. For beams and columns with a bi-triangular distribution of the bending moment, having in some parts curvature with opposite sign, whose end moments are $M_1 > M_2$ (both positive when the zero point finds two lines with curvature of opposite sign), the results can be used assuming:

$$l_x = \frac{l_b}{1 + \frac{M_2}{M_1}}$$
(2.79)

and:

$$k = 0.7 \left(\frac{1.75}{c_b} \right)^{\frac{1}{2}}$$
(2.80)

being:

$$c_b = 1.75 + 1.05 \cdot \frac{M_2}{M_1} + 0.3 \cdot \left(\frac{M_2}{M_1} \right)^2 \leq 2.3$$
(2.81)

From the experimental analyses carried on 121 specimens, Nakamura [54] has extracted the rotation capacity of the beams for different lateral torsional slenderness imposing the condition:

$$R = \frac{\beta}{\bar{\lambda}_{LT}} - 1$$
(2.82)

Where $\bar{\lambda}_{LT} = \sqrt{M_p / c \cdot M_{cr}}$ is the non-dimensional lateral-torsional slenderness.

- M_p is the plastic moment;

- M_{cr} is the elastic critical moment of a simple supported beam under uniform moment;

- c is the coefficient of behaviour to evaluate the moment of lateral instability ($c \cdot M_{cr}$) of a beam under a distribution of a variable moment.

- β is a coefficient that represents the effect of moment gradient on the rotation capacity. It is obtained from:

$$\beta = 1 - \frac{1}{2} \cdot \alpha \qquad\qquad \text{for } -1 \leq \alpha \leq 0$$

$$\beta = 1 - \alpha \qquad\qquad\qquad\qquad \text{for } 0 \le \alpha \le \frac{2}{3}$$

$$\beta = \frac{1}{3} \qquad\qquad\qquad\qquad \text{for } \frac{2}{3} \le \alpha \le 1$$

being α the ratio between the end moments, assumed positive when the curvature does not change the sign along the member. The experiments studied by the authors are relative to the case $\alpha = 0$ and $\alpha = 1$.

The Sedlacek – Spangemacher method is based on the results obtained from numerical simulations using the F.E.M. method. Particularly, these simulations are divided into different series, in which a single parameter that influences the rotation capacity has been modified, being constant all the others. The analysis of the results has been necessary to obtain the following empirical relationship:

$$R = R_o \cdot \left(\frac{f_u}{f_y} \right) + \Delta R \cdot \left(t_f \right) + \Delta R \cdot \left(\frac{b_f}{t_f} \right) + \Delta R \cdot \left(\frac{L}{b_f} \right) - \Delta R \cdot \left(k_g \right) \qquad (2.83)$$

where

$$R_o \cdot \left(\frac{f_u}{f_y} \right) = 0.75 \cdot \left(\frac{f_u}{f_y} \right)^{6.5} \qquad (2.84)$$

$$\Delta R \cdot \left(t_f \right) = \left[2.53 \cdot \left(\frac{f_u}{f_y} \right) - 2.63 \right] \cdot \alpha \cdot \left(15 - t_f \right) \qquad (2.85)$$

$$\alpha = 1.0 \qquad\qquad\qquad\qquad \text{for } t_f < 15mm$$
$$\alpha = 0.5 \qquad\qquad\qquad\qquad \text{for } t_f \ge 15mm$$

$$\Delta R \cdot \left(\frac{b_f}{t_f} \right) = \left[2.81 \cdot \left(\frac{f_u}{f_y} \right) - 2.74 \right] \cdot \left(20 - \frac{b_f}{t_f} \right) \qquad (2.86)$$

$$\Delta R \cdot \left(\frac{L}{b_f} \right) = \left[2.70 \cdot \left(\frac{f_u}{f_y} \right) - 2.70 \right] \cdot \left(5 - \frac{L}{b_f} \right) \qquad (2.87)$$

and

$$\Delta R \cdot (k_g) = S_{k_g} \cdot \Delta k_g \tag{2.88}$$

$$\Delta k_g = 9.31 - 0.035 \cdot \left(\frac{f_u}{f_y}\right)^{6.5} - \frac{G_h \cdot t_w^3}{3 \cdot d_w} \tag{2.89}$$

$$S_{k_g} = 0.35 \cdot \left(\frac{f_u}{f_y}\right)^4 \quad \text{for } \Delta k_g > 0 \tag{2.90}$$

$$S_{k_g} = 0 \quad \text{for } \Delta k_g \leq 0 \tag{2.91}$$

In the equation $\left\{ \Delta k_g = 9.31 - 0.035 \cdot \left(\dfrac{f_u}{f_y}\right)^{6.5} - \dfrac{G_h \cdot t_w^3}{3 \cdot d_w} \right\}$ G_h is the tangential

modulus strain hardening of the web evaluated according to the equation of Lay.

The axial load has not been considered; nevertheless, the expressions of Sedlacek and Spangemacher can be applied only for the beams.

2.4 FACTOR THAT INFLUENCE THE ROTATION CAPACITY

2.4.1 Local and global instabilities

It has been explained that the rotation capacity of a member is a function of the ratio between the critical stress that brings to the instability and the first yielding one.

The evaluation of critical stress can be performed both through theoretical and experimental relationships. In the first case, the method to define the rotation capacity is theoretical while, in the second case, it can be considered semi-empirical because the experimental relationships for the determination of the critical stress are combined with the theoretical ones. The instability phenomena can be divided in local (A) and flexural-torsional (B)

A)   Local instability
The critical stress that brings the local instability of the compressed flange, neglecting the constraint offered by the web, is given from Massonnet and Save, [56]:

$$\sigma_{cr} \cdot b_f \cdot t_f = \frac{12}{b_f^2} \frac{b_f \cdot t_f^3}{3} G_h \tag{2.92}$$

being:
- b_f the width of the flange;
- t_f the thickness of the flange;
- G_h the tangential modulus in the gardening step;

Besides, Lay [57] has shown that:

$$G_h = \frac{E}{1 + \nu + \dfrac{E}{4 \cdot E_h}} \tag{2.93}$$

being $\nu = 0,3$ the Poisson's coefficient. So:

$$s = \frac{\sigma_{cr}}{\sigma_y} = \left(\frac{t_f}{b_f}\right)^2 \frac{16 \cdot E_h}{5.2 \cdot E_h + E} \frac{1}{\varepsilon_y} \tag{2.94}$$

A more detailed expression to define the conditions of local instability of the compressed flange can be obtained by the analysis, in plastic field, of a plate connected with a torsional spring whose stiffness is the boundary condition represented by the web. In terms of critical deformation, the following expression has been obtained Lay e Galambos, [50,58] - Stowell, [59] – Southward, [51]:

$$\varepsilon_{cr} = \frac{12}{E_h \cdot b_f^3 \cdot t_f} \cdot \left[G_h \cdot \frac{b_f \cdot t_f^3}{3} + E_h \cdot I_\omega \cdot \left(\frac{2n\pi}{l_f}\right)^2 + K\left(\frac{l_f}{2n\pi}\right)^2 \right] \tag{2.95}$$

being:
- I_ω is the moment of inertia;
- K is the torsional stiffness of the web;

- $\dfrac{l_f}{n}$ is the semi-wave length of instability of flange. The minimum value of the critical stress is obtained imposing the condition:

$$\frac{\partial \sigma_{cr}}{\partial \left(\dfrac{l_f}{n}\right)} = 0 \tag{2.96}$$

that provides the semi-wave length corresponding to the minimum value of critical stress:

$$\frac{l_f}{n} = 2\pi \left(\frac{E_h \cdot I_\omega}{K}\right)^{0.25} \tag{2.97}$$

replacing the (2.97) in the (2.95), the expression of the critical deformation, in function of the geometrical and mechanical characteristics of the flange and of the web, is obtained (Lay e Galambos, [50]:

$$\varepsilon_{cr} = \frac{12}{E_h \cdot b_f^3 \cdot t_f} \cdot \left[G_h \cdot \frac{b_f \cdot t_f^3}{3} + 2 \cdot \sqrt{K \cdot E_h \cdot I_\omega} \right] \tag{2.98}$$

The (2.98) shows that the critical deformation depends on the mechanical properties in plastic field E_h and G_h and from the boundary conditions of the flange. Particularly the stiffness K of the torsional spring has to be compared to the action of the constraint, elastic or plastic, that the web asserts towards the flange or, the condition that the web is connected to the flange. It is observed [51] that the (2.98) points out that the contributions of the second and the third term of the (2.95) have the same influence; consequently, the (2.97) can be used for remove from (2.95) the unknown contribution of the web reaching to an expression in which the fundamental influence of the wavelength appears:

$$\varepsilon_{cr} = \frac{12}{E_h \cdot b_f^3 \cdot t_f} \cdot \left[G_h \cdot \frac{b_f \cdot t_f^3}{3} + \frac{8 \cdot \pi^2 \cdot E_h \cdot I_\omega}{l_f^2} \right] \tag{2.99}$$

The moment of inertia can be expressed through the following relationship (Southwanrd, [51]):

$$I_\omega = \frac{b_f \cdot t_f^3}{144}$$ (2.100)

Obtaining the final expression of the critical deformation:

$$\varepsilon_{cr} = 4 \cdot \frac{G_h}{E_h} \cdot \left(\frac{t_f}{b_f}\right)^2 + \frac{2}{3} \cdot \pi^2 \cdot \left(\frac{t_f}{l_f}\right)^2$$ (2.101)

The relationships previously described allow the theoretical prediction of the critical stress that provides the local instability of the compressed flange. An alternative is represented by the employment of empirical relationships based on the experimental tests. Through the data of a great number of "stub column test" Kato [36], [49] has obtained the followings relationships (2.58), (2.59), (2.60), (2.61).

These relationships can be employed for every steel type. Besides, more accurate relationships than keep in account the effects of mechanical properties of the steel, are provided by the same author for I sections and for steels used in Japan (Kato, [37]). It is necessary to evidence that these experimental relationships are based on "stub column test" in which the web results wholly compressed while the webs of the beams and the columns have a stress gradient. This difference can be kept into account introducing "real width" of the web that represents the compressed part of the web when the section is fully plasticized. It results:

$$N_w = N = \rho \cdot A \cdot \sigma_y = (1 - 2 \cdot \beta) \cdot A_w \cdot \sigma_y$$ (2.102)

so:

$$\beta = \frac{A_w - \rho \cdot A}{2 \cdot A_w}$$ (2.103)

and

$$d_{we} = \frac{1}{2}\left(1 + \frac{A}{A_w} \cdot \rho\right) \cdot d_w \qquad (2.104)$$

being

$$\rho = \frac{N}{N_{pl}};$$

d_w the length of the web;
A the total area of the section;
A_w the area of the web of the section.

B) Flexural-torsional Instability
It often happens that the phenomenon of the local instability starts before the flexural-torsional instability. This condition results verified if the distance between the torsional restraints is sufficiently small to prevent the lateral displacement of the compressed flange. In the opposed case the non-dimensional critical stress must be evaluated as the minimum value between the ones that conducts to local and to flexural-torsional instabilities.
This value can be calculated, keeping in mind the variation of the bending moment along the beam, through relationships that provide the bending moment that brings to the flexural-torsional instability and the relationships that correlate the end moments to the equivalent moment. With this purpose can be made reference, for instance, to the relationships provided by the Eurocode 3 [60].

2.4.2 Material properties

The response of material in a structure is a very intricate problem, which must be reduced to simple one, by emphasizing its native performance, useful for the design engineer practice. The uniaxial tensile test under monotonic load is conventionally recognized as an unified basis to compare structural materials. But it must be underlined that the result of the axial test never represents the actual behaviour of steel in a structure [61]. The good ductility of steel determined by tensile tests does not certainly assure a good ductility at the structural level. This difference in behaviour was for a long time the main cause of great confusion in the reception of steel as an ideal material for seismic-resistant structures.

(i) *Main mechanical properties.* The definitions of the most important mechanical properties, which interest structural engineering applications, are the following [29]:

- *yield point* is the stress corresponding to the plateau in the stress-strain curve; in other words, it is the stress value at which an increase of strain occurs without an increase of stress. In the case of steels that do not exhibit a distinct yielding behaviour, reference is made to the *yield stress* which is defined as the stress providing, after the unloading phase, a residual plastic deformation equal to 0.2 %. *Yield strength* is often used as a generic term to denote either the yield point or the yield stress;

- *ultimate strength,* or tensile strength is the maximum stress reached in the tensile test;

- *modulus of elasticity* (Young's modulus) is the stress to strain ratio at levels for which stress is linearly proportional to strain. For all the structural steels the modulus of elasticity can be assumed equal to 205000 N/mm^2;

- *initial strain-hardening modulus* is the slope of the stress-strain curve at the beginning of the strain-hardening range. The initial strain-hardening modulus and the strain at which strain-hardening begins are particularly important for evaluating the deformation capacity of structural steel members;

- *yield strain* is the strain corresponding to the yield strength;

- *uniform strain* is the strain attained at the maximum point of the engineering stress-strain curve, which corresponds to the beginning of necking;

- *total strain* is the maximum strain attained in the stress-strain curve immediately before fracture occurs;

- *Poisson's ratio* is the ratio between the absolute value of transversal strain and axial strain in elastic range; it can be assumed equal to 0.3. Its value increases as far as strain increases and reaches the maximum value 0.5 after the occurrence of complete yielding.

The tension test is performed on specimens with circular or rectangular cross-section, the latter being obtained by cutting some structural elements (Fig. 18a). The stress-strain curve may be determined in two ways: displacement-controlled or load-controlled tensile tests.

(ii) Displacement-controlled test in which the displacement is increased at a constant rate until the specimen is fractured. The form of the stress-strain curve for a specimen of typical low-carbon structural steel is shown in Figure 18b. The strain-rate proposed by the RILEM testing method is 0.5 x 10^{-4}/sec until plastic flow occurs, after which a strain-rates of 10^{-4}/sec is recommended for the remainder curve [37]. Due to the low strain rate, this test can be considered as a static one. The general shape of the stress-strain curve is typically represented by four regions corresponding to elastic, plastic, strain-hardening and necking ranges.
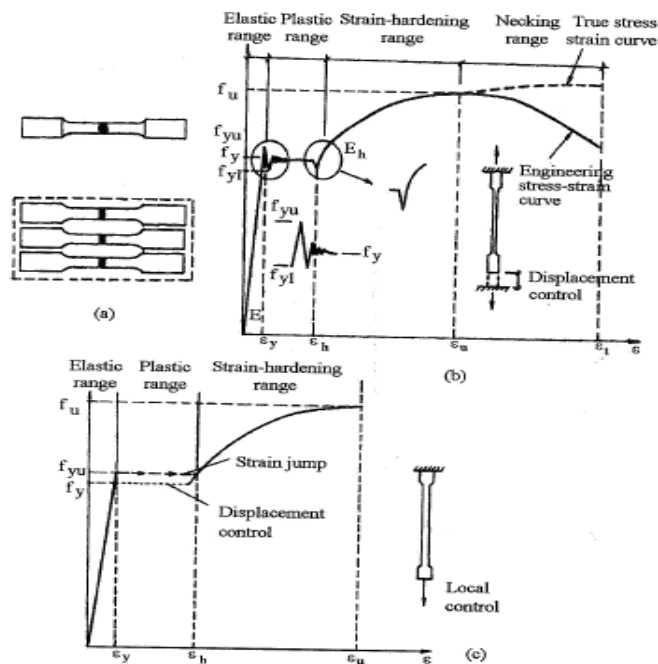

Fig. 18.   Stress-strain curve for structural steel: (a) Specimen types; (b) Displacement-controlled test; (c) Load-controlled test

- The *linear elastic region* is defined for $0<\varepsilon<\varepsilon_y$. The tensile stress-strain relationship is given by a straight line $\sigma= E\varepsilon$, where E represents the initial elastic modulus. The yield strain ε_y is given by $\varepsilon_y=f_y/E$

- The *yield plateau*, defined for $\varepsilon_v < \varepsilon< \varepsilon_h$, is assumed to be horizontal, but as Figure 18b shows, this is not actually the case, because small stress fluctuations arise with upper or lower values of yield stress. The upper yield stress, f_{yu} is the maximum attaining stress in elastic range, after which an increase of strain occurs, without an increase of stress. The lower yield stress, f_{yu} is the lowest level of yield stress, immediately following the upper value. Using the dislocation theory to explain the yielding of steel, the upper yield stress mobilizes dislocations and the lower yield stress maintains the movement of the dislocations [61]. The yield stress f_y is the average stress during the actual yielding in the plastic range. It is necessary to underline that the decreasing of stress from upper to lower yield stress is possible only in case of displacement-controlled test.

At yield point, regular line systems appear on the surface of steel specimens, indicating that the plastic strain is concerted in some bands (Fig. 19a), their traces on the surface being referred as Luders-Hartmann (LH) lines [57], [62]. This behaviour is due to the slip of crystalline planes in the direction of the critical shear stress. Generally, the direction of slip plane coincides with the maximum shear stress direction, at 45° inclination from specimen axis. The LH lines occur on the specimen surface only in a limited zone, where the strain traverses all the plastic plateau, reaching the hardening strain ε_h, while in the remained zones, the strain corresponds to yield one. Therefore, the behaviour of specimens is inhomogeneous, having discontinuous characteristics. The overall strain is

$$\varepsilon = \frac{\delta L}{L} = (1-s)\varepsilon_y + s\varepsilon_h \tag{2.105}$$

where δL measures the length of slip planes. The increasing of strain in plastic range is due to the formation of new slip planes, until the entire specimen reaches the hardening strain (Fig. 19b). So, the yield plateau does not correspond to a continuous deformation, but it is characterised by a succession of deformation jumps from yield strain to hardening strain.

-The *strain-hardening region* is defined for $\varepsilon_h < \varepsilon < \varepsilon_u$. The point at which the yield plateau ends and strain-hardening begins is not clearly identified, because a dip generally occurs at the end of the yield plateau before strain-hardening initiates [63].
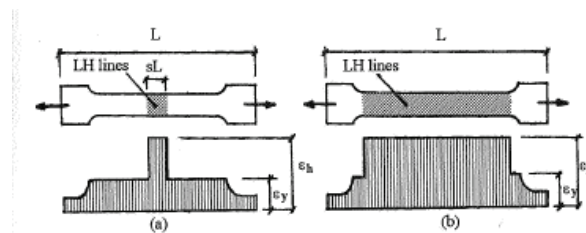
Fig. 19.   Luders-Hartmann lines: (a) Limited plastic zones; (b) Extended plastic zones

This dip is followed by a steep increase that suddenly changes the slope into relative smooth strain-hardening range, at the beginning of the hardening strain ε_h. The curve slope in this point is referred to as hardening modulus E_h. The strain-hardening range is extended until the maximum tensile stress, f_u, corresponds to the uniform strain ε_u. At this point the stress-strain curve has a zero slope and the necking range begins.

-The *post-ultimate stress* or *strain-softening region* is defined for $\varepsilon > \varepsilon_u$. In this region an apparent decrease in the engineering stress-strain curve occurs, due to the specimen necking. In reality, if the actual area is used for determining the actual stress, a continuous increasing of stress is obtained (true stress-true strain curve). The stress corresponding to the specimen fracture is f_t and the strain is ε_t. Due to the fact that this range cannot be used in practice, the ultimate stress f_u and uniform strain ε_u mark the end of the practical useful region of the stress-strain curve.

(iii) Load-controlled test, in which the load is increased at a constant rate until the specimen fractures. The corresponding stress-strain curve is presented in Figure 18c. The first elastic range until the upper yield stress is identical as for displacement-controlled test. When the stress reaches the upper yield stress, a decreasing to lower yield stress occurs and a continuous formation of slip bands can be observed in the case of displacement-controlled tests. But in the case of load-controlled tests this decreasing is impossible and thus all the bands slip directly until the hardening range with great velocity. This produces a jump of strain from ε_y till ε_h, local strain variation between these two limits being

physically impossible. The test stops at the ultimate stress and uniform strain, because it is not possible to obtain the decreasing of load in the necking range.

(iv) Behaviour in compression. Generally, if the effect of buckling is neglected, it is considered that the monotonic stress-strain curve for compression is equal and opposite to the curve in tension. There are some proposals to modify the tension curve, but the differences are not so high. So, the two curves shall be considered equal in the following Sections.

(v) High strength steel. The above native properties of steel are presented for mild carbon steel with yield strength in the range of 230-350 N/mm^2. Due to the advances in fabrication technology, the recent trend leads to built structures using higher strength steel, having yield strengths in the range of 400-700 N/mm^2. The effect of the increasing of yield strength on the stress-strain curve is presented in Figure 20. It is clear that the stress-strain behaviour of high strength steels is considerably different from that of low strength steel, exhibiting lower material deformability. For this reason high strength steels must be used with caution for moment-resistant structures in seismic areas.
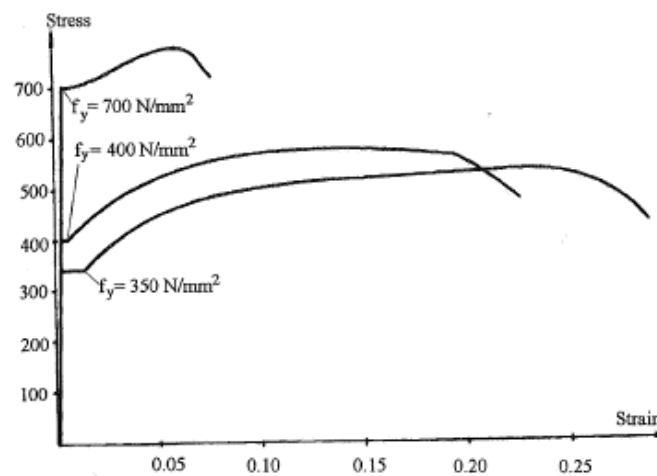
Fig. 20.   High strength steel constitutive low

(vi) Structural steels. The principal material properties which determine the structural ductility are: the yield stress, the length of yield plateau, the strain-hardening characteristics and the ratio between yield stress and tensile strength. The yield stress of structural steel is dependent on the chemical composition of the alloy and the method of manufacturing. These variables are reflected in the

designated grade of the steel. According to Eurocode 3 [60], Chapter 3 "Materials" and to EN 10025 code, the structural steels usually adopted for civil engineering structures are FeE 235 (Fe 360), FeE 275 (Fe 430), FeE 355 (Fe 510).

The nominal values of yield stress and ultimate strength are given in Table 2; they are the minimum values guaranteed by the producer. But the actual yield stress and tensile strength values are much higher than those guaranteed and a tendency to increase this difference exists, due to the improving technology of steel production. If this is a very good situation for strength problems, it is not true for seismic applications. The strain-hardening property is mainly defined by the initial strain-hardening modulus, E_h, for which no standard procedure of measuring exists, so various values are proposed. Generally, its value is evaluated as a fraction of the elastic modulus; say 30 to 50 times smaller. In addition there are two very important parameters: the value of uniform strain, ε_u, which marks the end of hardening range and the total elongation at rupture, ε_t, which limits the necking range.

(vii) Material ductility, named also kinematic ductility, can be defined as the ratio between the hardening strain ε_h and the yield strain ε_y:

$$\mu_h = \frac{\varepsilon_h}{\varepsilon_y} = 10 \div 12 \qquad (2.106)$$

Table 2. Stress-strain characteristics of usual steel for carpentry

Steel	t mm	fy N/mm^2	fu N/mm^2	ε_y %	ε_h %	ε_u %	ε_t %	E_h N/mm^2
S235	<40	235	360	0,115	1,41	14,0	25,0	5500
	>40	215	340	0,105				
S275	<40	275	430	0,134	1,47	12,0	22,0	4800
	>40	255	410	0,124				
S355	<40	355	510	0,173	1,70	11,0	20,0	4250
	>40	355	490	0,163				

or as the ratio between the uniform strain, ε_u, and the yield strain ε_u

$$\mu_u = \frac{\varepsilon_u}{\varepsilon_y} = 60 \div 120 \qquad (2.107)$$

One can see that the material ductility is very high, but the ductility of steel in a structure can be eroded at very low values. So, the material ductility can give an unreliable representation of the actual ductility.

(viii) *Yield ratio.* Due to the fact that structures are subjected to internal force gradients along the member axis, a good ductility is provided for low values of the ratio between yield stress and tensile strength:

$$\rho_y = \frac{f_y}{f_u} \tag{2.108}$$

The relation between yield ratio and yield stress is shown in Figure 21, Low yield ratio is considered for $\rho_y < 0.75$ and height yield ratio for $\rho > 0.75$ [64]. The yield ratio increases with the increasing of yield stress. As a consequence, ductility is substantially impaired by the elevated yield ratio. A yield ratio which assures a good behaviour is within 0.5-0.7. From Figure 21 one can see that the used steels frame in this condition.
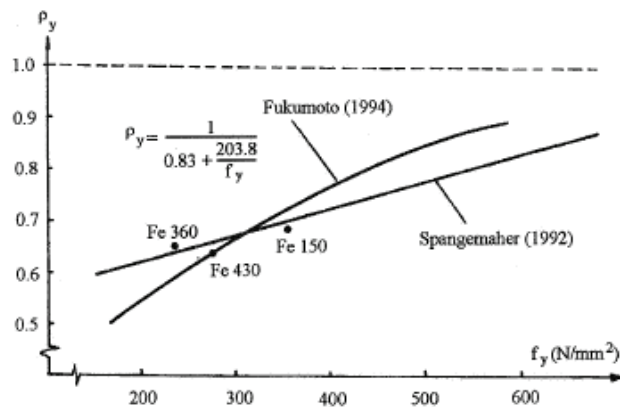
Fig. 21.   Yield ratio variability

The problem of yield ratio is very important for recent steel production, in which a tendency exists to realize high strength steels with tensile strength greater than 600 N/mm^2 and yield ratio greater than 0.9. Therefore, these high strength steels show very poor structural ductility and this is the reason why they are not recommended to be used for seismic-resistant structures. However, recent developments in steel production obtained high strength

steels with yield ratio of about 0.75 [64], [65], which can be considered acceptable for structures in seismic areas.

2.4.3 Cyclic loads

When a specimen, which has been plastically deformed in tension, is unloaded and subsequently reloaded in compression, the stress-strain curve in the new loading phase deviates from the linearity at a stress level far below the one corresponding to the yield point of the virgin material. This phenomenon is known as the Bauschinger effect [29], [63], [66] and depends on the position of stress reversal. The Bauschinger effect depends on the carbon content, lower carbon steels having a stiffer effect than higher carbon steels.

(i) Reversal within yield plateau regions. This is only a theoretical case, because, during an important earthquake, the structure is loaded in strain-hardening region. Figure 22a illustrates the typical stress-strain behaviour of a steel specimen after a load reversal of a point of the yield plateau region. The first part of the unloading branch can be approximated by a straight line parallel to the elastic loading, with the same slope corresponding to the elastic modulus E. In reality, the unloading modulus decreases and depends on plastic strain [63], but the differences are not so high ($E_r = (0.85 \div 1.00)E$). In the reversal stress, a stiffness softening gradually occurs due to the earlier yielding. If the specimen is loaded in tension again, then the stress-strain curve will deviate from the linear response far below the virgin yield stress, but it will be able to reach the stress and strain obtained in the first tension loading cycle. The stress-strain curve for the subsequent cycles will follow the same path of the first cycle, provided that the maximum strains are not greater than the ones reached in the first cycle.

(ii) Reversal from strain-hardening region. This is the usual case for the behaviour of structures under severe earthquakes. When a reversal starts from the strain-hardening, the shape of the reversal curve is independent of the virgin stress-strain curve; the yield plateau effectively disappears in both directions (Fig. 22b). The reversal curve depends on the maximum tensile load which has been reached.
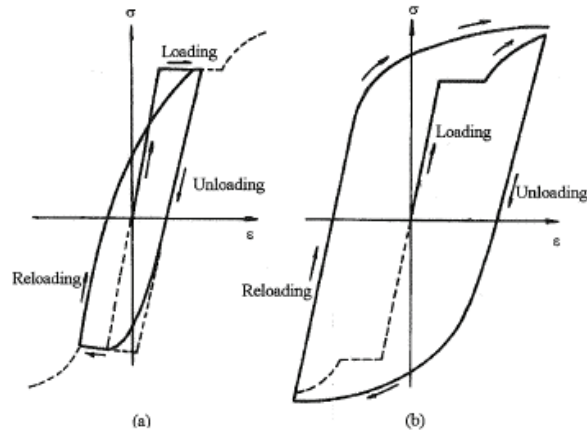
Fig. 22.   Cyclic strain-stress curves: (a) Reversal within yield plateau; (b) Reversal from strain-hardening region

(iii) Hysteretic ductility. The loading, unloading and reloading curves form a hysteretic loop (Fig. 23). The area included within these curves is the dissipated energy. Figure 23a shows the first cycle, while the Figure 23b the its cycle. The kinematic ductility given by the equations (2.106) and (2.107) is appropriate only for one cycle. For deformation histories characterized by many cycles, the use of energy criterion seems more realistic. Two energy criteria have been adopted [16]:

-hysteretic ductility in one direction:

$$\mu_h = \frac{E_{h,max}}{f_y \varepsilon_y} + 1 \qquad\qquad (2.109)$$

where

$$E_{h,max} = \max(E_h^+, E_h^-) \qquad\qquad (2.110)$$

-total hysteretic ductility:

$$\mu_h = \frac{E_{h,total}}{f_y \varepsilon_y} + 1 \qquad\qquad (2.111)$$

where

$$E_{h,total} = E_h^+ + E_h^-$$ (2.112)
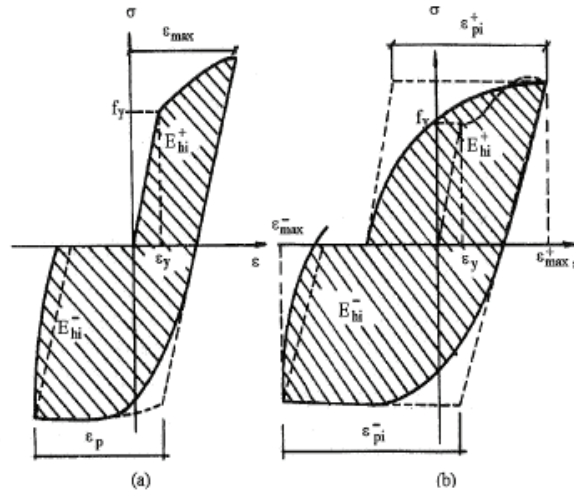
Fig. 23.   Hysteretic energy: (a) First cycle; (b) i cycle

(iv) *Control parameters of cyclic test.* As in the case of a monotonic tensile test, the cyclic test can be performed by means of the control of strain or stress. In the first case, under constant periodicity of strain, a continuous degradation of stress occurs for a given level of strain (Fig. 24a). In the second case, when the stress is under control, a degradation of strain is produced for a given level of stress (Fig. 24b). The control of strain is characteristic for laboratory tests, while the stress control is more realistic for interpreting the behaviour of structures under seismic actions.

(v) *Cyclic loading types.* The cyclic loading types generally used in research works are summarized in Figure 25. The first case is characterized by a fixed imposed value of the control parameter CP (strain or stress) with repetition up to failure (Fig. 25a). This cyclic loading type is used for determining the low cycle fatigue effects. The second type is characterized by an increasing of the control parameter after each cycle, or after three cycles, according to ECCS Recommendations (Fig. 25b). This loading type is generally recommended for the analysis of structures under ground motions corresponding to earthquakes far from source. The last type is characterized by a continuous decreasing of the control parameter (Fig. 25c), following the same rule as for the second case.
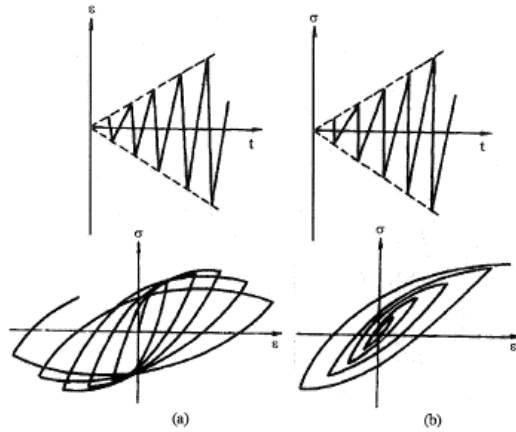
Fig. 24.   Cyclic tests: (a) Strain control; (b) Stress control
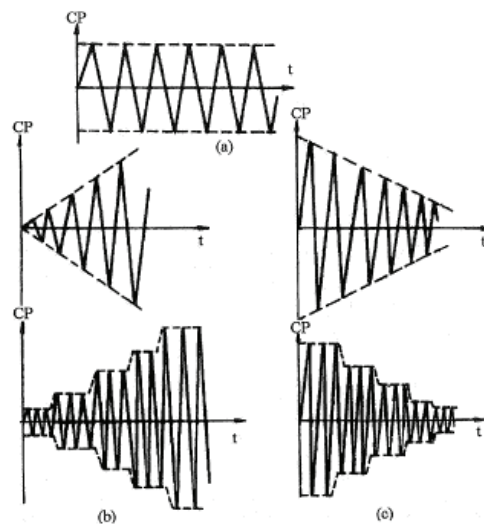
Fig. 25.   Cyclic loading type: (a) Fixed imposed control parameter; (b) Increasing of the control parameters; (c) Decreasing

This is the loading history characteristic for the structural behaviour under earthquakes near to source. It is worth reminding ourselves that cyclic loading tests are performed following many other types of laws, very different from the above mentioned ones and their definition is an open problem in the standardization of tests [67].

CHAPTER 3: THE OVERSTRENGTH OF STEEL MEMBERS

3.1 INTRODUCTION

The value of the overstrength factor "s", that represents the ratio between the critical stress that brings to the local instability and the yielding one, can be obtained using three different procedures:

- Theoretical method of Kemp [35];
- Semi-empirical method of the OPCM n° 3274 [68];
- Empirical method of Kato [36];

The method of Kato makes reference to the classification of sections, while the other two procedures refer to a classification of the whole member. In fact in the evaluation of the parameter "s" they do not only consider the geometrical and mechanical characteristics of the transversal section but also the length of the member.

Once calculated the value of "s" it will be possible to make some considerations that allow to understand the influence of "s" in the subdivision of the section or member in ductility categories.

For bending members the definition of the overstrength factor "s" assumes the following particular expression:

$$s = \frac{M_{max}}{M_{pl}} \tag{3.1}$$

where M_{max} represents the maximum moment that can be reached by the same structure, while M_{pl} is the theoretical full plastic moment.

On the other, for bending members the definition of the ductility factor (rotation capacity) "R" assumes the following expression:

$$R = \frac{\theta_u}{\theta_p} - 1 \tag{3.2}$$

where θ_u represents the rotation corresponding to the full plastic moment M_p in the softening part of the curve (Fig. 26).
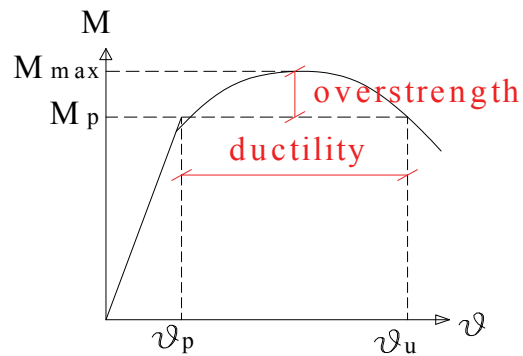
Fig. 26.   Definitions of ductility and overstrength of a member

A simple interpretation of the concept of overstrength can be obtained showing the following Figure 27 which simplifies the concept at the material level:
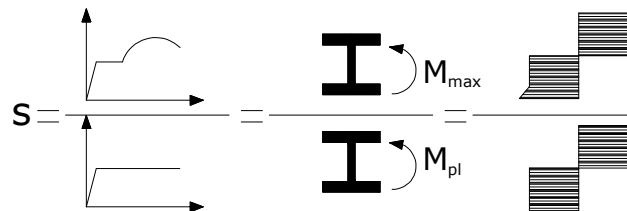
Fig. 27.   Interpretation of the overstrength concept

3.2 PREDICTIVE METHODS OF THE OVERSTRENGTH

3.2.1 Theoretical methods

The employment of the relationships finalized to the evaluation of the rotational capacity of steel beams and columns requires the calculation of the overtrength factor "s" which represents the ratio between the critical stress that brings to the local instability and the first yielding one ($s = \sigma_{cr}/\sigma_y$).The individualization of this parameter has been proposed by Kemp [35] through a theoretical procedure based on the following hypotheses:

- an elastic-perfectly plastic-hardening constitutive low of the material $\sigma - \varepsilon$;
- the determination of the moment-curvature relationship for an ideal I section.
- analysis makes reference to the beams with $\rho = 0$

Starting from the relationship proposed in the Chapter 3:

$$R = \frac{1}{s} \cdot \left[2 \cdot \frac{\varepsilon_h}{\varepsilon_y} \cdot \frac{h}{h_e} \cdot (s-1) + (s-1^2) \cdot \frac{E}{E_h} \cdot \frac{I}{I_e} \right] - 1 \qquad (3.3)$$

where for hypothesis $h/h_e = 1$ and $I/I_e = 1$ through the theoretical analysis developed by Kemp [35] with reference to the beams, the following relationship has been obtained:

$$R = \gamma \cdot \left[2 \cdot \frac{\varepsilon_h}{\varepsilon_y} + \frac{E}{E_h} \cdot \frac{\gamma}{1-\gamma} \right] \qquad (3.4)$$

being:

$$\gamma \cdot l = \frac{s-1}{s} \cdot l \qquad (3.5)$$

the extension of the plastic zone.
The employment of the relationship (3.5) requires the definition of the conditions that cause the local instability of the compressed flange. With this

purpose, it results fundamental the observation of Lay and Galambos [57], [58] according to which local instability is present when the extension of the plastic zone is really equal to the length of the wave according to which the compressed flange buckled. Insofar critical condition is given from:

$$l_f = \gamma \cdot l \tag{3.6}$$

The hypothesis introduced by Kemp [35] it is that the critical deformation ε_{cr}, furnished by the relationship of Southward [51] is equal to:

$$\varepsilon_{cr} = 4 \cdot \frac{G_h}{E_h} \cdot \left(\frac{t_f}{b_f}\right)^2 + \frac{2}{3} \cdot \pi^2 \cdot \left(\frac{t_f}{l_f}\right)^2 \tag{3.7}$$

it is reached in correspondence of the middle of the plastic zone.
In such hypothesis it results:

$$s = \frac{\sigma_{cr}}{\sigma_y} = 1 + \frac{0.5 \cdot \gamma}{1 - \gamma} \tag{3.8}$$

Insofar, combining the relationship (3.8) with the (3.7) and assuming, according to the Southward prescriptions [51] $G_h/E_h = 1/3$ the following result is obtained:

$$\frac{4}{3} \cdot \left(\frac{t_f}{b_f}\right)^2 + \frac{2}{3} \cdot \pi^2 \cdot \left(\frac{t_f}{\gamma \cdot l}\right)^2 = \varepsilon_h + \frac{\sigma_y}{E_h} \cdot \frac{0.5 \cdot \gamma}{1 - \gamma} \tag{3.9}$$

what results to be a third degree equation being unknown γ.
The value of γ, obtained for attempts by the relationship (3.9) provides through the (3.4) the value of the rotation capacity. Following the values of σ_y, E_h and ε_h used in the different formulations are presented:

Fe 360 $\dfrac{E}{E_h} = 37.5; \dfrac{\varepsilon_h}{\varepsilon_y} = 12.3; E = 210000; \sigma_y = 2350; E_h = 56000; \varepsilon_h = 0.0138;$

Fe 430 $\dfrac{E}{E_h} = 42.8; \dfrac{\varepsilon_h}{\varepsilon_y} = 11.0; E = 210000; \sigma_y = 2750; E_h = 49065; \varepsilon_h = 0.0144;$

Fe 510 $\dfrac{E}{E_h} = 48.2; \dfrac{\varepsilon_h}{\varepsilon_y} = 9.8; E = 210000; \sigma_y = 3550; E_h = 43568; \varepsilon_h = 0.0165.$

Besides, since Kemp defines a classification of the member and not of the transversal section in the relationship it has to be considered also the length of the structural element. Three lengths in function of the height of the member are generally considered: L/H = 10, L/H = 20 and L/H = 30.
It is possible to observe that the value of "s" decreases in correspondence with the increase of the length of the member, this means that when the extension of the structural element is great there are problems of local instability.

3.2.2 Semi-empirical methods

On the base of experimental evidence, it can be stated that the average length of the zone where local buckling of the compressed flange occurs is approximately 1.20b_f [42]. Therefore, the influence of the stress gradient on the critical stress which produces the local buckling of the compressed flange depends upon the b_f/L ratio (being, in general, L the distance between the section in which the bending moment is zero and the one in which it assumes its maximum value). The analysis of the experimental data collected in [35], [36], [42] has led, by means of a multiple regression analysis, to the following empirical relation:

$$\frac{1}{s} = 0.5463 + 1.6325\lambda_f^2 + 0.062\lambda_w^2 - 0.602\frac{b_f}{L} + 0.0014\frac{E}{E_h} + 0.0077\frac{\varepsilon_h}{\varepsilon_y} \quad (3.10)$$

being

$$\lambda_f = \frac{b_f}{2t_f}\sqrt{\varepsilon_y} \qquad\qquad\qquad\qquad (3.11)$$

$$\lambda_w = \frac{d_{we}}{t_w}\sqrt{\varepsilon_y} \qquad\qquad\qquad\qquad (3.12)$$

with

$$d_{we} = \frac{1}{2}\left(1 + \frac{A}{A_w}\rho\right)d_w$$

Relation (3.10) is more complete than the ones provided by Kato, because it includes the influence of the slenderness of the flange (λ_f) and of the web (λ_w) as well as the effects due to the stress gradient (b_f/L) and the influence of the mechanical properties of the material ($\varepsilon_h/\varepsilon_y$, E/E_h).

Moreover, it seems that the simplified model (ideal two flange section), which has been assumed for evaluating the ultimate rotation, has to be rationally kept also in the computation of the first yielding rotation.

The proposed method is based upon the use of equations (3.13) and (3.14) for evaluating the rotation capacity:

$$R_{st} = \frac{1}{s-\rho}\left\{(1-\rho)\frac{h}{h_e} + \frac{s-1}{1-\rho}\left[(1-2\rho)\frac{h}{h_e} + \frac{\varepsilon_h}{\varepsilon_y}\frac{h}{h_e} + (s-1)\frac{E}{E_r}\frac{I}{I_e}\right]\right\} - 1 \qquad (3.13)$$

$$R_{st} = \frac{1}{(s-\rho)(1-\rho)}\left\{\begin{array}{l}\left[1+\rho^2 - 2\rho(s-1)\right]\frac{h}{h_e} + 2\frac{\varepsilon_h}{\varepsilon_y}\frac{h}{h_e}(s-\rho-1) + \\[2mm] + \frac{E}{E_r}\frac{I}{I_e}4\rho(s-\rho-1) + (s-2\rho-1^2)\frac{E}{E_h}\frac{I}{I_e}\end{array}\right\} - 1 \qquad (3.14)$$

and, obviously, upon the computation of the critical stress leading to the local buckling of the compressed flange by means of equation (3.10).

The buckling stress ratio s can be computed if local buckling occurs before flexural-torsional buckling. This condition is verified when the distance between torsional restraints is sufficiently small in order to prevent the lateral displacement of the compressed flange. In the opposite case, the buckling stress ratio has to be computed as the minimum value between the one leading to local buckling and the one leading to lateral-torsional buckling.

This last value can be computed, taking into account moment-gradient, by means of the relations which provide the ultimate equivalent uniform bending moment for lateral-torsional buckling and the relations correlating end moments to the equivalent uniform bending moment.

The degree of accuracy of the described procedure for evaluating rotation capacity of steel beams and beam-columns has been investigated [51], [58] by

means of the comparison with the experimental data available in technical literature [35], [54], [56].

This method, including the influence of the part of the member which remains in elastic range, together with the influence of the stress gradient and of the mechanical properties of the material, seems to be able to provide a considerable reduction of the scatters between predicted and experimental values as well as sufficiently conservative results [51], [58].

Moreover, taking into account the complexity of the phenomenon and the advantages due to the use of an equation in «closed form», the approximation obtained by means of this method (±30%) can be considered satisfactory. Regarding to the obtained degree of accuracy, we can remember that some researchers have performed a numerical simulation of the experimental tests of Lukey and Adams [39], by using the finite element method and adopting nine node Lagrangian shell finite elements with 2x2 Gauss integration and a bounding surface model based on the linear flow theory; but the obtained scatters between predicted and experimental values of the rotation capacity varied from -40% to +60%, in spite of the use of such sophisticated approach.

It has been pointed that the rotation capacity of steel beams and beam-columns is influenced not only by the width-to-thickness ratios of the compressed parts of the cross-section, but also by the magnitude of the axial load, by the stress gradient along the cross-section (which can be taken into account by means of the concept of effective width of the web), by the longitudinal stress gradient due to the bending moment variation and by the distance between torsional restraints which plays a fundamental rule in preventing flexural-torsional buckling.

As a consequence of such amount of influencing effects, it seems that the concept of cross-section behavioural classes should be substituted by the concept of member behavioural classes.

From the operational point of view, equations (3.13) and (3.14) can be also used in order to provide the values of the non dimensional buckling stress s which are necessary in order to obtain a given value of the rotation capacity (R=2, 4, 6..) for any given value of the non-dimensional axial load. The obtained value of s provides through the relation:

$$\frac{1}{s} = 1.6325\lambda_f^2 + 0.062\lambda_w^2 - 0.6021\frac{b_f}{L} + K \qquad (3.15)$$

the limit value of the width-to-thickness ratios for any given value of the distance L between the zero moment point and the plastic hinge section. The parameter K depends on the material properties only, as it can be recognized from the comparison between (3.15) and (3.10) which gives

$$K = 0.5463 + 0.0014 \frac{E}{E_h} + 0.0077 \frac{\varepsilon_h}{\varepsilon_y} \tag{3.16}$$

With reference to the parameters expressing the material properties, the ratios E/E_h and $\varepsilon_h/\varepsilon_y$ are given by the following values:

$$\frac{E}{E_h} = 37.5 \quad \text{and} \quad \frac{\varepsilon_h}{\varepsilon_y} = 12.3 \qquad \text{for Fe360 steel}$$

$$\frac{E}{E_h} = 42.8 \quad \text{and} \quad \frac{\varepsilon_h}{\varepsilon_y} = 11.0 \qquad \text{for Fe430 steel}$$

$$\frac{E}{E_h} = 48.2 \quad \text{and} \quad \frac{\varepsilon_h}{\varepsilon_y} = 9.8 \qquad \text{for Fe510 steel}$$

The corresponding values of K are:

K=0.697005 for Fe360
K=0.694706 for Fe430
K=0.693330 for fe510

The limit values of the width-to-thickness ratios obtained by means of the above procedure guarantee the assigned value of the rotation capacity, provided that lateral-torsional buckling is prevented.

At this point can be concluded that the deformation capacity of steel beams and beam-columns depends not only on the width-to-thickness ratios of the compressed parts of the cross-section, but also on the magnitude of the axial load, the stress gradient along the section, the longitudinal stress gradient due to bending moment variation and the non-dimensional slenderness for flexural-torsional buckling.

As a consequence, it can be observed that the simple cross-sectional classes of EC3 are not able to include all the phenomena which affect the structural behaviour. As a generalized alternative the concept of member behavioural

classes has been introduced and it has been shown how this concept can become operational by means of the described method for evaluating the rotation capacity.

3.2.3 Empirical methods

An alternative is represented by the employment of empirical relationships based on experimental results. Using a total of 68 test data on "stub-columns" tests, B. Kato [36], [49] has proposed a series of relationships using an equivalence. To obtain the moment-curvature relationship the stress-strain curve of structural steels is simplified by assuming the rigid-plastic flow-strain hardening relation as shown in Figure 28:
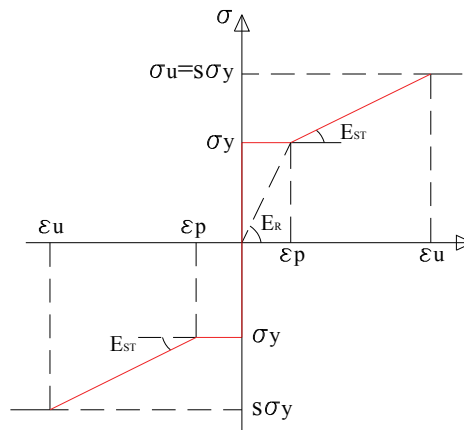
Fig. 28.   Simplified stress-strain relation

where

σ_y is the yield point, σ_u is the maximum strength of the material, s= σ_u/σ_y is the overstrength of the material, $\varepsilon_p = \varepsilon_{st} - \varepsilon_y$ is the plateau length, where ε_{st} is the strain at the strain-hardening point, ε_u is the strain at the maximum strength point in this model which is related to the real maximum strength and E_{st} is the strain-hardening modulus.

The I section is replaced by an equivalent two flange model as shown in Figure 29, where the equivalence can be maintained by equating the full plastic moment and the sectional area for both sections.
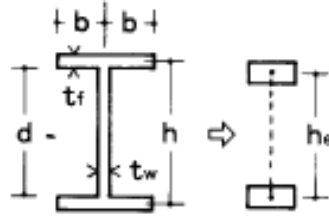
Fig. 29.   Equivalent section

The geometrical relations between these two sections are:

$$\frac{h}{h_e} = \frac{2 + 0.3(h/b)}{2 + 0{,}15(h/b)} \tag{3.17}$$

$$\frac{I}{I_e} = \frac{\left[2 + 0.3\left(h/b\right)\right]\left[2 + 0.1\left(h/b\right)\right]}{\left[2 + 0.15\left(h/b\right)\right]^2} \tag{3.18}$$

A series of stub-column tests with different combinations of b/t_f and d/t_w are carried out for various grades of steel, the mechanical properties of which are shown in Table 3.

Table 3.   Mechanical properties of steel grades

	Yield stress σ_y(N/mm^2)	Tensile stress σ_u(N/mm^2)	Yield ratio $Y = \sigma_y / \sigma_u$	$\varepsilon_p/\varepsilon_y$	E/E_{st}
SM41	299	458	0,65	10,5	52
SM50	377	521	0,72	9,2	63
SM58L	460	635	0,73	2,4	38
SM58H	525	599	0,88	6,4	116

In this table, SM58L is a new high-strength steel with low yield ratio which is under development to improve ductility, and SM58H is a conventional high-strength steel with high yield ratio. The plateau length ratio, $\varepsilon_p/\varepsilon_y$, and strain-hardening modulus ratio, E/E_{st}, of SM58L are rather small compared with those of SM41 and SM50, although the yield ratio is comparable. The numbers of stub-columns tested are 25 for SM41, 20 for SM50, 21 for SM58L and 22

for SM58H. The normalized maximum strength, $s = \sigma_{cr} / \sigma_y$ obtained from stub-column tests is related to the slenderness parameter, α_f and α_w by means of multiple regression analysis for each grade of steel obtained through multiple regressions as follows:

For SM41 steel ($8 \leq b/t_f \leq 16$, $40 \leq d/t_w \leq 80$)
$$1/s = 0.689 + 0.651(1/\alpha_f) + 0.0553(1/\alpha_w) \pm 0.0303 \tag{3.19}$$

For SM50 steel ($7 \leq b/t_f \leq 15$, $35 \leq d/t_w \leq 65$)
$$1/s = 0.689 + 0.586(1/\alpha_f) + 0.0711(1/\alpha_w) \pm 0.0538 \tag{3.20}$$

For SM58L steel ($6 \leq b/t_f \leq 14$, $20 \leq d/t_w \leq 60$)
$$1/s = 0.716 + 0.518(1/\alpha_f) + 0.0389(1/\alpha_w) \pm 0.0325 \tag{3.21}$$

For SM58H steel ($6 \leq b/t_f \leq 14$, $30 \leq d/t_w \leq 60$)
$$1/s = 0.881 + 0.270(1/\alpha_f) + 0.0365(1/\alpha_w) \tag{3.22}$$

These relationships generalized for any steel type become:

- for I sections

$$\frac{1}{s} = 0.6003 + \frac{1.600}{\alpha_f} + \frac{0.1535}{\alpha_w} \tag{3.23}$$

- for welded square hollow section (SHS)

$$\frac{1}{s} = 0.710 + \frac{0.167}{\alpha} \tag{3.24}$$

- for cold-formed square hollow section (cold-formed SHS)

$$\frac{1}{s} = 0.778 + \frac{0.13}{\alpha} \tag{3.25}$$

- for cold-formed circular hollow section (cold-formed CHS)

$$\frac{1}{s} = 0.777 + \frac{1.18}{\alpha} \tag{3.26}$$

being

- $\alpha_f = \dfrac{E}{\sigma_y}(\dfrac{t_f}{b_f/2})^2$ \qquad the slenderness parameter of the flange

- $\alpha_w = \dfrac{E}{\sigma_y}(\dfrac{t_w}{d_w})^2$ \qquad the slenderness parameter of the web (d_w is

the web height)

- $\alpha = \dfrac{E}{\sigma_y}(\dfrac{t}{b})^2$ and $\alpha = \dfrac{E}{\sigma_y}(\dfrac{t}{D})^2$ the slenderness parameter for SHS and CHS

sections respectively (B is the edge of the SHS section, D is the diameter of the CHS section and t is the thickness).

The aforesaid relationships can be employed for any steel type. It is necessary to put in evidence that the aforesaid experimental relationships are based on the test "stub column" in which the web results uniformly compressed while the webs of the beams and the columns are characterized by a stress gradient. These differences can be kept in account introducing the "effective width" of the web that represents the compressed part of the web when the section is fully plasticised. With references to the Figure 30 results:

$$N_w = N = \rho A \sigma_y = (1 - 2\beta)A_w \sigma_y \tag{3.27}$$
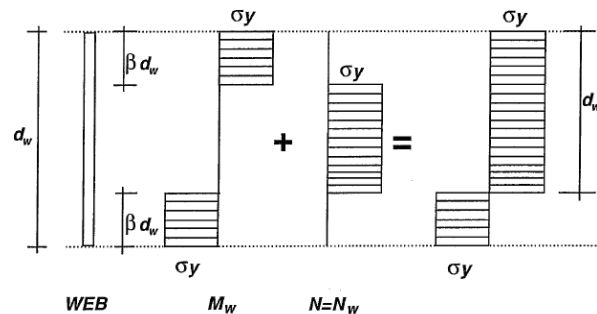
Fig. 30.   Definition of "effective width" of the web

Insofar:

$$\beta = \frac{A_w - \rho A}{2A_w} \tag{3.28}$$

and

$$d_{we} = \frac{1}{2}\left(1 + \frac{A}{A_w}\rho\right)d_w \tag{3.29}$$

The non-dimensional critical tension s can be calculated through the proposed formulations if the local instability occurs before the flexural-torsional instability. This condition results satisfied if the distance between torsional restraints is sufficiently small to prevent the lateral buckling of the compressed flange. In the opposite case, the non-dimensional critical tension must be calculated as the minimum value between the local instability and the flexural-torsional instability. This one can be obtained, taking into account the longitudinal variation of the bending moment, through the relationships corresponding to flexural torsional instability and through the ones that correlate moments at the end of the beam with the equivalent uniform moment. With this purpose, the relationships provided by EC3 code can be adopted [60].

CHAPTER 4: CODE PROVISIONS FOR "R" AND "s"

4.1 THE EXAMINED CODES

When designing a structure and its components, the designer is faced to the question of which model he is allowed to use. The concept of model is related to, on one hand, i) the analysis of the structure, which is aimed at the determination of the stress resultants (also termed internal forces or member forces) under the action of design loads, and, on the other hand, ii) the verification of the cross- sections which consists is checking whether the cross-sections are able to resist these design internal forces. Thus a model implies the use of a method of global analysis combined to a method of cross-section verification. Insofar the ultimate limit state design of structures is concerned, there are several possibilities to combine methods of analysis and methods of cross-section verification, according as these methods are referring to elastic or plastic approach. The possible combinations are listed in Table 4.

Table 4.   Definition of models

Model	Method of analysis	Method of cross-section verification
I	Plastic	Plastic
II	Elastic	Plastic
IIIa	a. elastic	a. elastic (full section)
IIIb	b. elastic	b. plastic (effective section)

Model I is related to plastic design of structures. Fully plasticity may be developed within cross-sections (i.e. the stress distribution corresponds to a fully rectangular block) so that plastic hinges can form. These have suitable moment rotation characteristics to allow for a sufficient rotation capacity and the formation of a plastic mechanism, as the result of moment redistribution in the structure.

For a structure composed of sections which can achieve their plastic resistance but have not a sufficient rotation capacity to allow for a plastic mechanism in the structure, the ultimate limit state must refer to the onset of the first plastic hinge. Thus, in Model II, the internal forces are determined based on an elastic analysis but are compared to the plastic capacities of the corresponding cross-sections. For statically determinate systems, the onset of the first plastic hinge leads to a plastic mechanism; both methods I and II should thus give the same result. For statically indeterminate structures, the moment redistribution is not possible according to Model II, in contrast to what is allowed for with Model I. when the cross-sections of a structure cannot exhibit their plastic capacity, both analysis and verification of cross-sections must be conducted elastically. The ultimate limit state according to Model III is achieved when yielding occurs at the most stressed fibre. Sometimes yielding in the extreme fibre cannot even be attained because of premature plate buckling of one component of the cross-section due to an excessive slenderness of this component plate. In such cases, above ultimate limit state should apply to effective cross-sections. Of course it is not possible to have a model where a plastic method of analysis is combined to an elastic cross-section verification. Indeed, the moment redistribution which is required by the plastic analysis cannot take place without some cross-sections being fully yielded. According as the model considered, it must be warranted that no local instability can occur before either the elastic bending capacity (Model III), or the plastic bending capacity (Model II) of the cross-section, or the formation of a complete plastic mechanism (Model I) is achieved. Such a mechanism shall form provided that any plastic hinge at first developed be able not only to rotate but, in addition, to rotate sufficiently; that presupposes that the cross- sections where plastic hinges form may exhibit the rotation capacity required by the formation of a plastic mechanism.

With this regard during seismic analyses, the evaluation of available and required ductility plays a key role. For MRF structures, designed applying the capacity design criterion, the attainment of a globally ductile behaviour of the structure, measured in terms of δ_u / δ_y, is possible only if, members have

adequate local ductility which can be measured in terms of plastic rotation ϑ_p (Fig. 31).
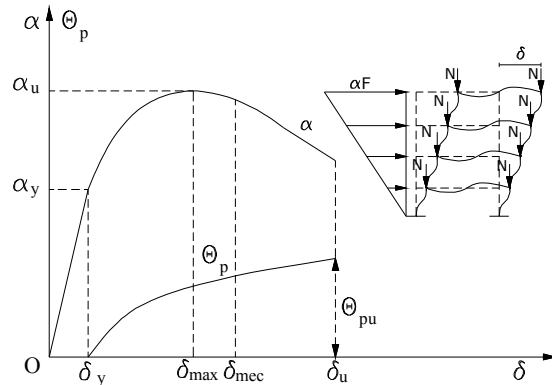
Fig. 31. Push-over curve for frame structure

The load bearing capacity of structural systems to withstand seismic actions in the non-linear range allows the design under actions lower than those corresponding to a purely linear elastic response of the structure. The force reduction is actually defined by a coefficient, namely behavioural factor *q*, which is a measure of the structural ductility. The relationship between this factor and local ductility of members is stated in all current seismic codes. The local ductility of steel beams can be evaluated from their rotation capacity which can be measured in different ways [35], [36], [41].

Starting from the generalized moment-rotation curve, obtained through the three point bending test, the rotation capacity can be defined as (Fig. 32):

$$R = \frac{\vartheta_{max}}{\vartheta_y} - 1 \tag{4.1}$$

This parameter can be compromised by the occurrence of local and global buckling phenomena that can affect the plates composing the section, and the whole member in absence of torsional restraints. The evaluation of the R parameter can be obtained through experimental tests, measuring and calculating the rotations ϑ_{max} and ϑ_y, or with *Theoretical methods, Semi-empirical methods* and *Empirical methods*.

In the seismic design of MRF, the available rotation capacity of beams is of primary importance. The subdivision of members into ductility classes is necessary because, as mentioned before, the rotation capacity influences the behavioural factor of the structure.

At the same time, the subdivision of the members into overstrength classes is necessary in order to apply the capacity design criteria both to local level (connections among dissipative and not dissipative zones), and to global level (overstrength of non-dissipative members).

Fig. 32.   M-θ curve of bending member

The twice classification of the steel members in ductility and overstrength classes, based on relevant criteria, should be the most appropriate approach for the seismic applications. Unfortunately, current seismic codes adopt only one classification criterion, from which both the consequences in terms of global ductility (behavioural factor) and in terms of capacity design are dependent.

The current section is finalised to provide a contribution on the discussion about this topic, through a critical analysis of the classification criteria currently proposed by some European codes and the evaluation of their reliability starting from available experimental results. In particular Eurocode 3 [60] subdivides cross-sections starting from their geometrical characteristics, the steel type and the internal actions. The new Italian seismic code OPCM 3274 [68] classification is instead based on the evaluation of the overstrength factor s, which takes into account not only the slenderness of the different parts in the transversal section and the mechanical characteristics of the material, but also the moment gradient along the axis of the member. In the current chapter different classification criteria adopted by the OPCM 3274 and by Eurocode 3 are compared with the purpose to identify the more reliable one for the application of the Technical Codes for Constructions (NTC '08) [69].

4.2 EUROCODE 8

The Eurocode 8 [9] adopts the classification criterion proposed by the Eurocode 3 [60], which subdivides the cross-sections into four classes: ductile or plastic (class 1), compact (class 2), semi-compact (class 3) and slender (class 4). Ductile sections are able to develop large inelastic deformations and plastic hinges having high rotation capacity; compact section, even if achieve the maximum plastic flexural strength, provide limited rotation capacity; semi-compact sections are able to reach the bending moment leading to first yielding, but, due to the occurrence of local buckling phenomena, plastic redistribution cannot develop; slender sections suffer failure in the elastic range due to local buckling of the compressed parts (Fig. 33).
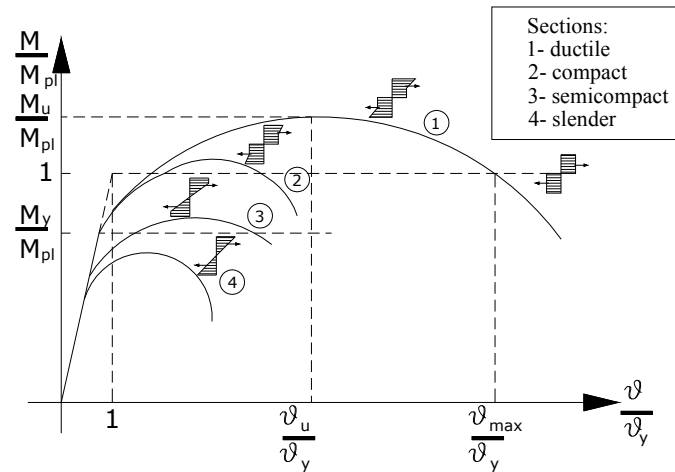
Fig. 33.   EC3 classification of cross sections

4.2.1 Proposed criterion and effects on seismic design

To ensure a sufficient rotation capacity, the extreme fibres must be able to exhibit very large strains without any drop-off in capacity occurs. In tension, usual steel grades exhibit a ductility which is largely sufficient to allow for the desired mount of tensile strains; in addition, no drop-off is to be feared before the ultimate tensile strength be reached. When compressive stresses, it is not so much a question of material ductility properly but well of ability to sustain these stresses without instability occurs. Therefore, the more simple way to warrant a sufficient rotation capacity is to limit the width-to-thickness ratio of

the component plates which are subject to compressive stresses due to bending moment and/or axial load.

For these reasons the definition of the cross-section class is based on the evaluation of the slenderness ratio (b/t) of compression parts which are subdivided into internal parts and outstand flanges. The web and the flange are considered independent, neglecting their mutual interaction. Indeed, the larger b/t ratio, the sooner plate buckling shall occur and consequently, the smaller the available rotation capacity. The range of the b/t ratios to which a simplified model is applicable is illustrated in Figure 34.
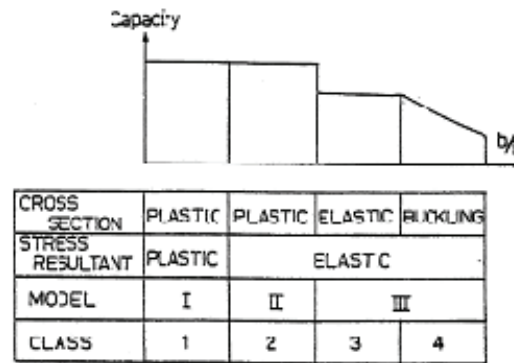
Fig. 34.   Relation between models and classes of cross-sections

Depending on the structural ductility class and on the behavioural factor *q*, the requirements regarding the cross-sectional classes of the dissipative elements are reported in Table 5.

Table 5.   Requirements on cross-sectional class of dissipative elements depending on ductility class and behavioural factor

Ductility class	Behavioural factor	Cross section class (dissipative zone)
DCM	$1.5 < q < 2$	Class 1,2 o 3
	$2 < q \leq 4$	Class 1 o 2
DCH	$q > 4$	Class 1

According to Eurocode 8 [9], the cross-section class is the only parameter that influences the global ductility of the structure, but it does not influence the application of the capacity design neither at local nor at global level.

At local level, for example, it is necessary that moment resisting connections have adequate overstrength to allow the development of plastic hinges at the end of the beams. For this reason, in accordance with EC8, connection has to provide the following bending capacity:

$$M_{jRd} \geq 1.1\gamma_{ov}M_{bRd} \tag{4.2}$$

where:
M_{jRd} is the joint design resistance;
M_{bRd} is the plastic moment of the connected beams;
γ_{ov} is an overstrength factor accounting for the random variability of the steel yield stress;
1.1 is a coefficient which covers the effects of the material strain hardening.

According to the EC8, γ_{ov} is a National Determined Parameter and its value can be defined at national level. Eurocode 8 does not provide a criterion for an appropriate evaluation of γ_{ov}, but suggests the use of $\gamma_{ov}=1.25$.
The hardening factor is assumed as a constant value (equal to 1.1) and it is not related with the class of the transversal cross section. These two assumptions lead to a local overstrength factor ($\gamma_{ov}\cdot1.1=1.375$) which has an important role not only in the connection design but also in the application of capacity design at global level. In fact, in the case of moment resisting frame structures, the columns shall be verified under seismic actions considering the following combination:

$$S_{Ed}=S_{Ed,G}+1.1\gamma_{ov}\Omega S_{Ed,E} \tag{4.3}$$

where:
$S_{Ed,G}$ represents the resistances (the compression force, the bending moment and shear force) in the column due to the non-seismic actions;
$S_{Ed,E}$ represents the resistances (the compression force, the bending moment and shear force) in the column due to the design seismic action;
γ_{ov} is the overstrength factor defined in (4.2);
Ω is the minimum value of

$$\Omega_i = \frac{M_{pl,Rd,i}}{M_{Ed,i}} \tag{4.4}$$

of all beams in which dissipative zones are located; $M_{Ed,i}$ is the design value of the bending moment in beam i in the seismic design situation and $M_{pl,Rd,i}$ is the corresponding plastic moment.

4.3 ITALIAN CODE OPCM 3274

In the previous section it has been empathized that the EC3 cross-section classification criterion, adopted by EC8, is based on a very few number of parameters, related only to the material and to the cross-section geometrical properties. Several studies have emphasized that the available rotation capacity of steel beam and beam-columns is influenced also by the characteristics of the full member [70]. As a consequence, if finalised to seismic design, the concept of member behavioural classes appears to be more appropriate than the one related only to the cross-section. For these reasons the Italian code OPCM 3274 [68] provide a classification criterion which subdivides members into three categories:

- *Ductile*: the local buckling of the compressed parts of the section develops in plastic range without significant reduction of the load carrying capacity, after the member exhibits large plastic hardening deformations;
- *Plastic*: the local buckling of the compressed parts of the section develops in plastic range, allowing significant plastic rotations;
- *Slender*: the local buckling of the compressed parts of the section occurs in the elastic range.

4.3.1 Proposed criterion and effects on seismic design

The classification criterion adopted by Italian code OPCM 3274 is based on the evaluation of the overstrength factor s, which can be defined as the ratio between critical tension corresponding to local instability of the compressed flange and the yield strength:

$$s = \frac{f_{cr}}{f_y} \tag{4.5}$$

This expression can be particularized for bending members and assumes the following expression:

$$s = \frac{M_u}{M_{pl}} \tag{4.6}$$

In Eq. (4.6) M_u is the maximum moment that can be reached by the structure, while M_{pl} is the beam plastic moment. A simplified representation is shown in Figure 35.
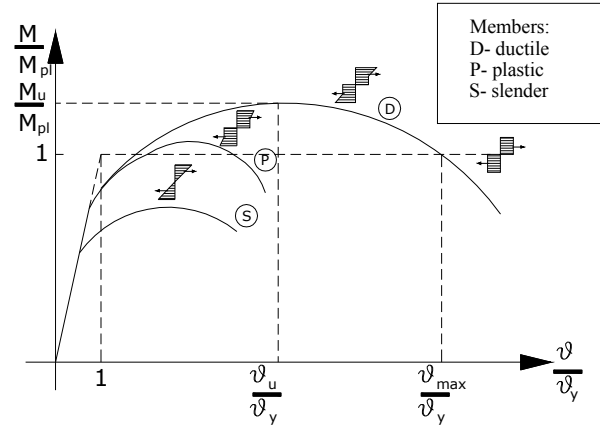
Fig. 35. OPCM 3274 classification of members

For I section subjected to axial and/or flexural loads, considering usual steel types, the overstrength factor *s* can be calculated by means of the following analytical formulation:

$$s = \frac{1}{0.695 + 1.632 \cdot \lambda_f^2 + 0.062 \cdot \lambda_w^2 - 0.602 \cdot \dfrac{b_f}{L^*}} \leq \min\left\{\frac{f_u}{f_y}; 1.25\right\} \tag{4.7}$$

being:

$$\lambda_f = \frac{b_f}{2 \cdot t_f} \sqrt{\frac{f_y}{E}} \qquad \text{the flange slenderness}$$

$$\lambda_w = \frac{d_{w,e}}{t_w} \sqrt{\frac{f_y}{E}} \qquad \text{the web slenderness}$$

b_f the flange width;

L^* the distance between the plastic hinge and the point of zero moment;

$d_{w,e} = \dfrac{1}{2}\left(1 + \dfrac{A}{A_w}\rho\right) d_w$ the parameter which takes into account the influence of

the axial load because it represents the compressed part of the beam web.

The Eq. (4.5) starts from theoretical-experimental studies [30] in which the dependence of the *s* factor from the internal actions (particularly from the intensity of the axial load), from the variation of moment gradient along the transversal section and along the longitudinal axis of the structure, are considered. About the influence of the cross-section classification on the seismic design, it is important to underline, the explicit relationship between the value assumed by the *s* factor for the beams which contain plastic hinges and the behavioural factor. The latter, in fact, is expressed, for each steel structural type, such as moment resisting frames, concentric and eccentric braced frames, by the following relationship:

$$q = q_0 K_D K_R \tag{4.8}$$

In which:
q_0 is the reference value of the q-factor, as a function of both the structural typology and the ductility category of the structure;
K_D is a factor related to the local ductility resources of the dissipative zone by *s* factor;
K_R is the coefficient of structural regularity, which takes into account the elevation and the in-plane regularity characteristics of the building;

The limit values of the *s* parameter, which identify the ductility categories of members, are given in Table 6, where the corresponding K_D values assumed for the determination of the design *q* factor are indicated too.

Table 6.   Classification of members in terms of ductility

Member categories	s	K_D
Ductile	s>1.2	1
Plastic	1<s<1.2	0.75
Slender	s≤1	0.5

As for the Eurocode 8, the application of capacity design to local level is possible only if the equation (4.2) is satisfied. In particular, in this case, the condition assumes the following expression:

$$M_{jRd} \geq s\gamma_{ov}M_{bRd} \tag{4.9}$$

In which the γ_{ov} factor is not unique, but it is defined for every steel type as indicated in Table 7.

Table 7. γ_{ov} values for different steel type

Steel	γ_{ov}
S235	1.2
S275	1.15
S355	1.1

Besides the hardening parameter, that has a constant value in the EC8 (1.1), in the OPCM 3274 is equal to *s* factor and, for this reason, it is calculated through the equation 4.5.

Consequently, contrary to the EC8, for which the necessary overstrength at the local level is constant (*37.5%*) and independent from the steel type and from of the transversal cross-section, the OPCM 3274 local overstrength is changeable as function of the γ_{ov} and *s* factors. Particularly, in the most unfavourable situation, the necessary overstrength according to the OPCM 3274 reaches the value of about 50% ($\gamma_{ov}=1.2; s=s_{max}=1.25$).

As far as the capacity design at global level (beam-column) is concerned, the OPCM 3274 requires its control only if the structural system is designed in high ductility. In this case the columns have to be verified considering the most unfavourable combination of the axial load and bending moments:

$$S_{c,Sd}=S_{c,Sd,G}+\alpha S_{c,Sd,E}$$ (4.10)

where:

$S_{c,Sd,G}$ represents the resistance (the compression force, the bending moment and shear force) in the column due to the non-seismic actions;

$S_{c,Sd,E}$ represents the resistance (the compression force, the bending moment and shear force) in the column due to the design seismic action;

a is the minimum value of a_i of all beams connected to the examined column:

$$\alpha_i=min\left\{\frac{\gamma_{ov}s_i M_{b,pl,Rd,i}-M_{b,Sd,G,i}}{M_{b,Sd,E,i}};q\right\}$$ (4.11)

where $M_{b,pl,Rd,i}$ is the plastic moment value for *i* beam, $M_{b,Sd,G,i}$ is the bending moment value due only to vertical actions, $M_{b,Sd,E,i}$ is the design bending moment value due to seismic actions.

A comparison between the EC8 and the OPCM 3274, regarding the application of the capacity design at global level, shows that, first of all, both codes require the amplification of the internal actions produced by the seismic input on the column, through a coefficient.

In the EC8, since the local overstrength is constant, the coefficient is $1.1\gamma_{ov}\Omega$; while in the OPCM 3274 it is also dependent on the variability of the local overstrength.

In addition, in the case of the EC8, the coefficient Ω is calculated neglecting vertical loads contribution, which are, instead, taken into account in the a expression. Nevertheless, with reference to ordinary structures, this discordance does not involve a significant difference respect to OPCM 3274. Besides, small variations of these multipliers do not behave substantial differences in the choice of the adopted profiles, because of the great discontinuity of the available commercial sections.

4.4 ITALIAN CODE NTC '08

The Technical Codes for Constructions (NTC '08)[69], following a performance approach, subdivide the steel sections in four classes according to EC3 prescriptions, but providing limit values of rotation capacity (R). Particularly the code differentiates the sections of class 1 and 2 (compact) from those of class 3 and 4 (fairly slender and slender). The first ones are able to reach and overcome the full plastic moment, while the last ones do not reaches such performance.

4.4.1 Proposed criterion and effects on seismic design

Appling the classification criterion proposed by NTC '08 four different classes can be distinguished:
-   *class 1* when the section is able to develop a plastic hinge having the rotation capacity required for the structural analysis with the plastic method without strength reductions. These sections are characterized by rotational capacity of $R \geq 3$
-   *class 2* when the section is able to develop its plastic moment, but with limited rotation capacity. These sections are characterized by rotational capacity of $1.5 \leq R < 3$.

- *class 3* when the stresses in the external compressed fibres of the section can reach the yielding stress, but local instability prevents the development of the plastic moment ($M_y < M_u < M_{pl}$)
- *class 4* when, to define the bending, shear or normal strength it is necessary to take into account the effects of the local instability in elastic range in the compressed parts of the section ($M_u < M_y$). In this case in the evaluation of the strength, the actual geometric section can be replaced of with an effective one.

From the conceptual point of view this classification criterion is consistent with the one adopted by the EC3, even there are some substantial differences:

- the performance level in terms of rotation capacity, that differentiates sections of first and second class, is made explicit.

- no one specific prescription is provided respect to the evaluation models of R, leaving such choice exclusively to the designer.

For the design in seismic zone, or rather for what concerns to the consequences of such classification in terms of global ductility and capacity design, nothing can be add to how is already underlined in the previous paragraphs about the EC8 and the OPCM 3274, making reference to the NTC '08 about applicative rules.

4.5 COMPARISONS AND CRITICAL ANALYSIS OF RESULTS

In this section, the examined classification criteria are compared in order to individuate the most reliable one. Such comparison is exclusively conducted with reference to the I sections, which are the most used in the seismic design. First of all, a database of available experimental tests, regarding I sections, has been set up (Table 8). Subsequently the classification of the relevant cross-sections and members, according to the two considered codes, and the evaluation of the experimental overstrength factors ($s_{exp} = M_{u,exp}/M_{pl}$) and rotation capacities have been done [72].

Table 8.   Experimental tests on I section beams

Tests number	Author	Profiles typology
24	Kuhlmann [41]	I section welded
23	Spangemacher [44]	I section hot rolled
4	Kemp [35]	I section hot rolled
5	Boeraeve-Lognard [71]	I section hot rolled
12	Lukey-Adams [39]	I section hot rolled

The Figures 36, 37 and 38 summarize the obtained results. In these Figures the minimum rotation capacity level R=3 is also reported according to the NTC '08 prescriptions.

A comparison between the theoretical class, evaluated with the application of the codes criteria, and the experimental class, has been firstly carried out.

According to EC3, the theoretical class has been assigned evaluating the ratios between web and flanges slenderness, while the experimental class calculating the rotation capacity values (R>3 for class 1; R<3 and M_{ult}>M_{pl} for class 2).

According to OPCM 3274 instead, the theoretical class has been assigned evaluating the overstrength factor *s*, through the already defined equation (4.5), while the experimental class calculating the value of the ratio $s_{exp}=M_{u,exp}/M_{pl}$.

The first consideration is that the examined classification criteria do not always represent the actual behaviour of the steel members in terms of rotation capacity and overstrength. In addition they often provide results in disagreement among them.

By applying the EC3 provisions, despite of 63 sections showed an experimental rotation capacity greater than 3, only 23 of them belong to the theoretical class 1, with reliability (coincidence between experimental and theoretical results) of about 37%. In the case of the OPCM 3274, despite of 38 members had s_{exp}>1.2 so they were experimentally "ductile", 17 of them are also theoretically ductile, so the level of reliability is about 45%.

The second consideration is that most of the examined tests has an experimental overstrength greater than *1.1γ_{ov}* (EC8 assumed value), with a maximum value s=1.48 and an average value s=1.21.

In conclusion, for ductile members the classification criterion based on the evaluation of the overstrength factor involves that a greater number of tests has the same theoretical and experimental class and the overstrength of the member is calculated in a more correct way.
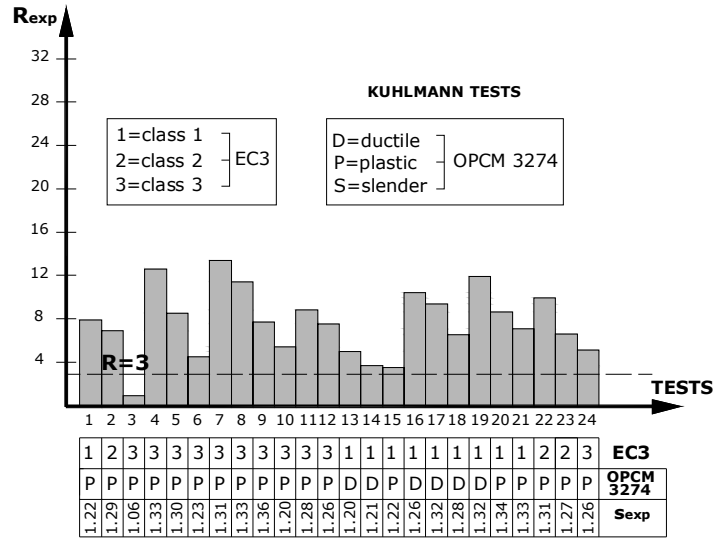
Fig. 36. Rotation capacity of sections classified applying the EC3 and the OPCM 3274 prescriptions (Kuhlmann tests)
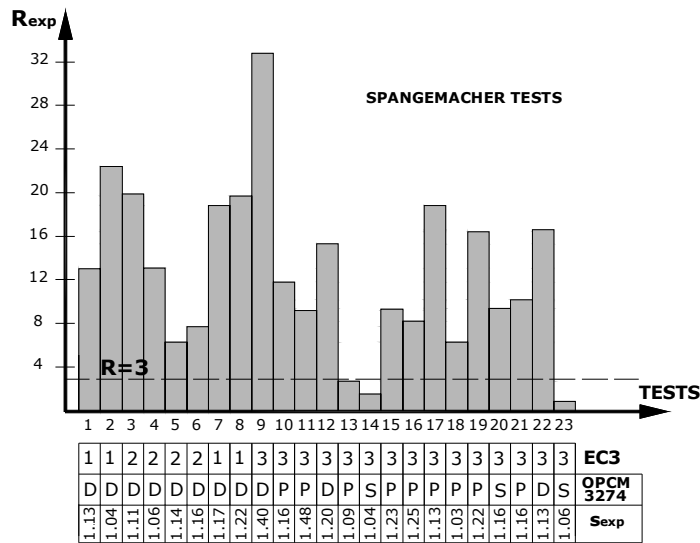
Fig. 37. Rotation capacity of sections classified applying the EC3 and the OPCM 3274 prescriptions (Spangemacher tests)
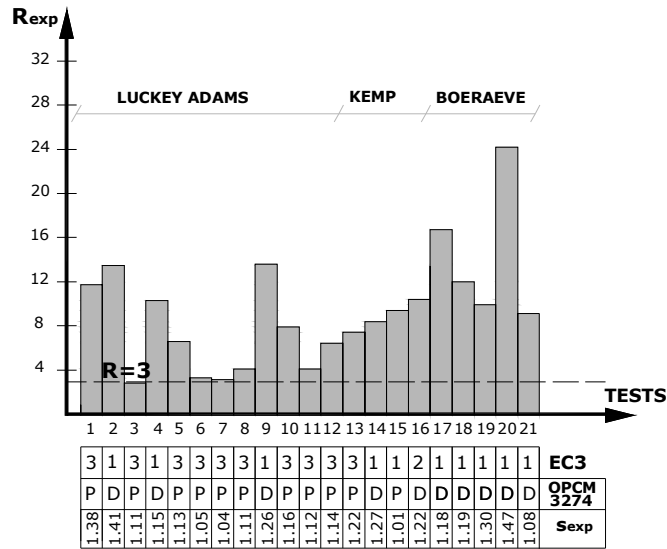
Fig. 38.   Rotation capacity of sections classified applying the EC3 and the OPCM 3274 prescriptions
(Luckey-Adams, Kemp and Boeraeve tests)

The obtained results, clearly show that the adopted classification criteria are not able to describe the actual behaviour of the steel members in post-critical field, because of the difficulties to model the local instability phenomena.

The Eurocode 3 classification criterion, does not allow to establish a correspondence between the theoretical class of the section and its rotation capacity R. In fact such model is only based on the web and flange slenderness parameters which are not sufficient to assess the cross-section class. In the Figures 39 and 40, with reference to the tests reported in Table 8, the values of the rotational capacity are plotted as function of slenderness of web and flange respectively.

Such slenderness, as shown in these Figures, do not allow the evaluation of the available rotation capacity if they are individually considered. In fact, different values of R for similar values of slenderness λ_f and λ_w occur. This means that, in the codified approaches these two slenderness must be combined for defining the cross-section class.

For bending members, the flange is largely interested by phenomena of local buckling, while the web contributes however, with its stiffness, to stabilize it. The Eurocode 3 takes into account the interaction between web and flange by assigning the higher class to the section (less favourable) among the web and flange ones. An interpretation of the results reached using this approach is

emphasized in the Figure 41, where slenderness are combined according to EC3.

On the contrary, the overstrength factor *s*, introduced in the OPCM 3274, takes into account not only the geometrical characteristics of the section at whole (web and flange), but also the moment gradient in the zone of the plastic hinge and the mechanical parameters of the material are accounted too. For this reason the latter approach appears to be more reliable for the classification of I steel members.

Three different approaches for the classification of steel section and members adopted by EC8 and Italian seismic codes have been considered. The main aim was to emphasize their influence on the application of the capacity design, at global and local level, and on the behavioural factor of the structure. The comparison among these codes has shown that the use of the EC3 classification criterion, despite its simplicity, is less satisfactory in seismic field. On the contrary, the criterion proposed by the Italian code appears to be more reliable because it is based on the study of the whole member and it assures the correspondence among theoretical and experimental class in more cases [73].
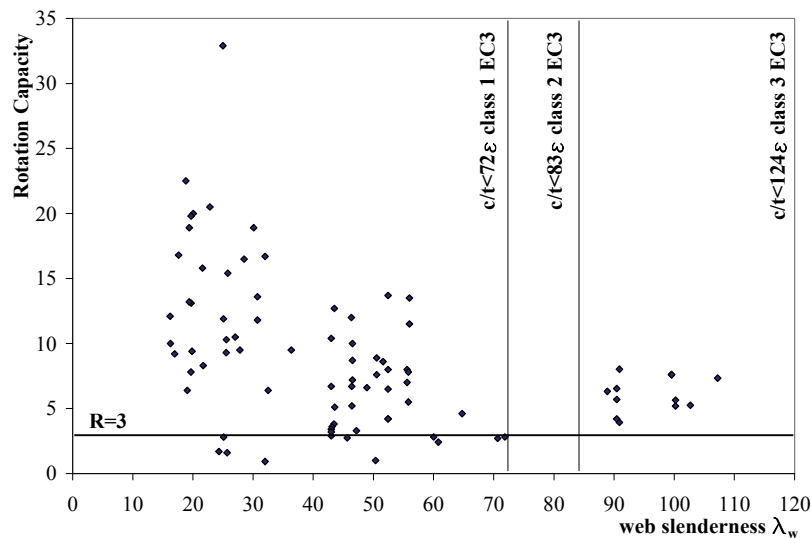
Fig. 39.   Rotation capacity values for different web slenderness
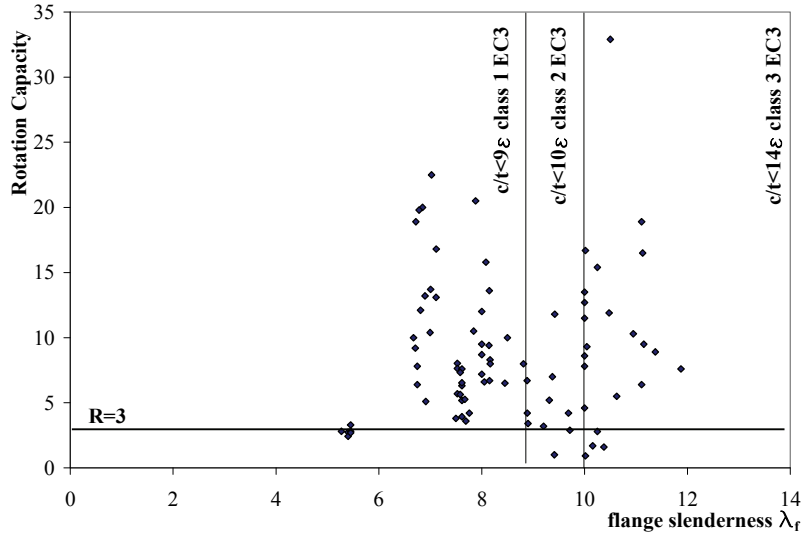
Fig. 40.   Rotation capacity values for different flange slenderness
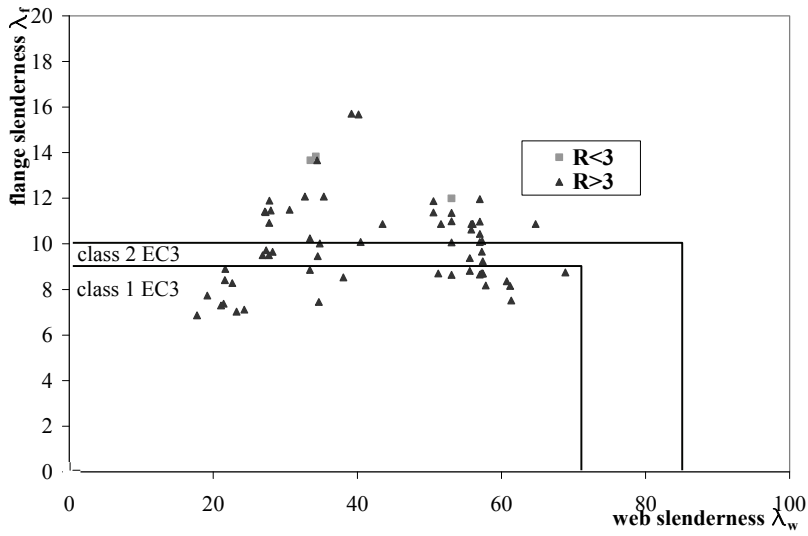
Fig. 41.   Rotation capacity values for different flange and web slenderness combinations

CHAPTER 5: THE EXPERIMENTAL STUDY

5.1 PLANNING OF EXPERIMENTAL ACTIVITIES

In the current Chapter all the aspects of the experimental campaign on rotation capacity and overstrength of steel members, carried out in the laboratory of structures of the faculty of Engineering of the University of Salerno, are illustrated. This cooperation among University of Naples and Salerno is started in January 2006 with good results.

The laboratory has a large plate of base in reinforced concrete with the thickness of 1 m and to which, through the use of dywidag bar with high resistance, it has been possible to anchor a vertical frame of contrast and a sleigh of base, both in steel (Fig.42):

Fig. 42.   Vertical frame of contrast

To the vertical frame, using the perforation prepared along its column, the hydraulic actuators (MTS 243), used for the application of the loads during the tests, have been positioned. To the sleigh of base has been directly connected the beam, besides it has been necessary to employ a horizontal frame of contrast to avoid problems of flexural-torsional instability of the beam founded in the pilot-test. The principal finalization of the experimental campaign is the study of the behaviour of steel members under monotonic and cyclic loads, for this reason the adopted scheme is the cantilever beam which reproduce the behaviour of a beam in a frame subject to seismic actions (Fig. 43).

Fig. 43.   Adopted set-up of cantilever beam

In the following Figure 44, the adopted test scheme, composed of the vertical frame of contrast , the horizontal frames, the plate of base in reinforced concrete, the steel sleigh of base and the beam, is illustrated:
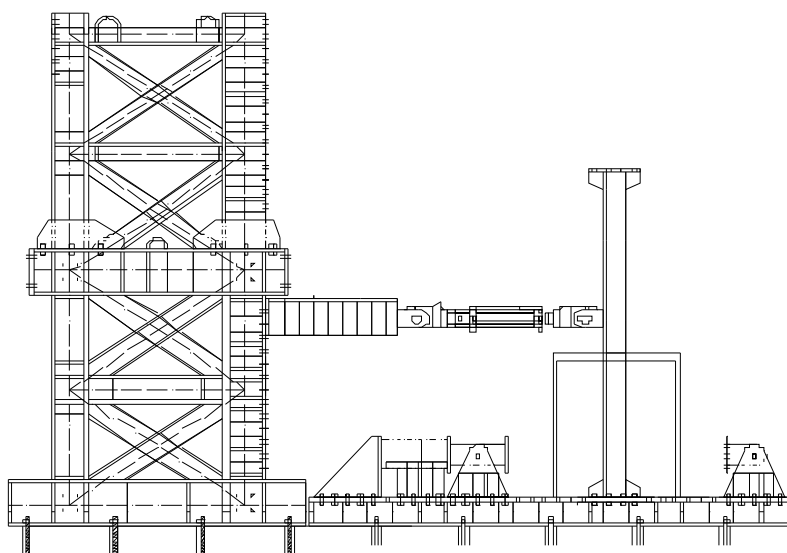
Fig. 44.   Adopted test scheme

5.2 SELECTION AND DESIGN OF TESTED MEMBERS

Rotation capacity and overstrength play a key role in the design of dissipative structures. The experimental campaign of monotonic and cyclic tests has been carried out with the purpose of investigate parameters that influences these factors, in particular:

- material strength
- ratios of slenderness between flange and web of plates in the section
- moment gradient
- cyclic loads

Three different typologies of cross-section have been investigated:

1) I Sections,
2) Rectangular Hollow Sections,
3) Square Hollow Sections.

The program of experimental tests has been planned considering the tests performed in technical literature to avoid the investigation of parameters already studied. I profiles are the most used in technical literature, the selection is based on ratios between parameters indicates in the following Figures 44, 45, 46, 47, 48 [74]:
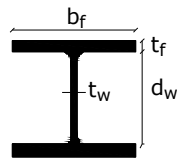
Fig. 45.   Parameters investigates for I profiles
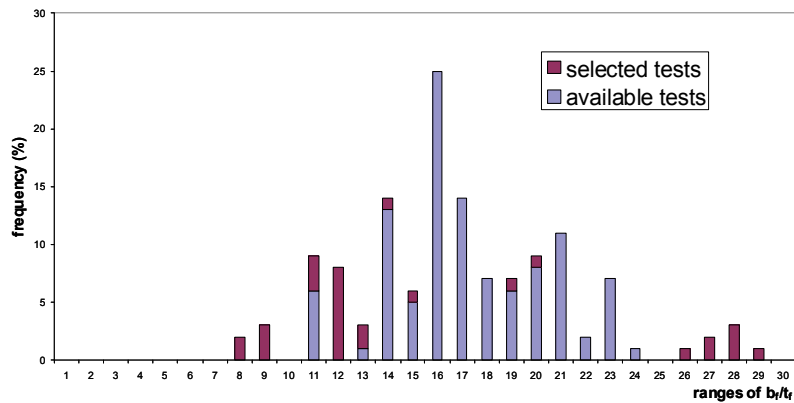
Fig. 46.   Variability range of the parameter b_f/t_f
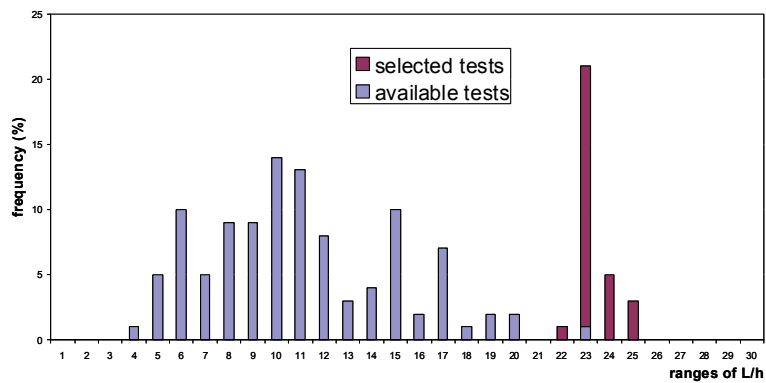
Fig. 47.   Variability range of the parameter L/h
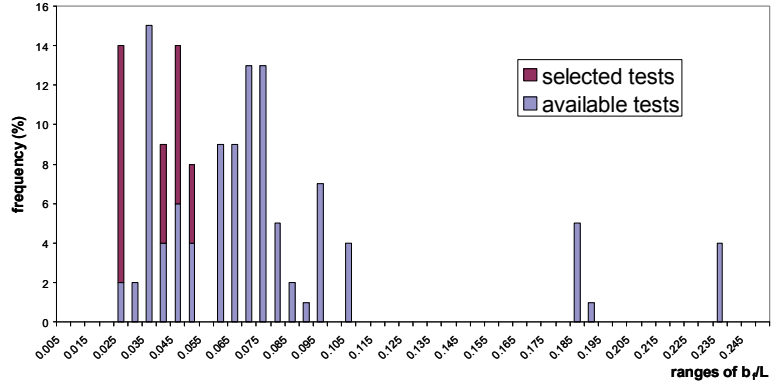
Fig. 48.   Variability range of the parameter b_f/L
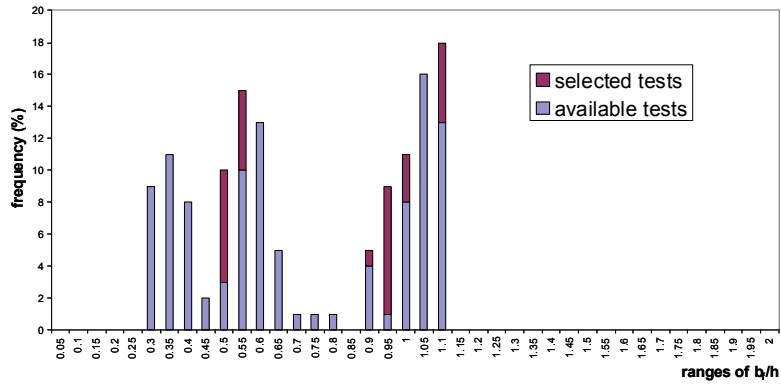
Fig. 49.   Variability range of the parameter b_f/h
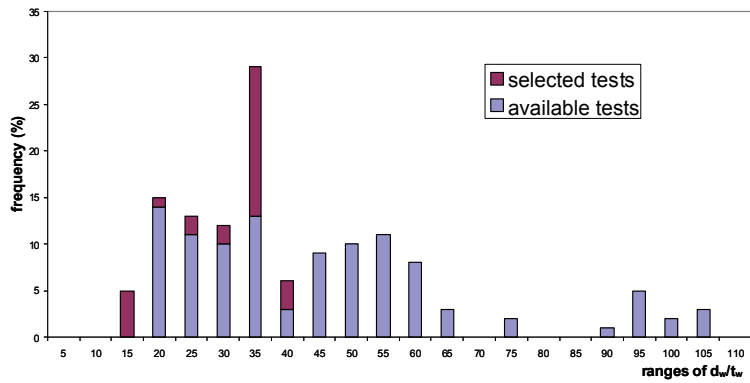
Fig. 50.   Variability range of the parameter d_w/t_w

After these comparisons, a database of experimental tests has been formulated. It is presented in the following Table 9:

Table 9.   Database of experimental tests

profiles	L/h	c/t_f	d/t_w
IPE 240	16.67	6.12	35.54
IPE 300	13.33	7.00	39.23
HEB 240	16.67	7.05	20.60
HEA 160	26.32	8.88	22.33
HEA 240	17.39	10.00	27.46
HEM 160	22.22	3.60	9.57
150x100x4	26.67	25.00	35.50
160x80x5	25.00	16.00	30.00
200x100x8	20.00	12.50	23.00
250x100x10	16.00	10.00	23.00
300x100x12.5	13.33	8.00	22.00
300x200x14.2	13.33	14.08	19.13
150x150x5	26.67	30.00	28.00
160x160x6.3	25.00	25.40	23.40
200x200x10	20.00	20.00	18.00
250x250x8	16.00	31.25	29.25
250x250x5	16.00	50.00	48.00
300x300x10	13.33	30.00	28.00

The choice of the number, the position and the dimension of bolts has been conditioned by the sleigh of base which is perforated with holes fixed at a distance of 151 mm in the horizontal direction and of 160 mm in the vertical direction. For these reasons the only element to be dimensioned was the thickness of the plate which connect beam and column. The adopted scheme was the one of the extended end plate suitable also for braced frames. Often, as visible in this case, joints with extended end-plates are characterized by columns reinforced with transversal braces. This situation is illustrated in figure 51.
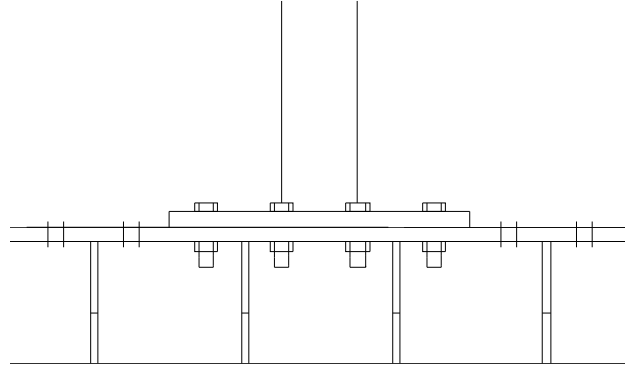
Fig. 51. Extended end-plate with transversal braces

To evaluate the strength of the flange of the column ad of the end plate they have to be associated to equivalent T-stub elements with a defined length called effective length (l_{eff}). If more than one line of bolts in tension are present, the equivalent T-stub element, in some cases, have to be modelled for each line singularly, in other cases, for groups of lines coupled. When the single line belongs to a group of bolts it will be necessary to verify that the sum of strength of the lines of the group does not exceed the strength of the same group.
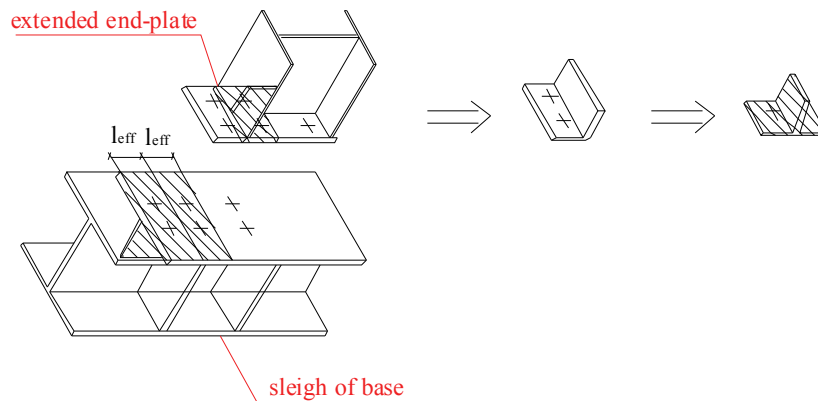
Fig. 52. Equivalent T-stub individualized in the test scheme

The design strength in tension $F_{t,Rd}$ of an equivalent T-stub have to be assumed equal to the minor of the following three collapse mechanisms:

- Type 1: complete collapse mechanism of the flange
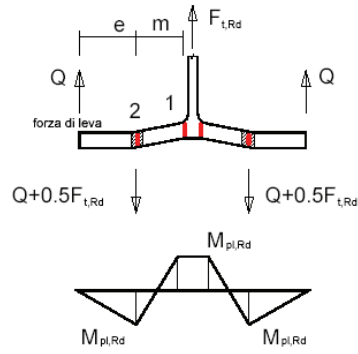
Fig. 53.   Mechanism Type 1

From the equilibrium of rotation of the plastic hinge 1:

$$(Q + 0.5F_{t,Rd})m - Q(e + m) = M_{pl,Rd}$$
$$0.5F_{t,Rd}m - Qe = M_{pl,Rd} \qquad\qquad (a)$$

From the equilibrium of rotation of the plastic hinge 2:

$$Qe = M_{pl,Rd} \qquad \text{substituting in the equation (a)}$$
$$F_{t,Rd} = \frac{4M_{pl,Rd}}{m}$$

where: $M_{pl,Rd} = 0.25 \sum l_{eff,1} t_f^2 f_y / \gamma_{MO}$

being $\sum l_{eff,1} =$ the effective length for the mechanism type 1

- Type 2: collapse of bolts with yielding of the flange

From the equilibrium at the translation:

$$\sum B_{t,Rd} - 2Q = F_{t,Rd} \qquad\qquad \rightarrow \qquad Q = (\sum B_{t,Rd} - F_{t,Rd})/2$$
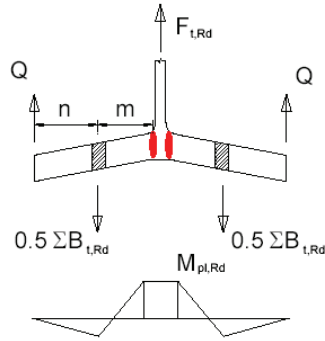
Fig. 54. Mechanism type 2

From the equilibrium of rotation at the plastic hinge:

$$0.5\sum B_{t,Rd}m - Q(n+m) = M_{pl,Rd}$$

Substituting in the expression of Q:

$$F_{t,Rd} = \frac{2M_{pl,Rd} + n\sum B_{t,Rd}}{m+n}$$

where: $M_{pl,Rd} = 0.25\sum l_{eff,2}t_f^2 f_y / \gamma_{MO}$

with $\sum l_{eff,2}$ = effective length for the collapse mechanism type 2

$\sum B_{t,Rd}$ = is the total strength in tension of all bolts of the equivalent T-stub.

$n = e_{min}$ with $n \le 1.25m$

- Type 3: collapse of bolts

From the equilibrium at the translation:

$$F_{T,Rd} = \sum B_{t,Rd}$$
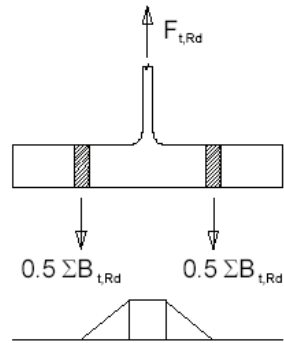
Fig. 55.   Mechanism type 3

- Numerical Example

In order to show the practical application of the component approach for predicting the flexural resistance of bolted end plate connections, this section develops a complete numerical example with reference to the beam IPE 300. In the following Figure 56, the considered distances are reported:
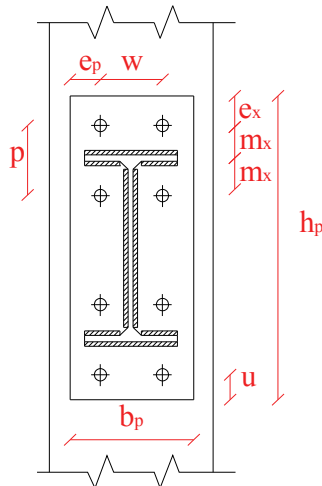
Fig. 56.   Dimensions of the considered section
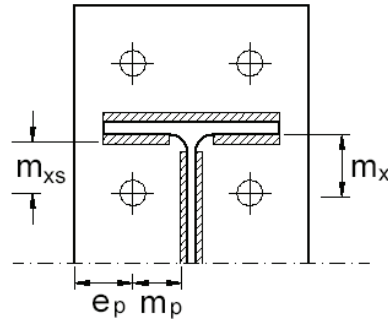
Fig. 57. Influence of the welding of the dimensions

Because of the presence of transversal braces along the sleigh of base, tension and compression in the web are absorbed by braces so the zones to be controlled are the extended end plate and the flange of the sleigh. Groups of bolts positioned upper and lower the braces are modeled as independent equivalent T-stubs. It is not necessary to control the strength resistance. In this considered case, the two independent T-stubs are equal.

- Strength of the flange of the sleigh with braces

sleigh of base with braces
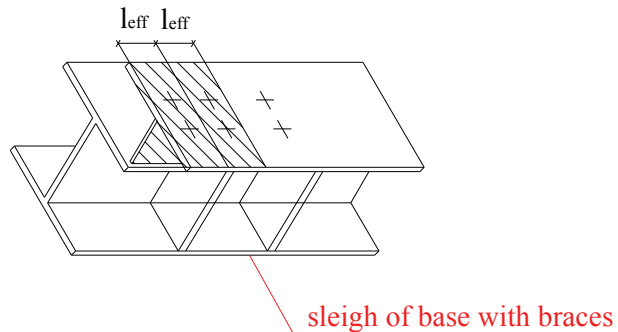
Fig. 58. T-stub individualized in the sleigh with braces

The effective length (l_{eff}) to be considered for each line of bolts is the smaller of the following values:

(a) for bolts adjacent to the brace:

$$l_{eff,a} = 201 = \min \begin{cases} 2\pi m_c = 201.7 \\ \alpha m_c = 224 \end{cases}$$

being α=7 obtained from the abacus illustrated in Figure 59:
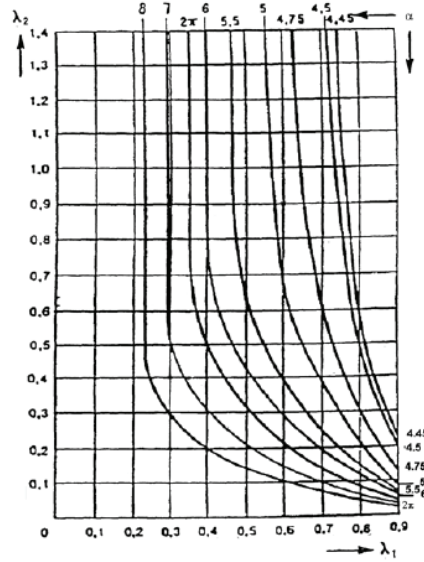
Fig. 59.   Abacus for the calculation of λ₁ and λ₂

with $\lambda_1 = \dfrac{m_c}{m_c + e_c} = \dfrac{32.1}{32.1 + 60} = 0.348$; $\lambda_2 = \dfrac{m_{xs}}{m_{xs} + e_c} = \dfrac{43.21}{43.21 + 60} = 0.491$

the plastic moment of the equivalent T-stub

$$M_{pl,Rd} = \frac{t_{fc}^2 l_{eff}}{4} \frac{f_y}{\gamma_{M0}} = 1.525 kNm$$

The resistant forces for three collapse mechanisms are:

$$F_{T1,Rd} = \frac{4M_{pl,Rd}}{m} = 190.1 kN \qquad\qquad \text{collapse mechanism n.1}$$

$$F_{T2,Rd} = \frac{2M_{pl,Rd} + n\sum B_{t,Rd}}{m + n} = 243 kN \qquad\qquad \text{collapse mechanism n.2}$$

$$F_{T3,Rd} = \sum B_{T,Rd} = 2B_{T,Rd} = 352.8 kN \qquad \text{collapse mechanism n.3}$$

being:

$$m = m_c = 32.1 mm$$
$$n = \min\{1.25 m_c; e_p; e_c\} = \min\{40.1; 50; 60\} = 40.1 mm$$

The prevailing collapse mechanism is the number 1:

$$F_{T,Rd} = \min\{F_{T1,Rd}; F_{T2,Rd}; F_{T3,Rd}\} = 190.1 kN$$

The strength of the flange of the sleigh in tension, the sum of the strength of the two independent T-stubs, is:

$$\boxed{F_{t,fc,Rd} = 2F_{T,Rd} = 2 \cdot 190.1 = 380.2 kN}$$

- Strength of the extended end-plate

About the end-plate the effective lengths (l_{eff}) to be considered are different for the internal and the external line of bolts because of the bracing provided from the web of the beam so the strength and the stiffness are greater than the external line (Fig.60).
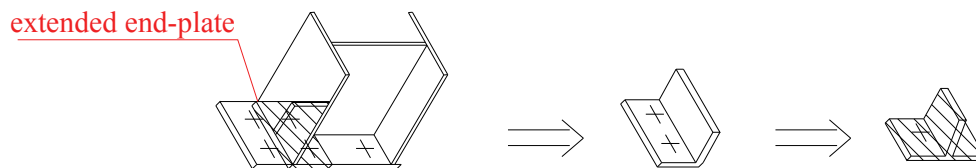
Fig. 60.   T-stub individualized in the extended end-plate

For sake of simplicity the strength of the internal line is considered equal to the one of the external line, but now we calculated together values.
The effective length (l_{eff}) to be considered for each line of bolts is the smaller of the following values:

(a) for bolts external to the flange of the beam:

$$l_{eff,a} = 0.5b_p = 0.5 \cdot 200 = 100mm$$
$$l_{eff,a} = 0.5w + 2m_x + 0.625e_x = 0.5 \cdot 100 + 2 \cdot 43.21 + 0.625 \cdot 50 = 167.7mm$$

But also the following conditions are considered:

$$l_{eff} = 100mm = \min \begin{cases} circular - pattern \\ 2\pi m_{xs} = 270 \\ \pi m_{xs} + w = 235 \\ \pi m_{xs} + 2e_p = 235 \\ other - patterns \\ 4m_{xs} + 1.25e_x = 234.5 \\ ep + 2m_{xs} + 0.625e_x = 167.2 \end{cases}$$

(b) for bolts of the internal line:

$$l_{eff,1} = 258 = \min \begin{cases} circular - pattern = 2\pi m_p = 263 \\ noncircular - pattern = \alpha m_p = 258 \end{cases}$$
$$l_{eff,2} = other - pattern = \alpha m_p = 258mm$$

where α=6.14 is obtained by the abacus in Figure 59

α represents the part of stiffness provided from the web of the beam to the equivalent T-stub for the internal line through the parameters λ_1 and λ_2.

$$\lambda_1 = \frac{m_p}{m_p + e_p} = \frac{42}{42 + 50} = 0.46$$
$$\lambda_2 = \frac{m_{xs}}{m_{xs} + e_p} = \frac{43}{43 + 50} = 0.46$$

the plastic moment of the equivalent T-stub

$$M_{pl,Rd} = \frac{t_p^2 l_{eff}}{4} \frac{f_y}{\gamma_{M0}} = 2.5 kNm$$

The resistant forces for three collapse mechanisms are in the case (a):

$$F_{T1,Rd} = \frac{4M_{pl,Rd}}{m} = 232 kN \qquad \text{collapse mechanism n.1}$$

$$F_{T2,Rd} = \frac{2M_{pl,Rd} + n\sum B_{t,Rd}}{m+n} = 243 kN \qquad \text{collapse mechanism n.2}$$

being

$$n = \min\{1.25 m_{xs}; e_x\} = \min\{51.6; 50\} = 50 mm$$
$$m = m_{xs} = 43 mm$$
$$e_x = 50 mm$$

$$F_{T3,Rd} = \sum B_{T,Rd} = 2B_{T,Rd} = 352.8 kN \qquad \text{collapse mechanism n.3}$$

The strength of the external part of the flange is:

$$F_{t,p,Rd}^{ext} = \min\{F_{T1,Rd}; F_{T2,Rd}; F_{T3,Rd}\} = 232 kN$$

The resistant forces for three collapse mechanisms are in the case (b):

$$M_{pl,Rd} = \frac{t_p^2 l_{eff}}{4} \frac{f_y}{\gamma_{M0}} = 6.45 kNm$$

$$F_{T1,Rd} = \frac{4M_{pl,Rd}}{m} = 614 kN \qquad \text{collapse mechanism n.1}$$

$$F_{T2,Rd} = \frac{2M_{pl,Rd} + n\sum B_{t,Rd}}{m+n} = 332 kN \qquad \text{collapse mechanism n.2}$$

being

$$n = \min\{1.25m_p; e_p; e_c\} = \min\{52.5; 50; 60\} = 50mm$$

$$m = m_p = 42mm$$

$$F_{T3,Rd} = \sum B_{T,Rd} = 2B_{T,Rd} = 352.8kN \qquad\qquad \text{collapse mechanism n.3}$$

The strength of the internal part of the flange is:

$$F_{t,p,Rd}^{\mathrm{int}} = \min\{F_{T1,Rd}; F_{T2,Rd}; F_{T3,Rd}\} = 332kN$$

Finally the strength of the end plate is the sum of the strength of the external and of the internal parts of the flange:

$$\boxed{F_{t,p,Rd} = F_{t,p,Rd}^{ext} + F_{t,p,Rd}^{\mathrm{int}} = 232 + 332 = 564kN}$$

Summary and conclusions

$$\boxed{F_{t,fc,Rd} = 380.2kN} \qquad\qquad \text{strength of the flange of the sleigh in tension}$$

$$F_{t,p,Rd} = 564kN \qquad\qquad \text{strength of the extended end plate}$$

As visible, the strength of the connection is dependent by the strength of the sleigh in tension, which globally is equal to= 380.2 kN. The moment resistant is the product of the strength at each line for the distance:

$$M_{jRd} = F_{t,fc,Rd}^{ext} z^{ext} + F_{t,fc,Rd}^{\mathrm{int}} z^{\mathrm{int}} = 190.1 \cdot 0.344 + 190.1 \cdot 0.233 = 109.68kNm$$

The moment resistant of the connection have to be compared with the one of the beam IPE 300:

$$\frac{M_{c,Rd}}{M_{j,Rd}} = \frac{157}{109.68} = 1.43$$

As visible the moment resistant of the beam is minor than the one of the beam so the choose thickness of the end plate is appropriate for the connection.

The already examined case represents a situation in which it is possible to apply the equivalent T-stub criterion for the end plate of a connection. With the purpose of extending the codified formulation of EC3 to the case of plate with more lines of bolts, new formulations of the resistant strength at the collapse, corresponding to the three collapse mechanism visible in Figures 61, 62 and 63, are proposed applying the same procedures previous illustrated:

- Type 1: complete collapse mechanism of the flange
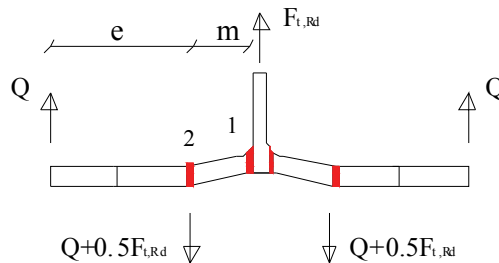
Fig. 61.   Mechanism type 1

Writing the equilibrium of rotation of the plastic hinge 1 and of the plastic hinge 2, the following value of the strength is obtained:

$$F_{t,Rd} = \frac{4M_{pl}}{m_1}$$

- Type 2: collapse of bolts with yielding of the flange
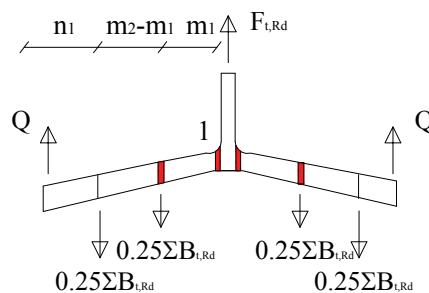
Fig. 62.   Mechanism type 2

From the equilibrium at the translation and of the rotation at the plastic hinge, the following value of the strength is obtained:

$$F_{t,Rd} = \frac{2M_p - 0.5\sum B_{t,Rd}m_1 + 0.5\sum B_{t,Rd}m_2 + \sum B_{t,Rd}n_1}{n_1 + m_2}$$

- Type 3: collapse of bolts
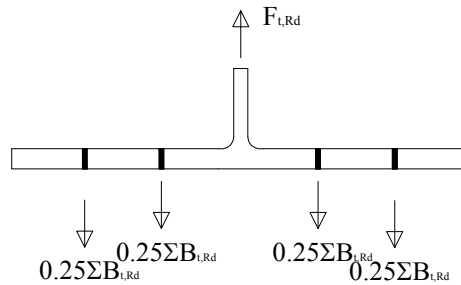
Fig. 63.   Mechanism type 3

Writing the equilibrium at the translation the following value of the strength is obtained:

$$F_{T,Rd} = \sum B_{t,Rd}$$

More details on the design of specimens and of connected parts are illustrated in the Appendix A.

5.3 THE EXPERIMENTAL ACTIVITY

The experimental activity, carried at the laboratory of the University of Salerno, has been composed of two parts:

- the identification of the material mechanical properties through the execution of tensile tests
- the evaluation of the rotation capacity and overstrength of the members through the execution of tests on cantilever beam

5.3.1 Identification of material mechanical properties

The tensile test, codified by the European standard EN 10002, is a test in which the specimen, applying a tensile effort, reaches the collapse. The purpose of the test is the evaluation of the mechanical characteristics of the material. The test has to be performed at a room-temperature between 10 and 35ºC.

The shape and the dimension of specimens are dependent by the shape and the dimension of the metallic products of which mechanical characteristics must be determined. The specimen is often obtained through the mechanical processing of a sample taken from a product. Furthermore, specimens with constant sections (profile, rebar, wire) can be submitted to the test without previous processing. The section of the specimen can be circular, rectangular, annular and in some cases of other shape.

Specimens for which the length is related to the area of the initial section through the relationship $L_0 = kS_0$ are called proportional. The value of K is known at international level as 5.65. the initial length between references points must be higher than 20 mm. Before starting monotonic and cyclic tests, mono-axial tensile tests are carried on specimens of material taken out from the flange and from the web of the beam (Fig. 64):

Fig. 64.   Specimens of material for tensile test

The tensile machine used for tests is the Schenck Hydropulos S56 (maximum load 630 kN, raced of the pistons 125mm) illustrated in the following Figure 65:

Fig. 65.   Tensile test for the characterization of material properties

With this test it is possible to obtain the stress-strain behaviour of the material. For the tensile test the used instrumentation is represented by a strain gage positioned on the middle part of the strip of the material. Following the average stress-strain curves of the material for each specimen are illustrated. The geometrical characteristics are evaluated considering the subdivision of the section presented in Figure 66 [75]:
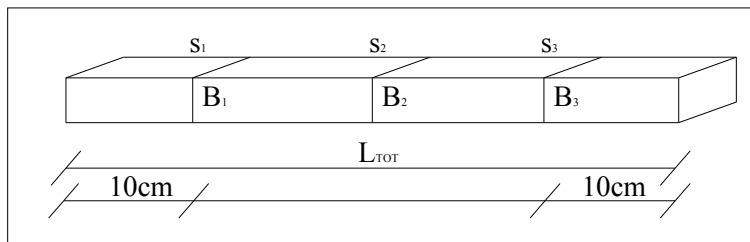
Fig. 66.   Measured parts of specimen

- I profiles
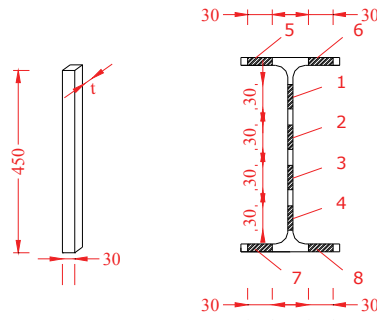
SPECIMEN HEA 160

	L (mm)	B_1 (mm)	B_2 (mm)	B_3 (mm)	s_1 (mm)	s_2 (mm)	s_3 (mm)	B_{ave} (mm)	s_{ave} (mm)	A_{ave} (mm^2)
Geometrical characteristics of specimen HEA 160										
WEB I	451,0	27,0	27,3	27,0	6,6	6,6	6,6	27,1	6,6	178,4
WEB II	450,5	31,1	31,5	31,7	6,7	6,7	6,7	31,4	6,7	210,5
FL. I	451,0	29,8	29,6	29,5	9,6	9,3	9,3	29,7	9,4	279,5
FL. II	451,0	29,3	29,4	29,5	9,2	9,3	9,6	29,4	9,4	276,2
FL. III	450,0	29,8	29,6	29,5	8,8	9,0	9,0	29,7	8,9	264,9
FL. IV	450,5	29,3	28,8	28,8	9,1	9,1	9,1	29,0	9,1	264,0
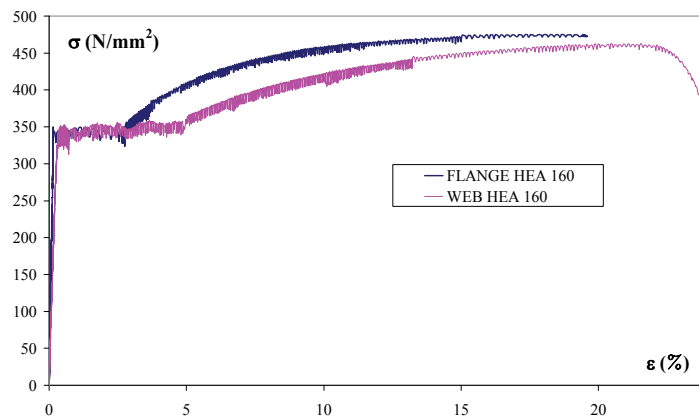
Fig. 67. Constitutive low of flange and web HEA 160

SPECIMEN HEB 240
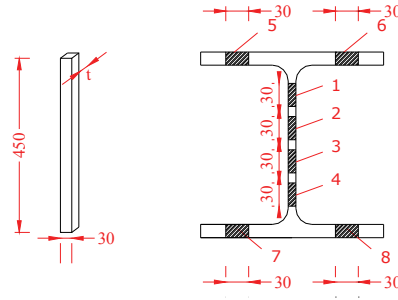
Geometrical characteristics of specimen HEB 240									
	L (mm)	B_1 (mm)	B_2 (mm)	B_3 (mm)	s_1 (mm)	s_2 (mm)	s_3 (mm)	B_{ave} (mm)	s_{ave} (mm)	A_{ave} (mm^2)
WEB I	471,0	31,0	31,0	31,0	9,8	9,8	9,8	31,0	9,8	304,0
WEB II	470,0	32,0	30,0	29,7	9,8	9,7	10,0	30,6	9,8	301,0
WEB III	472,0	30,5	31,4	31,2	9,8	9,8	9,8	31,0	9,8	304,3
WEB IV	471,0	31,4	30,9	29,6	10,0	9,9	10,0	30,6	10,0	305,4
FL. I	471,0	28,9	28,8	28,9	16,8	16,8	16,8	28,9	16,8	484,4
FL. II	470,0	29,9	29,1	29,2	16,3	16,2	16,3	29,4	16,3	478,4
FL. III	469,0	29,9	30,2	30,2	16,7	16,6	16,7	30,1	16,7	501,6
FL. IV	472,0	29,7	29,8	29,4	16,7	16,7	16,8	29,6	16,7	495,7
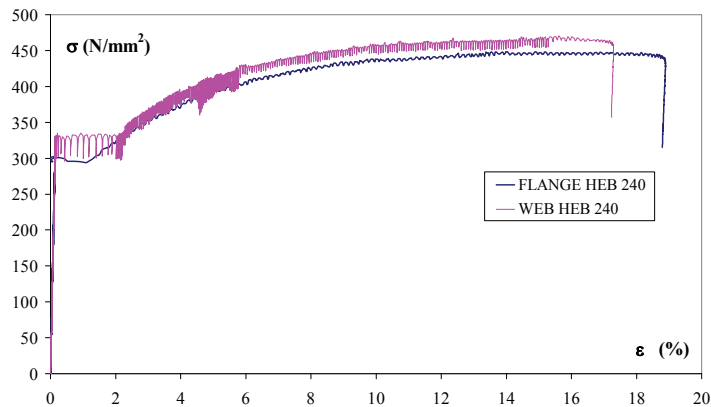
Fig. 68.   Constitutive low of flange HEB 240

- RHS profiles

SPECIMEN 150x100x5
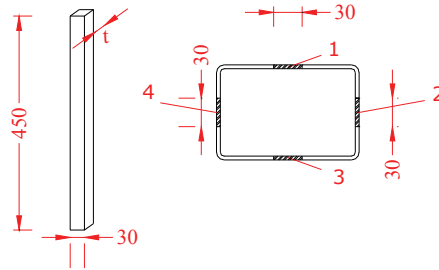
Geometrical characteristics of specimen 150x100x5									
	L (mm)	B_1 (mm)	B_2 (mm)	B_3 (mm)	s_1 (mm)	s_2 (mm)	s_3 (mm)	B_{ave} (mm)	s_{ave} (mm)	A_{ave} (mm^2)
SPEC. 1	470,0	29,5	30,0	30,4	6,0	6,0	5,9	30,0	6,0	178,8
SPEC. 2	471,0	29,4	29,1	28,9	5,7	5,7	5,5	29,1	5,6	164,1
SPEC. 3	470,0	30,0	30,0	30,3	5,5	5,7	5,7	30,1	5,6	169,6
SPEC. 4	471,0	30,0	30,1	30,3	6,1	6,2	5,9	30,1	6,1	182,3
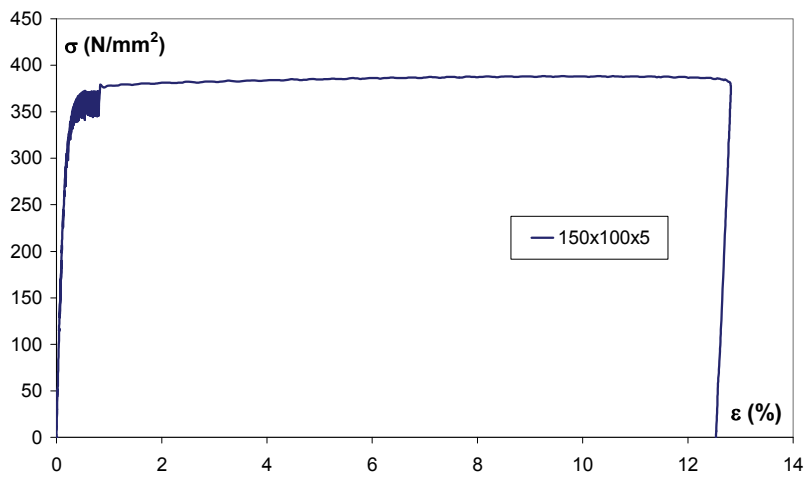
Fig. 69. Constitutive low of specimen 150x100x5

SPECIMEN 160x80x4
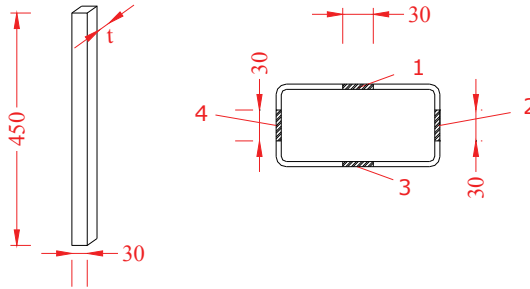
Geometrical characteristics of specimen 160x80x4									
	L (mm)	B_1 (mm)	B_2 (mm)	B_3 (mm)	s_1 (mm)	s_2 (mm)	s_3 (mm)	B_{ave} (mm)	s_{ave} (mm)	A_{ave} (mm^2)
SPEC. 1	470,0	29,7	28,9	28,9	4,0	4,0	4,0	29,2	4,0	116,0
SPEC. 2	471,0	30,1	29,8	29,6	4,0	4,0	4,1	29,8	4,0	120,2
SPEC. 3	470,5	31,3	31,4	31,4	4,0	4,0	4,0	31,4	4,0	124,3
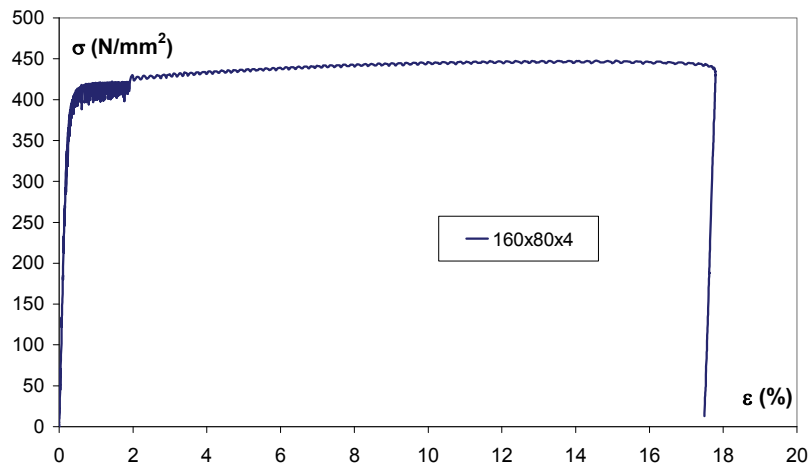
Fig. 70.   Constitutive low of specimen 160x80x4

- SHS profiles

SPECIMEN 200x200x10
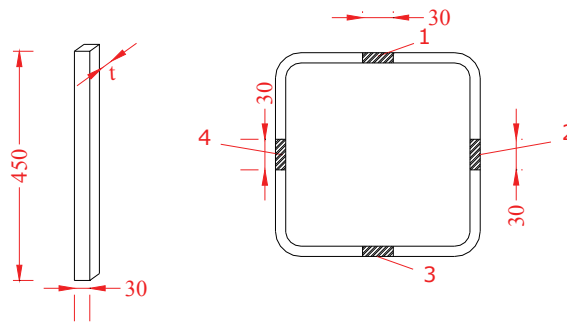
Geometrical characteristics of specimen 200x200x10									
	L (mm)	B_1 (mm)	B_2 (mm)	B_3 (mm)	s_1 (mm)	s_2 (mm)	s_3 (mm)	B_{ave} (mm)	s_{ave} (mm)	A_{ave} (mm^2)
SPEC. 1	470,0	29,9	29,9	29,7	9,8	9,7	9,7	29,8	9,7	290,8
SPEC. 2	471,0	30,6	30,5	30,5	9,9	10,0	10,0	30,5	10,0	304,4
SPEC. 3	469,0	31,5	31,4	31,2	9,8	9,8	9,9	31,4	9,8	308,9
SPEC. 4	471,0	29,6	29,9	30,1	9,9	9,8	9,9	29,9	9,9	295,2
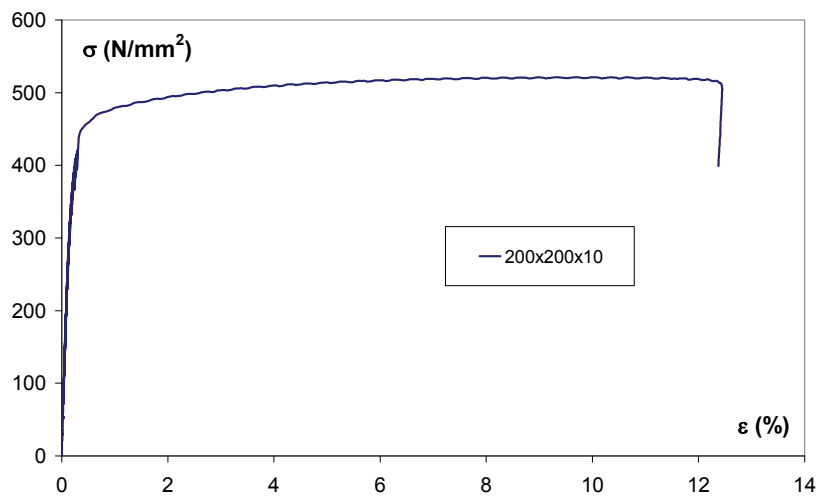
Fig. 71.   Constitutive low of specimen 200x200x10

SPECIMEN 160x160x6.3
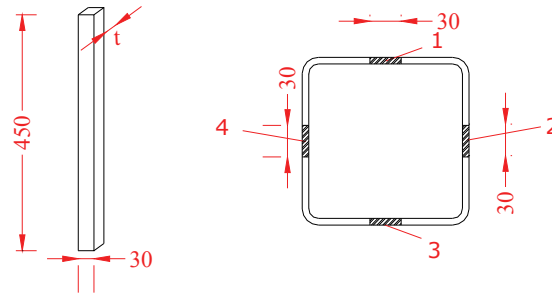
Geometrical characteristics of specimen 160x160x6,3										
	L (mm)	B_1 (mm)	B_2 (mm)	B_3 (mm)	s_1 (mm)	s_2 (mm)	s_3 (mm)	B_{ave} (mm)	s_{ave} (mm)	A_{ave} (mm^2)
SPEC. 1	471,0	30,1	30,2	30,2	5,9	6,0	5,9	30,2	5,9	179,3
SPEC. 2	470,9	32,0	31,5	31,1	5,9	5,9	5,9	31,5	5,9	186,8
SPEC. 3	472,0	29,7	30,1	30,4	5,7	5,9	5,9	30,1	5,8	175,0
SPEC. 4	471,0	30,4	29,7	30,0	6,1	6,1	6,0	30,0	6,1	182,1
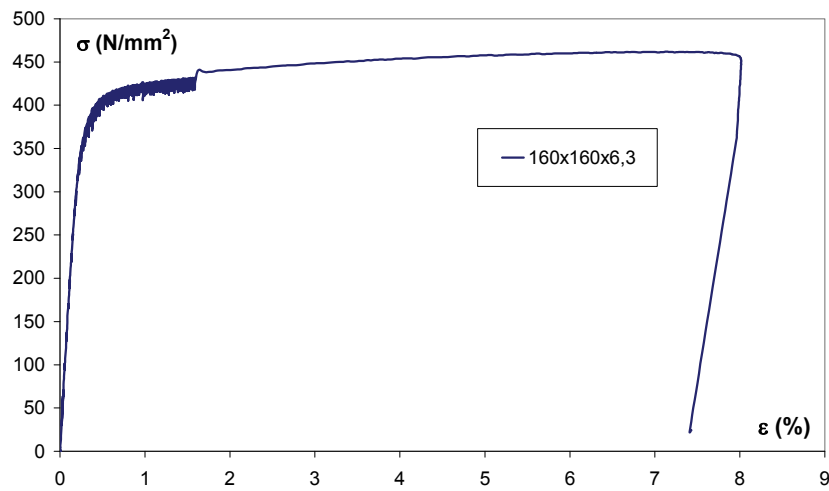
Fig. 72.   Constitutive low of specimen 160x160x6.3

5.3.1 Tests on members

The tests on members are performed through the use of a hydraulic actuator type MTS 243 with maximum effort of 250 kN. This equipment applies predetermined strengths or displacements checking their values through a control device.

The actuator works with controlled displacements and submits the member to an effort of bending simulating the solicitations on a cantilever beam. The same actuator applies the cyclical loads because the displacements are imposed.
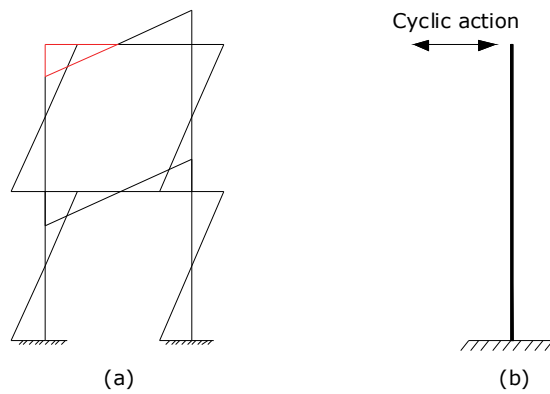
Fig. 73.   (a) bending moment on frame; (b) adopted cantilever beam scheme

- For monotonic tests the loading history applied is the one illustrated in Figure 74:
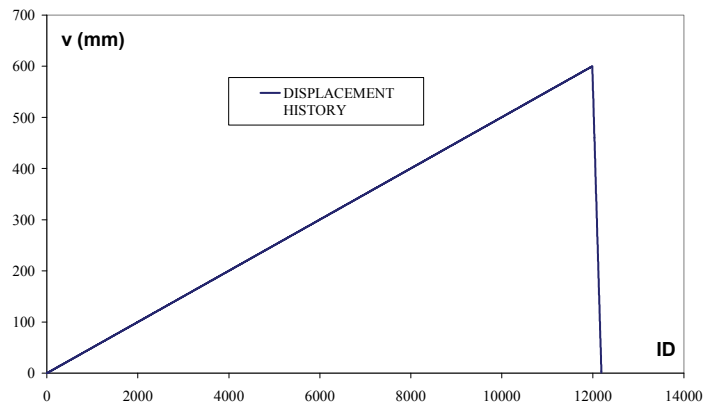
- For cyclic tests amplitude and number of cycles have been programmed according to the provisions of AISC codes [82] as illustrated in Figure 74:
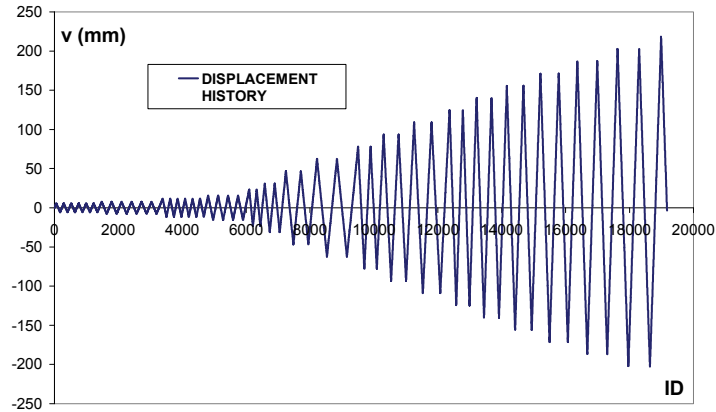
Fig. 74.   Loading history proposed by AISC codes

The proposed loading history is composed by:

- 6 cycles with $\theta = 0,00375$ rad
- 6 cycles with $\theta = 0,005$ rad
- 6 cycles with $\theta = 0,0075$ rad
- 4 cycles with $\theta = 0,01$ rad
- 2 cycles with $\theta = 0,015$ rad
- 2 cycles with $\theta = 0,02$ rad
- 2 cycles with $\theta = 0,03$ rad
- 2 cycles with $\theta = 0,04$ rad

While the following steps of load have 2 cycles for each one and an increase of 0,01 rad. Subsequently, selected the upper displacement of the beam as parameter to represent the test and considering the prescriptions of AISC, the programmed displacement history is the following:

v [mm/s]	Step	θ [rad]	n cicli	δ [mm]	t_r [s]	t_c [s]	t_{step} [s]
0,5	1	0,00375	6	5,85	11,7	47	293
	2	0,005	6	7,8	3,9	62	378
1	3	0,0075	6	11,7	3,9	47	285
	4	0,01	4	15,6	3,9	62	254
	5	0,015	2	23,4	3,9	47	98
2	6	0,02	2	31,2	3,9	62	129
	7	0,03	2	46,8	7,8	94	195
	8	0,04	2	62,4	7,8	125	257
	9	0,05	2	78	3,9	78	160
4	10	0,06	2	93,6	3,9	94	191
	11	0,07	2	109,2	3,9	109	222
	12	0,08	2	124,8	2,6	83	169
6	13	0,09	2	140,4	2,6	94	190
	14	0,1	2	156	2,6	104	211
	15	0,11	2	171,6	2,6	114	231

Fig. 75.   Loading history proposed by AISC codes

The values of the displacements have been obtained starting from the rotations and considering a length of the beam equal to 1885 mm; t_r ramp time; t_c time of the cycle; total time of the test equal to 60 min. During the test different parameters are investigated such as displacements and forces applied by the actuator in different points of the beam.

These values have been obtained positioning the following instrumentation:

- N.2 LVDT to measure the deflection in the region of plastic hinge equal to $1.2b_f$ (lateral)

- N.2 LVDT to measure the displacement of base plate (frontal)

- N.2 LVDT to measure the web out of plane displacements (back)

- N.2 INCLINOMETERS to measure rotations

- N.2 STRAIN GAGES to measure the flange strains

Figures 76 and 77 show the frontal and back position of the instruments used to measure displacements, deformation and rotations.

Fig. 76.   Frontal position of instrumentation

Fig. 77.   Back position of instrumentation

Each test has been developed through a series of steps:

1) preparation of the specimens: on the beam was welded the transversal braces and then the beam was bolted to the sleigh of base

2) the beam was positioned for the test. Plates for the anchoring of the actuator were positioned at a distance of 1885 mm from the base plate

3) the actuator was connected with the pc central unit

4) LVDT, inclinometers, and strain gages were positioned along the beam and on the base plate.

5) the central unit was connected to the computer and to the central unit of the actuator

6) the test started automatically: the load was indirectly applied: imposing the displacement at the head of the beam and reading the corresponding value of the force.

- I profiles
MEMBER HEA 160

Geometrical characteristics of member HEA 160					
member		base-plate		bolts	
length	weight	size	weight	type	number
(m)	(kg)	(m)	(kg)	M30	
3,7	112,5	0,4x0,4x0,03	40,5	8,8	10,0
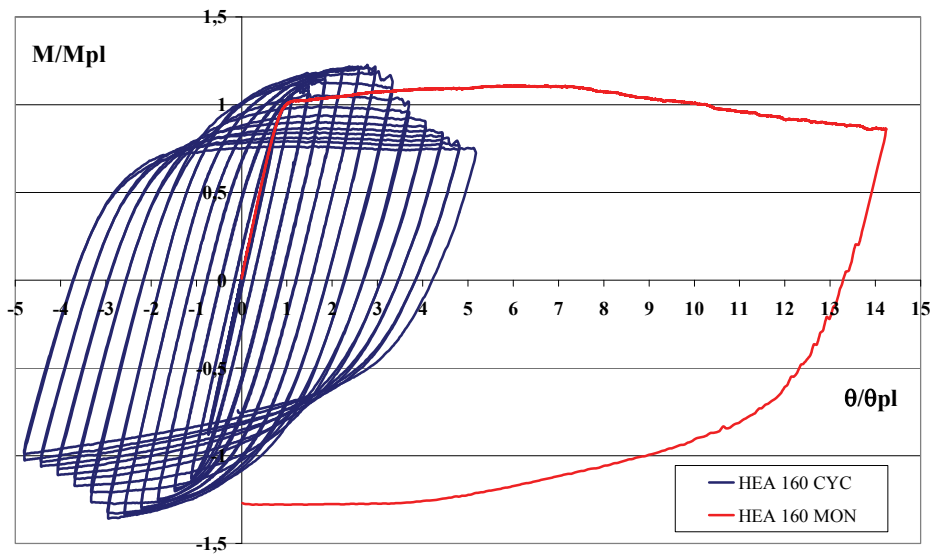
Mpl (kNm)	R	s
83,30	9,31	1,11

Monotonic deformation   Cyclic deformation

MEMBER HEB 240

Geometrical characteristics of member HEB 240					
member		base-plate		bolts	
length	weight	size	weight	type	number
(m)	(kg)	(m)	(kg)	M30	
3,7	307,8	0,6x0,4x0,35	70,9	8,8	12,0
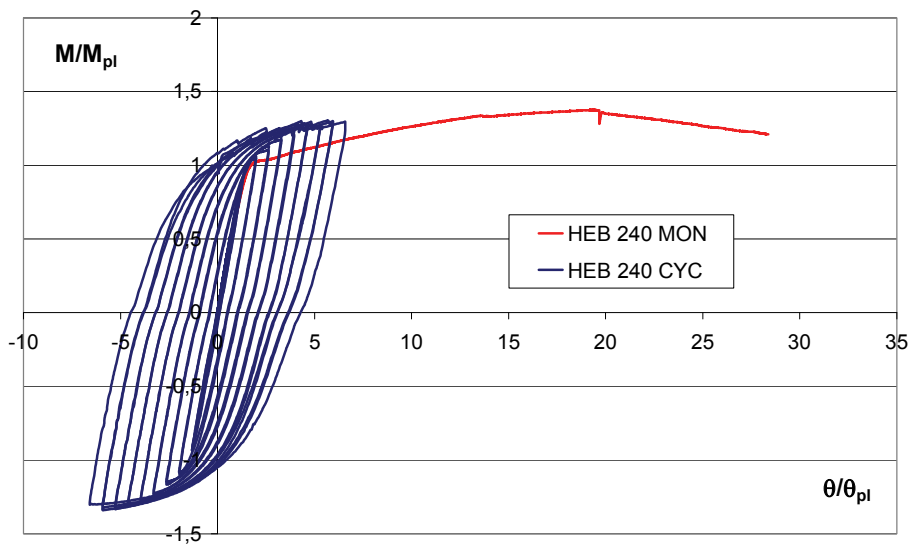
Mpl (kNm)	R	s
314,32	19,00	1,37

Monotonic deformation   Cyclic deformation

- RHS profiles
MEMBER 150x100x5

Geometrical characteristics of member 150x100x5					
member		base-plate		bolts	
length	weight	size	weight	type	number
(m)	(kg)	(m)	(kg)	M30	
3,7	55,9	0,6x0,25x0,03	35,3	8,8	8,0
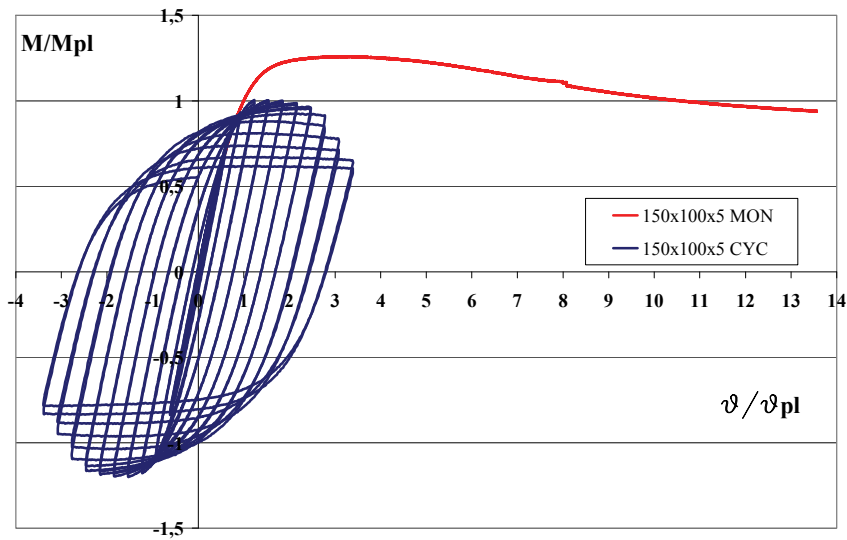
Mpl (kNm)	R	s
44,10	9,36	1,26
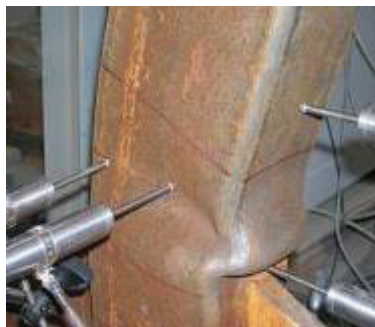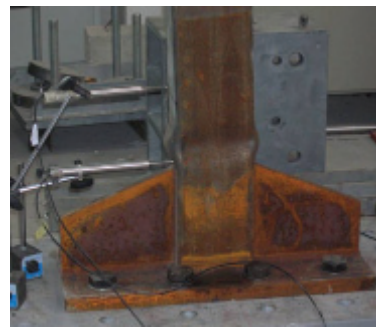
Monotonic deformation   Cyclic deformation

MEMBER 160x80x4

Geometrical characteristics of member 160x80x4					
member		base-plate		bolts	
length	weight	size	weight	type	number
(m)	(kg)	(m)	(kg)	M30	
3,7	65,9	0,6x0,25x0,03	35,3	8,8	8,0
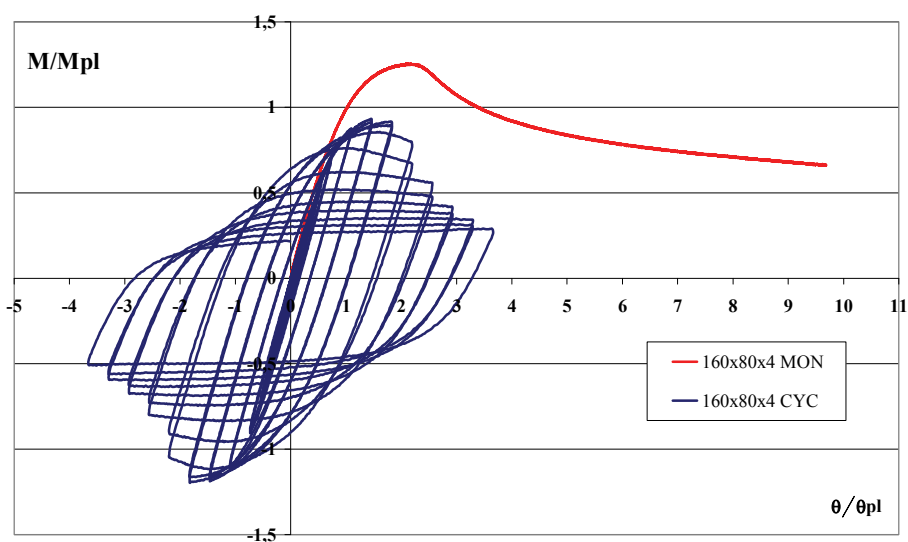
Mpl (kNm)	R	s
30,77	2,44	1,25

Monotonic deformation   Cyclic deformation

- SHS Profiles
MEMBER 200x200x10

Geometrical characteristics of member 200x200x10					
member		base-plate		bolts	
length	weight	size	weight	type	number
(m)	(kg)	(m)	(kg)	M30	
3,7	217,6	0,6x0,4x0,03	60,7	8,8	12,0
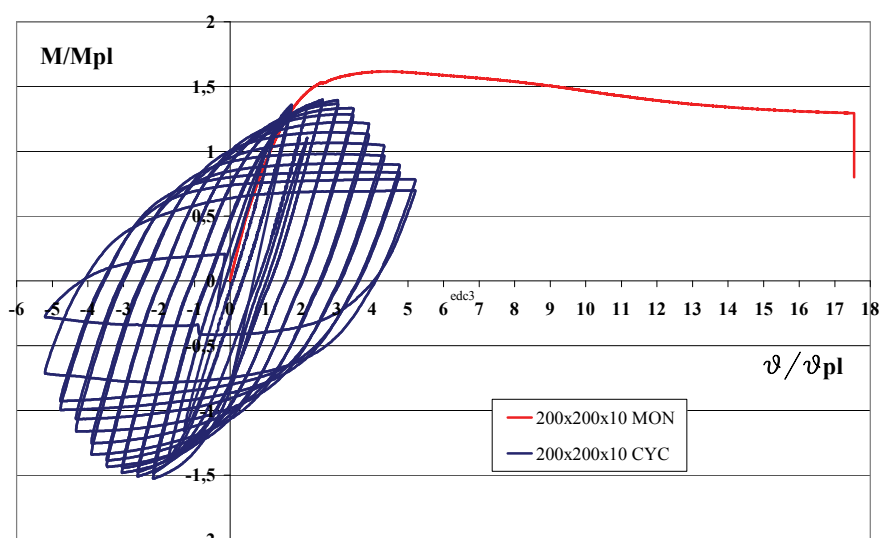
Mpl (kNm)	R	s
180,50	16,30	1,62

Monotonic deformation   Cyclic deformation

MEMBER 160x160x6.3

Geometrical characteristics of member 160x160x6,3					
member		base-plate		bolts	
length	weight	size	weight	type	number
(m)	(kg)	(m)	(kg)	M30	
3,7	111,4	0,6x0,4x0,03	60,7	8,8	12,0
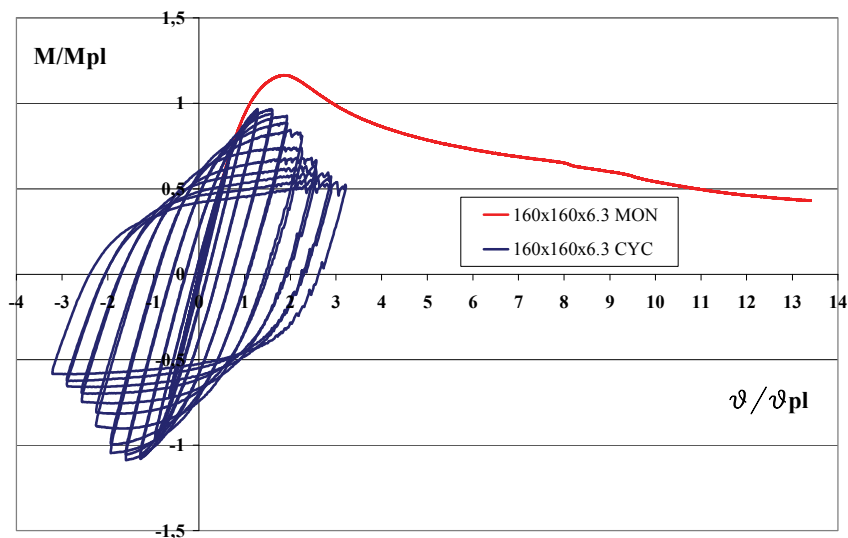
Mpl (kNm)	R	s
85,80	1,96	1,16
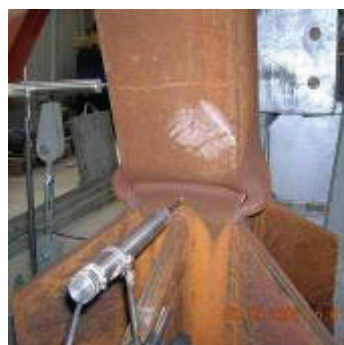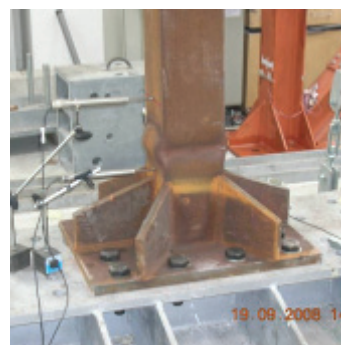
Monotonic deformation   Cyclic deformation

5.4 CRITICAL ANALYSIS OF TESTS RESULTS

After the execution of experimental tests on members already illustrated it has been possible, first of all, to classify these ones according to the provisions of seismic codes analyzed in Chapter 4: EC3 [60], NTC '08 [69] and OPCM 3274 [68]. In the following Table 10, the results of these comparisons are reported:

Table 10.   Classification of tested members using EC3, NTC'08, OPCM 3274 provisions

	R	s	Classe EC3	Classe NTC'08	Classe OPCM 3274
HEA 160	9,31	1,11	1	1	2
HEB 240	17	1,25	1	1	1
150x100x5	9,36	1,26	1	1	1
160x80x4	2,44	1,25	1	2	1
200x200x10	16,3	1,62	1	1	1
160x160x6,3	1,96	1,16	1	2	2

As visible, profiles are not classified in the same way by different criteria, in particular:

- EC3 classification criterion results to be the less conservative, because applying it all profiles results to be of the first class. This situation is due to the fact that this criterion focus the attention only on cross-section while a correct approach must be based on the study of whole member.
- NTC'08 and OPCM 3274 codes appear to be more conservative than EC3 but there is no coincidence in the results. This situation is due to the fact that NTC'08 classification criterion is based only on the ductility parameter while the OPCM 3274 one is based only on the overstrength parameter s.

The considerations regarding this results confirm the necessity of a classification criterion which takes into account the characteristics of the whole member and not of only cross-section and takes into account simultaneously rotation capacity and overstrength parameters.

Subsequently, to evaluate the influence of cyclic loads on rotation capacity and overstrength factors, comparisons between energy dissipated by monotonic and cyclic tests have been performed. The evaluation of dissipated energies by monotonic (E1) and cyclic (E2) tests have been calculated as areas subtended by curves.

- profile HEA 160
E1=25676 kNmm
E2=298265 kNmm
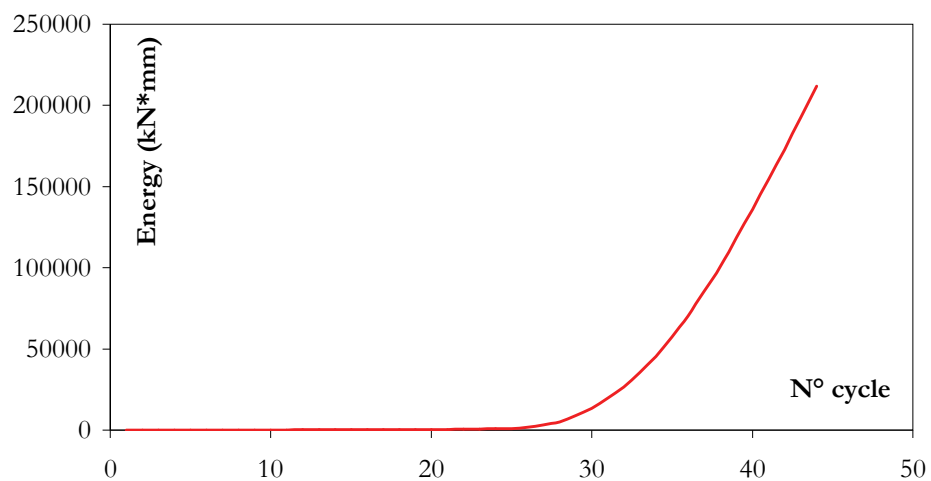
- profile HEB 240
E1=136030 kNmm
E2=563776 kNmm
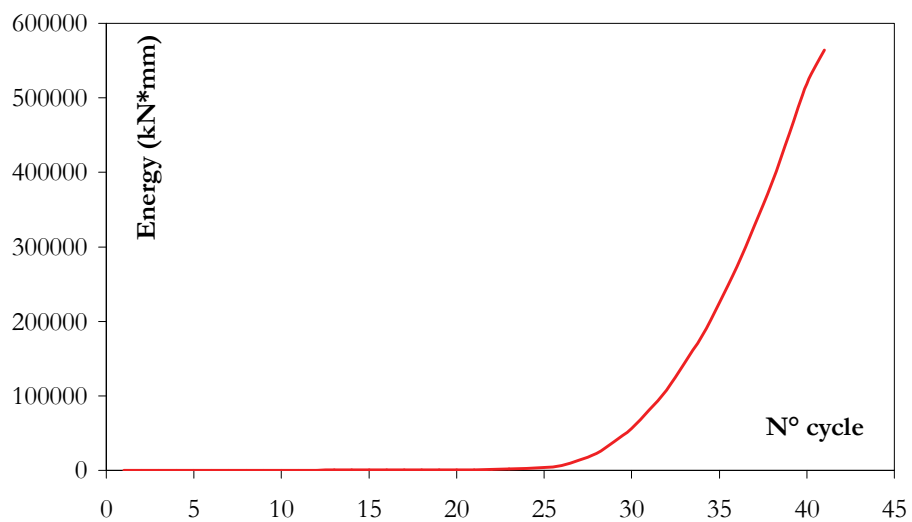
- profile 150x100x5
E1=17223 kNmm
E2=95053 kNmm
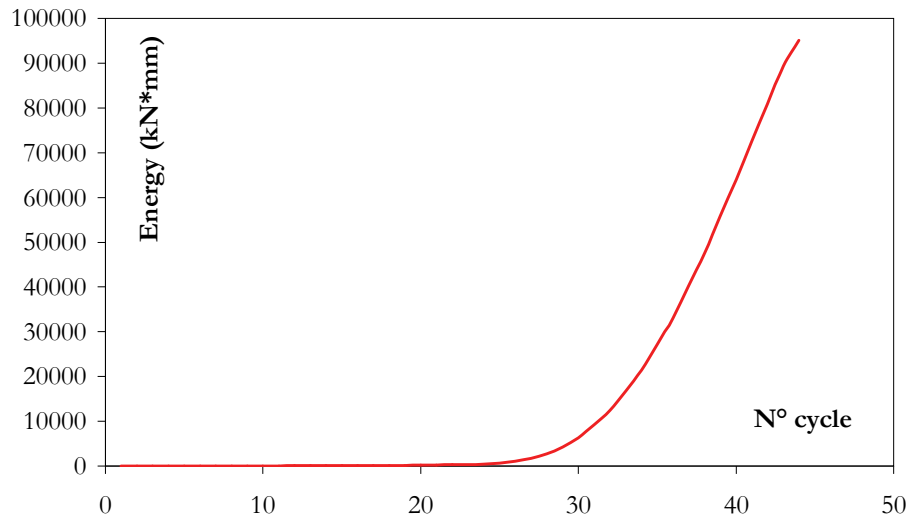
- profile 160x80x4
E1=5709 kNmm
E2=35675 kNmm
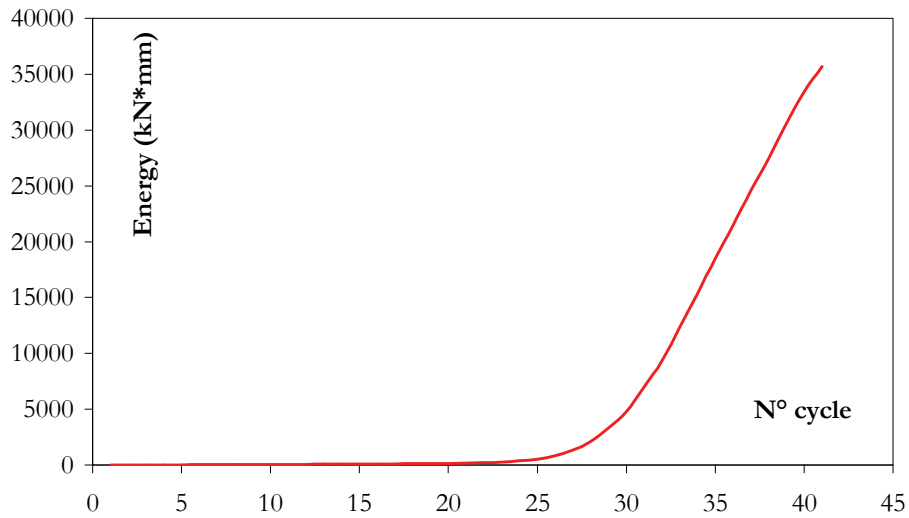
- profile 200x200x10
E1=83948 kNmm
E2=455212 kNmm
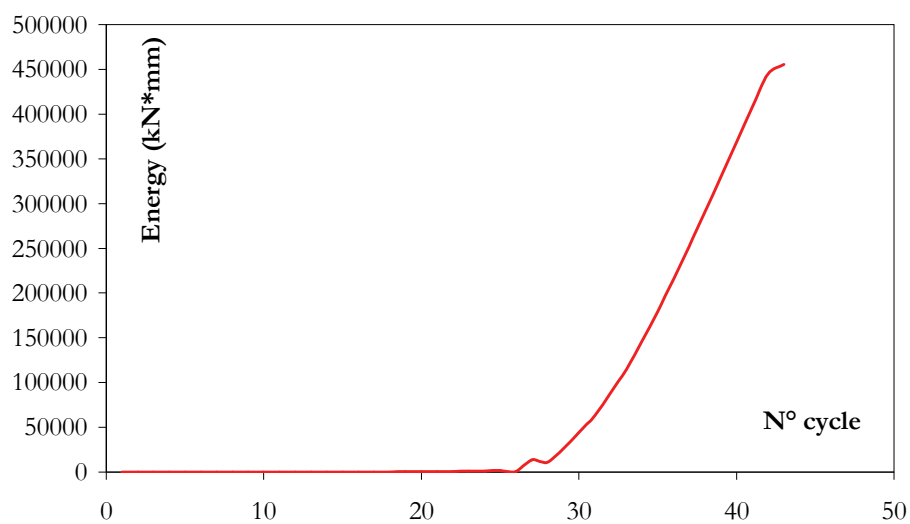
- profile 160x160x6.3
E1=20682 kNmm
E2=95752 kNmm
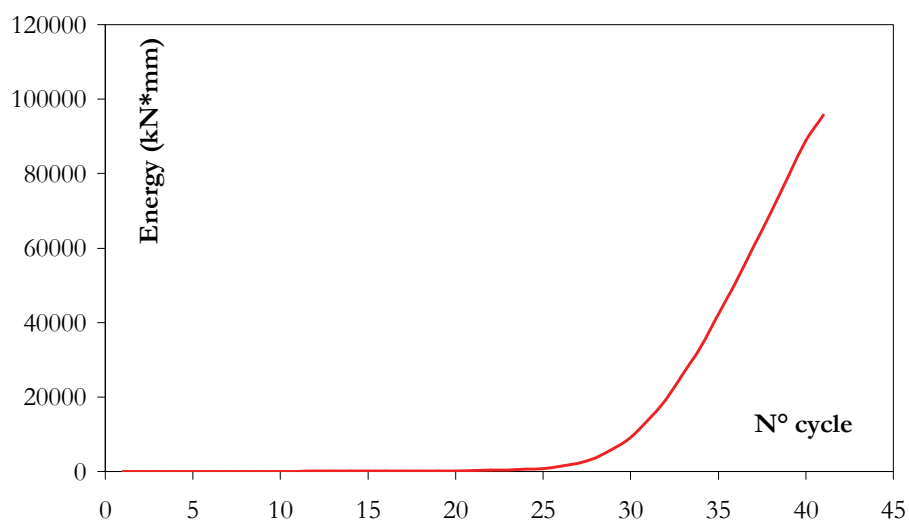
The principal result of these comparisons is that the average value of the energy dissipated during monotonic test is about the 18% of the corresponding energy dissipated during cyclic test as visible in the following Table 11 :

Table 11.   Comparison between dissipated energies

	E1 (kNmm)	E2 (kNmm)	E1/E2
HEA 160	25676	298265	0,09
HEB 240	136030	563776	0,24
150x100x5	17223	95053	0,18
160x80x4	5709	35675	0,16
200x200x10	83948	455212	0,18
160x160x6,3	20682	95752	0,22
average value (%)			17,82

CHAPTER 6: THE NUMERICAL STUDY

6.1 INTRODUCTION

The Finite Element Method (FEM) is widely used in design of structures. It can be used with different degrees of sophistication for different purposes. Most common is linear elastic analysis and also geometrically non-linear elastic analysis of frames. Such analysis give load effects and together with limiting criteria from codes forms a design method for structures. These methods are well established for frames using beam elements. The imperfections needed for a non-linear analysis are bow and sway imperfections, which are given in Eurocode 3 [60].

In order to deal with plate buckling problems the structure has to be modelled with shell elements or solid elements, which give models with many more degrees of freedom (DOF) than using beam elements. Non-linear FE simulations are usually needed in order to describe the behaviour at ULS. Such methods are today used mainly as a research tool. It is fairly time consuming to create a proper model and in cases where instability governs the results may be quite sensitive to the assumed imperfections. Also, the computer power needed for solving large problems used to be a limitation. With modern computers this restriction seems to be disappearing and it is today possible to solve most problems on a PC. Another breakthrough which facilitates use of FEA is object oriented pre-processing and efficient coupling between CAD programs with a pre-processor of computational software. Furthermore, new versions of computational software are more user friendly, with icon based options and very powerful documentation. For this reason it is to be expected that non-linear FE simulations will become a design tool in the near future.

6.1.1 Characteristics of the numerical F.E.M. model

The expression F.E.M. represents the generalization of common methods of calculation for mono-dimensional structures (reticular structures and portal frames), for bi-dimensional structures (slabs, plates and vaults) or three-dimensional continuous. The fundamental concept of this method is that it considers each structure as constituted by finite number of elements connected in a finite number of points called nodal points. Furthermore, the method identifies the response of the structure with the one obtained in these finite number of nodes.

This concept can be directly verified in the case of an ordinary frame structure in which there are beams and columns, while points of connection are internal nodes of the frame. In these cases, the structure is constituted by a finite number of elements connected among them in a defined number of points. In this case the elastic analysis can be lead back, through the forces and displacements methods, writing congruence and equilibrium equations corresponding to nodes connection of the elements. The Finite Element Methods consists, as already said, in the extension of this concept to bi-dimensional and three-dimensional structures. A slender slab with generic shape (Fig. 78a) can be considered ideally constituted by a finite number of shell element, for example with triangular shape (Fig. 78b), connected in nodal points. In this way, the idealization of the structure consists in the subdivision of the continuous in a finite number of elements with appropriate shape and dimension. The calculation of the structure can be carried out through the application, in a generalized way, of the force and displacement methods.
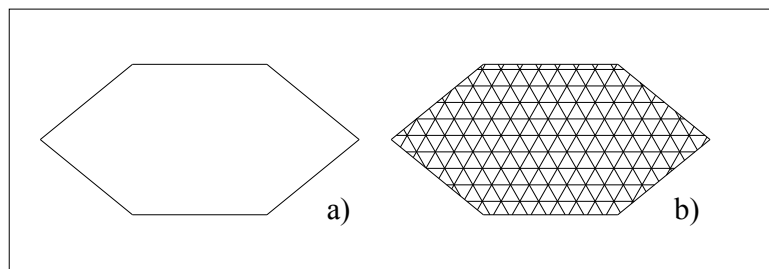
Fig. 78.   Example of subdivision into finite elements

Finite Element Method belongs to the category of numerical methods for structural analysis but it is different from traditional methods of finite differences because the subdivision of the system is not only related to the "algorithm" but also interests the physical structure of the model. The adopted

approximation has a physical nature, the actual continuous is substituted with an ideal structure obtained from the assemblage of a finite number of elements, but the solution is obtained in rigorous way. The calculation of structures through the Finite Element Method can be subdivided into the following three principal phases:

1) Idealization of the structure

2) Evaluation of the characteristics of each element which constituted the idealized structure

3) Structural analysis of idealized structure

The first phase consists in the subdivision of the original continuous in an opportune number of elements with appropriate shape and dimension. This operation requires particular attention because the obtained results are more close to actual values than the ideal structure is able to simulate the behaviour of the actual continuous; however good results are often obtained with a subdivision of the structure in a very small number of elements.

In the second phase it is necessary to evaluate, for each element of the idealized structure, the relationships between nodal forces and displacements. If, for example, we consider a generic triangular element of the idealized structure of Figure 78, the characteristics of each element can be evaluated when constitutive low between the system of nodal forces represented in Figure 79a and the system of nodal displacements represented in Figure 79b are defined.
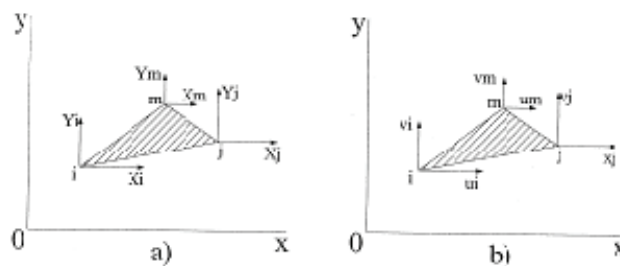
Fig. 79.   *Nodal forces and displacements in slabs: a) forces; b) displacements*

These relationships, if the system is elastic with linear elasticity, results to be linear, and assume the expression:

$$\begin{cases} X_i = K_{11}u_i + K_{12}v_i + ... + K_{16}v_m \\ Y_i = K_{21}u_i + K_{22}v_i + ... + K_{26}v_m \\ .... \\ Y_m = K_{61}u_i + K_{62}v_i + ... + K_{66}v_m \end{cases} \qquad (6.1)$$

being K_{ij} the stiffness coefficient which must be determined. If we indicate with F and δ the two column vectors (6,1):

$$F = \begin{pmatrix} X_i \\ Y_i \\ . \\ . \\ . \\ Y_m \end{pmatrix}, \ \delta = \begin{pmatrix} u_i \\ v_i \\ . \\ . \\ . \\ v_m \end{pmatrix} \qquad (6.2)$$

and with K the square matrix (6,6):

$$K = \begin{pmatrix} K_{11}K_{12}....K_{16} \\ K_{21}K_{22}....K_{26} \\ .... \\ K_{61}K_{62}....K_{66} \end{pmatrix} \qquad (6.3)$$

the equations (6.1) assume the expression:

$$F = K\delta \qquad (6.4)$$

The considered matrix has called stiffness matrix and characterizes the elastic behaviour of the examined element. Furthermore, it is evident that the determinant of the matrix (6.3) must be $|K| \neq 0$ so the (6.4) is reversible and can be written as:

$$\delta = K^{-1}F \qquad (6.5)$$

The principal problem regards the second phase of the structural calculation with the Finite Element Method and consists in the evaluation of the stiffness matrix K or in the evaluation of the deformability matrix K^{-1}, for each element of the idealized structure. If we apply the displacement method, the stiffness matrix will be calculated, if we apply the force method, the deformability matrix will be calculated.

The examination of the structure with the displacement method allows to obtain a solution that, in the context of displacements, is valid for the actual continuous and for this reason is valid not only for nodal points but also for lines in common between two adjacent elements. The definition of stiffness matrix for each element must be done choosing an opportune distribution of displacements that automatically allows the congruent solution along lines of contact when the congruent solution into nodal points is verified. If instead we want to analyze the structure with the forces methods, the purpose is to obtain a solution valid for the actual continuous for internal forces and so perfectly balanced in terms of nodal forces and also in correspondence of the common lines of adjacent elements. The definition of deformability matrix for each element has to be done choosing an opportune internal stress distribution that automatically allows the equilibrium along the contact lines when the equilibrium of nodal forces is allowed. Under these hypotheses the solution of all together cases is close to the actual one when the number of elements increases. For this reason the greater difficulty is the attribution of the displacement distribution in the element finalized to the evaluation of the stiffness matrix or the distribution of internal stresses finalized to the evaluation of deformability matrix.

In the third phase the solution is obtained applying the deformability method, starting from all constitutive methods of each element,

$$F = K\delta \qquad\qquad (6.6)$$

through the definition of the stiffness matrix K, the system of fundamental equations in the unknown quantities represented by nodal displacements is obtained imposing that in each external node the equilibrium and congruence condition are verified in relationship to existent constraints always in terms of nodal displacement. If we consider the forces method, starting from all constitutive methods of each element,

$$\delta = K^{-1}F \qquad\qquad (6.7)$$

through the definition of the deformability matrix K^{-1}, the system of fundamental equations in the unknown quantities represented by nodal forces is obtained writing at each internal node the congruence equations in terms of nodal displacements, and in each external node the equilibrium and congruence equations in relationship to the constraints existing always in terms of nodal forces [76].

6.2 MODEL FOR MONOTONIC TESTS

This paragraphs describes the finite element analysis of I, RHS, SHS members, to simulate the experimental tests of Chapter 5. The proposed numerical model is finalized to the study of the monotonic behaviour of steel members under seismic actions. Starting from experimental tests a numerical model has been realized with the purpose of obtaining a reliable predictive model. Numerical or finite element analysis provides a relatively inexpensive, and time efficient alternative to physical experiments.

It is vital to have a sound set of experimental data upon which to calibrate a finite element model. In this way, it is possible to investigate a wide range of parameters within the model. In order to model the plastic bending tests, the finite element program should include the effects of material like geometric and mechanical non-linearity, imperfections, and local buckling. The program ABAQUS (Version 6.7-1), performs the numerical analyses [79].

Introducing geometric imperfections into the model was essential to obtain results that were close to the experimental results. A perfect specimen without imperfections achieved rotation capacities much higher than those observed experimentally. The size of the imperfections had an unexpectedly large influence on the rotation capacity of the specimens. Larger imperfections were required on the more slender sections to simulate the experimental results. The finite element analysis determined similar trends as observed experimentally, namely that the rotation capacity was a function of both the flange and web slenderness.

Subsequently, all steps necessary for the calibration of the numerical model are reported, in particular the 150x100x5 specimen is illustrated.

6.2.1 Geometrical properties

In this first module the different parts which constitute the model are geometrically realized. ABAQUS has several element types suitable for numerical analysis: solid two and three-dimensional elements, membrane and truss elements, beam elements, and shell elements. The major aim of the analysis was to predict the formation of inelastic local instabilities in a cross section and the corresponding rotation capacity. Beam, membrane and truss elements are not appropriate for the buckling problem. Solid three dimensional elements ("brick" elements) may be suitable, but the solid elements have only translation degrees of freedom at each node, and require a fine mesh to model regions of high curvature. A finer mesh does not necessarily imply more total degrees of freedom, as one must consider the number of elements and the degrees of freedom of each element. The most appropriate element type is the shell element.

For these reasons through the use of the graphic processor CAE in this module the geometric characteristics of whole beam (l=1885 mm) and the loading plate have been modeled. The elements used for the representation of the beam was the three-dimensional extruded shell. Along this element, a partition has been realized with the purpose of individualize the extension of the plastic hinge, starting from the yielding point in which it will be necessary to thicken the mesh (Fig. 80).
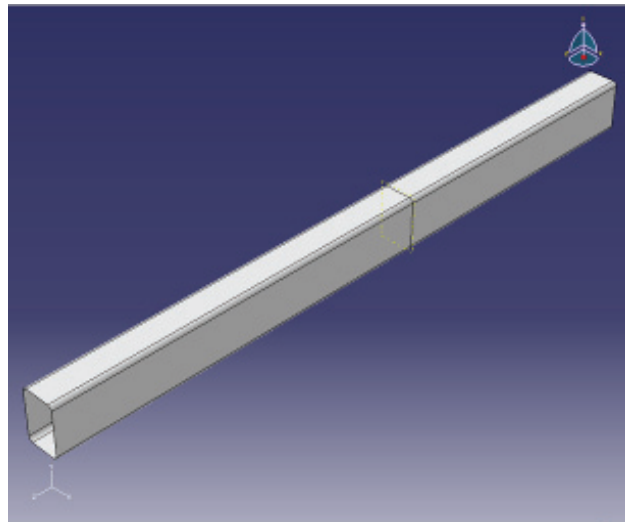
Fig. 80.   150x100x5 beam

The used elements for the representation of the loading plate was the three-dimensional planar shell (Fig. 81):
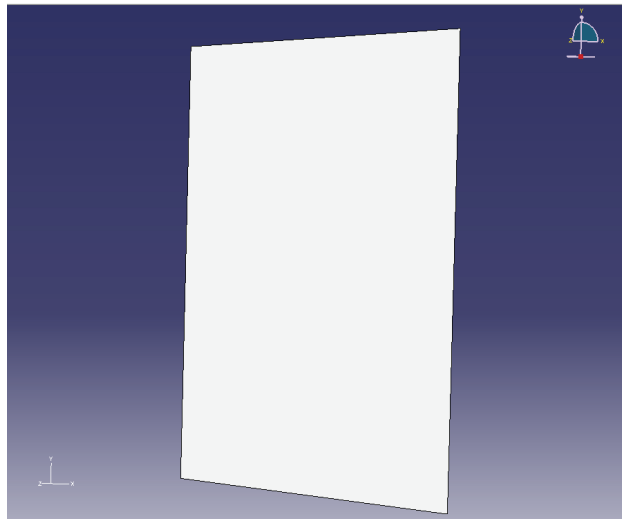
Fig. 81.   loading plate

6.2.2 Mechanical properties

In this second module the following steps are done:

1) Definition of material characteristics
2) Definition of sections characteristics
3) Assignment to the sections of the mechanical characteristics of the material which are previously defined.

To define the material characteristics, a couple of value in elastic field and a couple of value in plastic field have to be assigned.

In elastic field we have to consider:

-    Young's modulus (E) that is the modulus of tangential elasticity which for steel has a value of 210000 N/mm^2

- Poisson's modulus (ν) which represent the ratio between the transversal and longitudinal deformations of the specimens. For steel it assumes the value ν=0.3

In plastic field we have to consider:

- Yield stress, which is an unique value
- Plastic stain, which is the plastic deformation.

The material properties obtained from a standard tensile test were input to the ABAQUS model as a set of points on the stress - strain curve (Fig.82). ABAQUS uses true stress and true strain, and hence the values of engineering stress and engineering strain derived from a standard tensile test were modified and then inserted into the model using the following equations:

$$\sigma_{true} = \sigma_{ing}\left(1 + \varepsilon_{ing}\right)$$

$$\varepsilon_{true} = \ln(1 + \varepsilon_{ing})$$

being σ_{ing} and ε_{ing} respectively the conventional engineering stresses and the deformations.
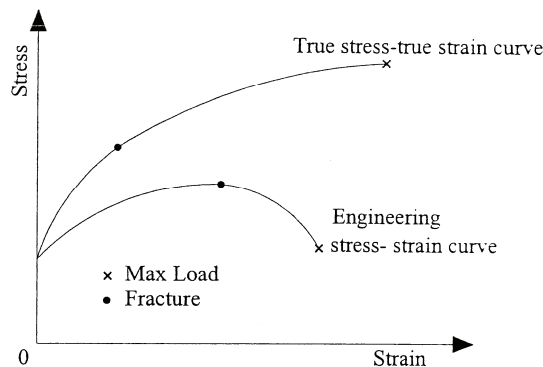
Fig. 82.   Comparison between engineering and true stress-true strain curves

This situation is due to the fact that the engineering true stress-true strain curve does not provide an actual indication of the characteristics deformation of a metal because it is based on the original dimensions of specimens, but these

dimensions changes during the tensile test. Using the actual stress based on the actual area of the section of the specimen, the stress-strain curve will monotonic increases on the value of fracture. If the evaluated deformation is based on snapshot measures, the obtained curve is called true stress- true strain.

The classical metal plasticity model in ABAQUS defines the post-yielding behaviour for most metals. ABAQUS approximates the smooth stress-strain behaviour of the material with a series of straight lines joining the given data points. Any number of points can be used to approximate the actual material behaviour and in this way it is possible to obtain a very close approximation. The plastic data define the true yield stress of the material as a function of true plastic strain. The first part of data given defines the initial yield stress of the material and, therefore, should have a plastic strain value of zero.

The strains provided in material tests data used to define the plastic behaviour are not likely to be the plastic strains in the material, for this reason it is necessary to decompose these total strain values into the elastic and plastic strain components. The plastic strain is obtained by subtracting the elastic strain defines as the value of true stress divided by the Young's modulus from the value of total strain (Fig. 83):
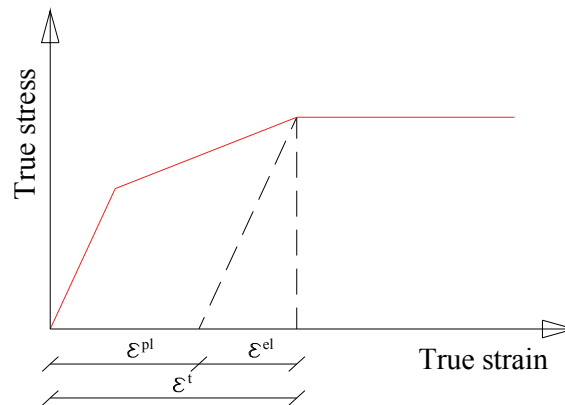
Fig. 83. Decomposition of the total strain into elastic and plastic components

This relationship is written:

$$\varepsilon^{pl} = \varepsilon^{t} - \varepsilon^{el} = \varepsilon^{t} - \sigma / \varepsilon$$

where:

ε^{pl} is true plastic strain

ε^{t} is true total strain

ε^{el} is true elastic strain

σ is the true stress

After the definition of mechanical properties the operation of assemblage of the different parts previously defined is required, through the control Instance → Create, positioning them in the final configuration they assume during the experimental tests. In this module a set has been create to individualize the line along the which the load must be applied (name of the set: linea-carico). This operation has been made through the control Tools → set→ Create. Subsequently are defend:

- the typology of analysis that the processor has to carry out.
- the geometrical and mechanical non-linearity of the model
- the number of degree of freedom to take under control during the analysis

The typology of analysis chosen is the Riks one, the most used for static analyses. The main application is the determination of structural response of tested specimens and, in particular, the determination of force-displacement curves. About this topic it is necessary to observe that during the collapse analyses of structural elements, the presence of instability phenomena of the compressed parts of the sections, often due a typical behaviour of the F-δ curves in which, after a linear behaviour a value of peak load is reached and then a sudden lose of the curve. Traditional methods of calculation based on displacement control have a lot of difficulties to catch this typology of curves:
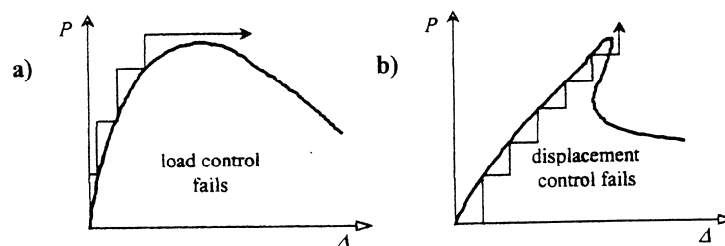
Fig. 84. Traditional failure of control methods: a) load control; b) displacement control

For these reasons, the use of methods based on the "arc-length" have a great development. These methods, introduced by Riks (1972), try to move, during the plotting of force-displacement curves, along the direction of the equilibrium. Common interpretation of these methodologies are partially linear and takes into account tangential stiffness as visible in Figure 85:
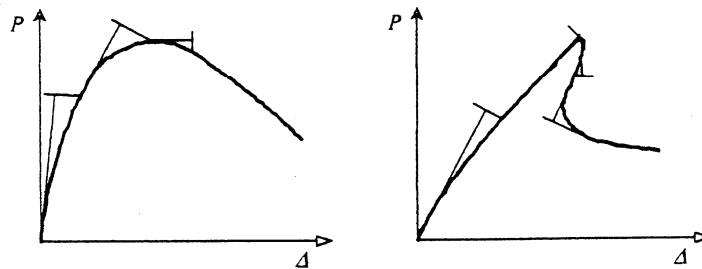
Fig. 85.   Linear "arc-length" method

ABAQUS, for the resolution of non linear problems, uses the "Modified Riks method". The solution is determined, first of all, assigning a specific length (Δl), in the space of solutions, along the tangential stiffness. The control of the length is made through automatic schemes based on predefined criteria of convergence. The equilibrated solution is researched along the line orthogonal to the tangential stiffness following the procedure illustrated in Figure 86:
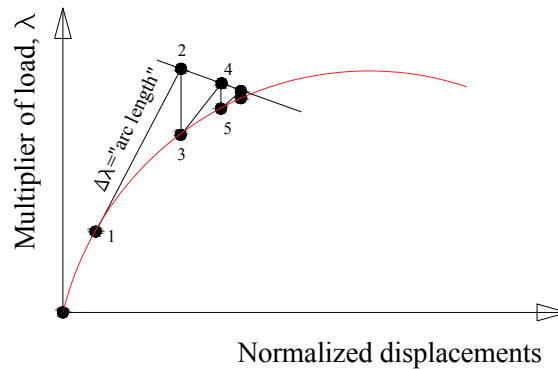
Fig. 86.   Modified Riks method

For the generic loading step, the tangential stiffness is determined in point 1; then with a displacement (Δl) the point 2 is reached; the loss of equilibrium of forces is determined (point 3). Using the convergence criteria the rightness of

this solution is verified; in particular if the loss of equilibrium is too great, from point 3 the parallel line to the tangential one (1-2) is plotted till the intersection, in point 4, with the orthogonal line to the above mentioned tangent line. From this point a new loss of equilibrium of force is determined (point 5) using a convergence criterion, verifying that it is sufficiently small to be accepted as solution. In this way it is possible to conclude the generic step that will carries to the determination of another point of the force-displacement curve. The adopted convergence criterion is constituted by three verifications both on nodal forces at each step and on variation of displacements associated. In this module also geometrical non linearity are activated [77].

After these operations, it is possible to define, in models constituted by more parts, the interaction among them establishing typologies of contact and of constraints. In this case, the beam is a three dimensional shell element which represent an "unique element" so the only definition of a tie constraint between beam and loading plate has been necessary (Fig. 87). With this purpose the definition of two surfaces, one belonging to the beam and one belonging to the loading plate, was necessary.
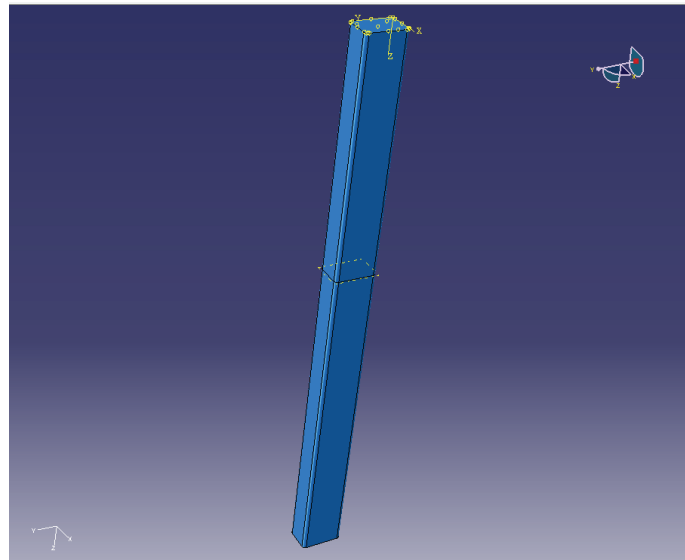
Fig. 87.   Tie constraint between beam and loading plate

6.2.3 Loads and boundary conditions

In this module the definition of load and boundary conditions is made. Several different situations may occur depending on the purpose of the FE-simulation. In this particular case the load condition is represented by the encastre at the base of the beam and by a predefined displacement assigned to the set linea-carico:

1) BC →create → step: initial → symmetry/Antisimmetry/encastre → (after selecting the base of the beam) →U1=U2=U3=UR1=UR2=UR3=0
2) BC →create → step: step-1 → displacement/rotation → (after selecting the set linea-carico) →U1=0 (to avoid flexural-torsional instabilities); U2=600 (Fig. 88)
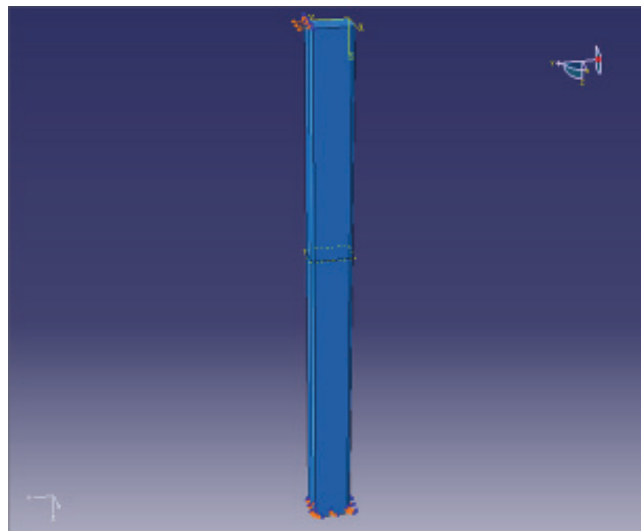
Fig. 88.   Boundary conditions

6.2.4 Mesh sensitivity analysis

Another question that is essential for the model is the meshing. A too coarse mesh may lead to non conservative results when local buckling governs. The common way of checking, if experience of similar structures is not available, is to successively refine the mesh until stable results are achieved. However, a too

fine mesh increases the numerical errors so there is a limit for how fine the mesh can be made. A rule of thumb for shell elements is that there should be at least six elements in the expected half wavelength of a buckle. Shell elements are commonly used for modeling plate structures. They usually give accurate enough results if the structure is properly modeled.

ABAQUS takes into account elements of interpolation of the first order (linear) and elements of the second order (quadratic) with tetrahedral, triangular prisms and hexametrical shapes as visible in Figure 89.
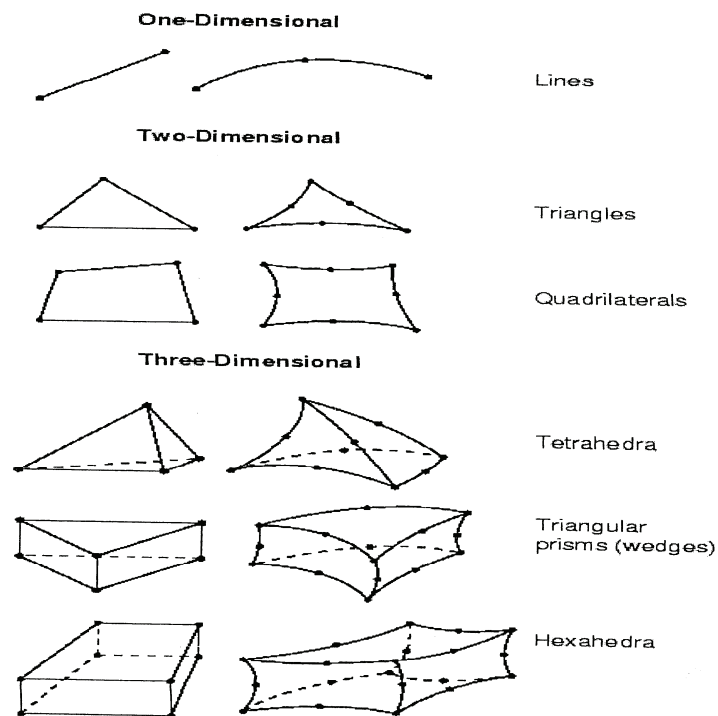
Fig. 89.   Typologies of elements used for the mesh

In general elements of the second order are characterized by a greater accuracy of the ones of the first order for problems of contact, impact and severe distortions of elements. They are also better for the representation of geometrical properties, in fact with them it is possible to model a curve surface with a minor number of elements. In any case, for the typology of simulation we are illustrating, elements of the first order have been used because they are

efficient for the computational point of view and shown a good behaviour during the Riks analysis.

Besides, into the ABAQUS library two different typologies of elements are considered:

- full integration
- reduced integration

The Gaussian integration is always used for the interpolation of polynomial products in these elements. The expression full integration means that the Gaussian scheme makes an integration of the stiffness matrix of an element considering an uniform behaviour of the material if the Jacobean of the map is constant and diagonal through the element. This situations happens when the element is rectangular and, for elements of the second order, when middle nodes of the edge are in the middle of the edges of the elements. If the element does not satisfy these conditions, the full integration is not correct because some terms of the stiffness matrix belongs to an order much higher of them integrated exactly through the preselected Gaussian scheme. Reduced integration means that in the Gaussian scheme an order under the fully scheme is used for the integration of internal forces and stiffness of the elements. The reduced integration appears an approximation but it has been demonstrated that offers some advantages. In fact it calculates the deformations with interpolation functions using a greater accuracy. With reference to the output results, it is also important when the constitutive model is non linear because the deformations passes through constitutive routines which are the best representation of deformations. It has been demonstrated that the reduced integration offers better results respect to the full integration but the mesh have to be more accurate.

In the specific case illustrated linear elements of the first order are used with S4R5 elements. They are quadrilateral shaped elements and, for simplicity of modeling, they were all defined as rectangles within the current analysis. If the aspect ratio of the rectangles becomes too high, the shell elements become less accurate.
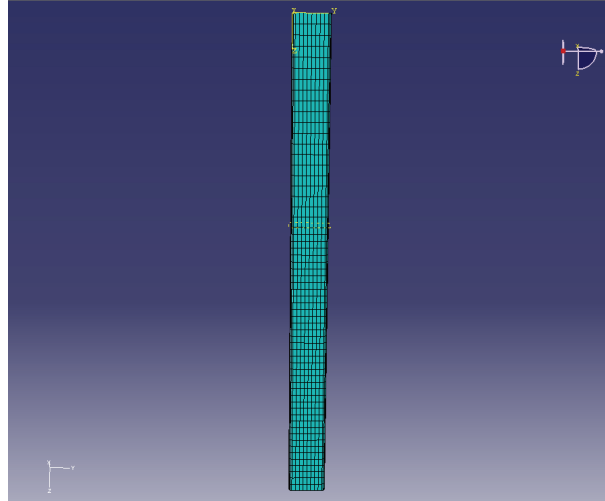
Fig. 90.   Mesh used for the model

The ultimate operation consists in the execution of the analyses are presents. The analysis starts when the input file has been created: Job manager → create → write input.

After the analysis it is possible to visualize the results of the analyses, to plot the deformed shape and the required curves. In this case the deformed shape is (Fig. 91):
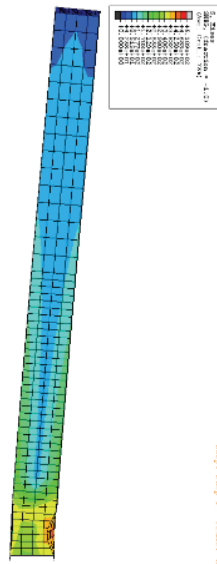
Fig. 91.   Deformed shape of the analyzed specimen

To obtain the F-v curve is necessary to apply the following procedure:

Tools → XY data → create → obd field output → position linea-carico→ RF2 (in particular sum(RF2)) → U2

Tools → XY data → create → operate on XY data →combine (U2, sum(RF2))

6.2.5 Geometrical imperfection

The model has to include imperfections corresponding to the most likely instability modes. For plated structures the imperfections can be either local or global. Local imperfections are buckles in a plate or twist of a flange or stiffener. Global imperfections or bow imperfections consist of a bow deformation of a stiffener or the whole member.

The imperfections guide the subsequent deformation and they should be directed such that the worst case is achieved. This means that it is sometimes necessary to check different directions of imperfections for unsymmetrical plates. Usually the imperfections are introduced as eigenmodes that are scaled to a proper magnitude.

The critical mode is easily obtained for simple cases. Figure 92 and 93 show some examples of modes of vibration coming from buckling analyses.
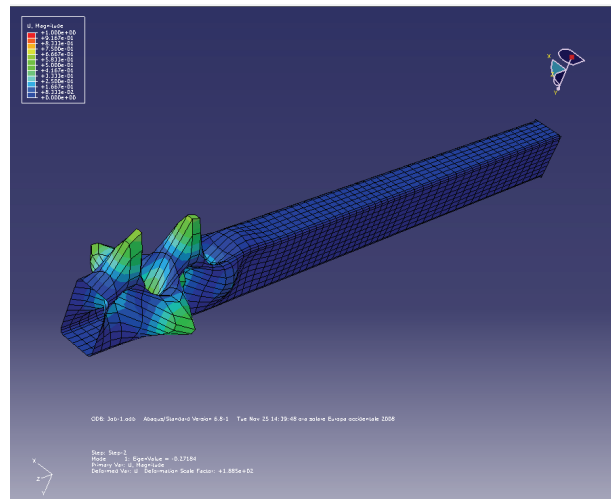
Fig. 92.   Example of buckling mode of vibration
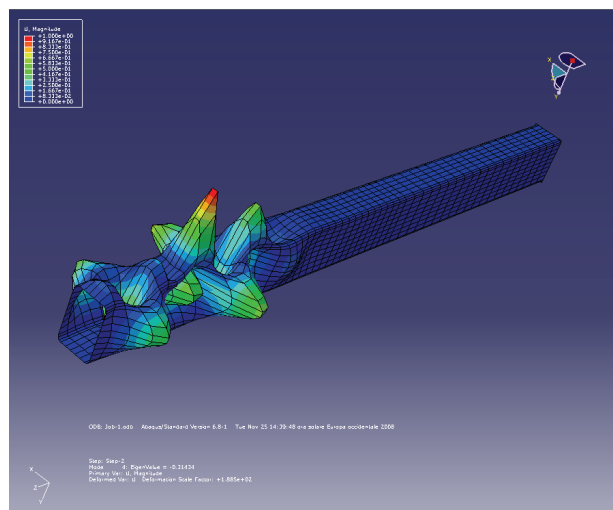
Fig. 93.   Example of buckling mode of vibration

If the magnitude of the largest web buckle is set to a prescribed design value the whole deformation pattern is defined. Assuming that it is not clear if buckling of the web or the flange is governing, it may be necessary to increase the flange buckle to its design value. This can be done by superposing another eigenmode where the flange buckling dominates. However, this will also change the deformation pattern of the web. An alternative method is rotating the flange without considering the compatibility with the web.

The magnitude of the initial deformations is often taken as the tolerance limits for fabrication. This may seem rational but it is not necessarily the right choice in the context of a probabilistic safety concept. The characteristic resistance is intended to be a 5% fractile taking all the scatter of the influencing parameters into account. Assuming that the statistical distribution of the initial deformations were known it would be possible to calculate a design value to be used. Systematic measurements of initial deformations are however rarely published so there is a lack of reliable data. The suggested level of imperfections equal to 0,8 times the tolerance limit is based on engineering judgement [76].

6.2.6 Numerical-Experimental comparisons

As illustrated in the previous paragraph, the FE model realized has the following characteristics:

- model of the whole beam
- displacement control analysis
- true stress-true strain curve for material
- geometrical imperfection (buckling modes)
- torsional constraint
- mesh composed of S4R element (shell with 4 nodes reduced integration)

The purpose of the numerical study has been the obtainment of a reliable model which correctly simulates the experimental behaviour of tested beams. In this way parametrical analyses can be carried out on members avoiding the great economic burden derived from an experimental campaign. Figure 94 compares F-v experimental and numerical responses of the specimens 150x100x5. As visible, the numerical simulation is in a good agreement with the experimental tests in terms of:

- stiffness
- strength
- ductility

For these reasons, the two parameters which are the object of the current study, overstrength and rotation capacity, are evaluated in a correct way.
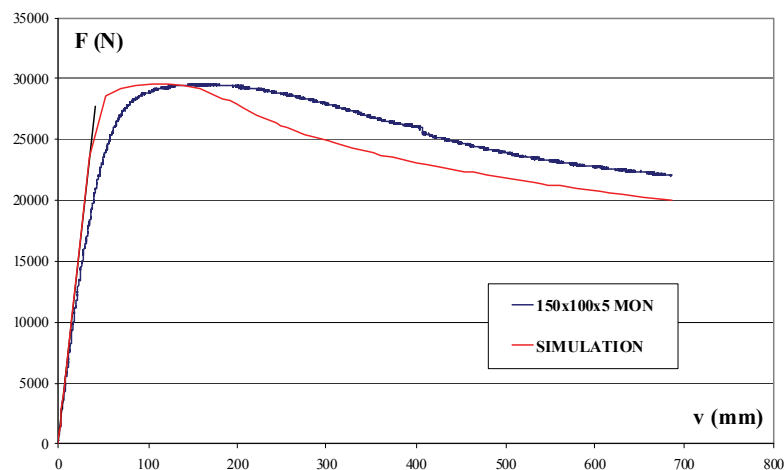
Fig. 94.   Numerical-experimental comparison

6.3 MODEL FOR CYCLIC TESTS

This paragraph describes the numerical model proposed for the simulation of cyclic behaviour of steel members under seismic actions.

The calibration of the cyclic model has been realized having a lot of characteristics in common with the monotonic model. In this paragraph the attention will be focuses only on the aspects modelled in different way. Subsequently, all steps necessary for the calibration of the numerical model are reported with reference to the specimen 150x100x5.

6.3.1 Geometrical properties

The module part in which the geometrical characteristics of the member are modelled, remains the same of the monotonic model

6.3.2 Mechanical properties

The true stress- true strain behaviour of the material is used to model the characteristics of the material both in monotonic and in cyclic analyses. Furthermore, during cyclic analyses another important aspect as to be considered: the hardening of the material.

A linear kinematic hardening model can be used in Abaqus to simulate the behaviour of materials that are subjected to cyclic loading. The evolution law in these model consists of a kinematic hardening component (which describes the translation of the yield surface in stress space). The Bauschinger effect and plastic shakedown can be modelled with this model. In the kinematic hardening models the centre of the yield surface moves in stress space due to the kinematic hardening component (Fig. 95).
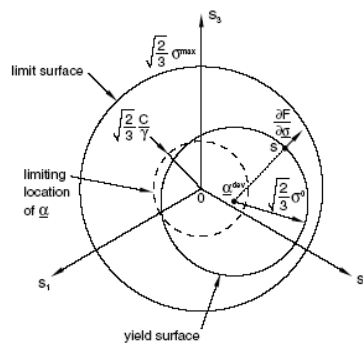
Fig. 95.   Three dimensional representation of the hardening in the non linear kinematic model

Considering the kinematic hardening it is possible to consider, as already said, the following phenomena:

• **Bauschinger effect:** This effect is characterized by a reduced yield stress upon load reversal after plastic deformation has occurred during the initial loading. This phenomenon decreases with continued cycling. The linear kinematic hardening component takes this effect into consideration, but a nonlinear component improves the shape of the cycles.

• **Cyclic hardening with plastic shakedown:** This phenomenon is characteristic of symmetric stress- or strain-controlled experiments. Soft or annealed metals tend to harden toward a stable limit, and initially hardened metals tend to soften. Figure 86 illustrates the behaviour of a metal that hardens under prescribed symmetric strain cycles (Fig. 96) [79].
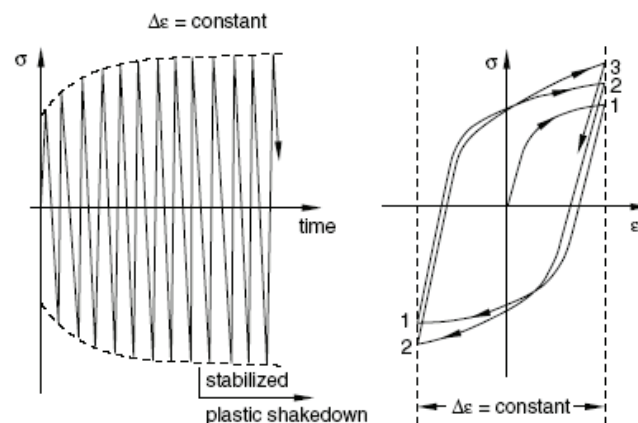
Fig. 96.   Plastic shakedown

This command is implemented in the following way: Material → Mechanical → Plastic → Hardening: kinematic

After the definition of geometrical and mechanical properties, the assemblage of the different parts that constituted the section is required, but also in this case it remains the same of the monotonic model. During the cyclic analyses the best choice is to carry a Static General Analysis to avoid problems of convergence which can be judges unlikely. In this module also geometrical non linearity are activated. Subsequently, the constraint type tie is created between the member and the loading-plate in the same way of the monotonic model, but in this case it is necessary to impose. also the amplitude of the

displacement, that is the time-history (Fig. 97). As explained in the Chapter 5, the adopted loading protocol is the ones provided by AISC codes:
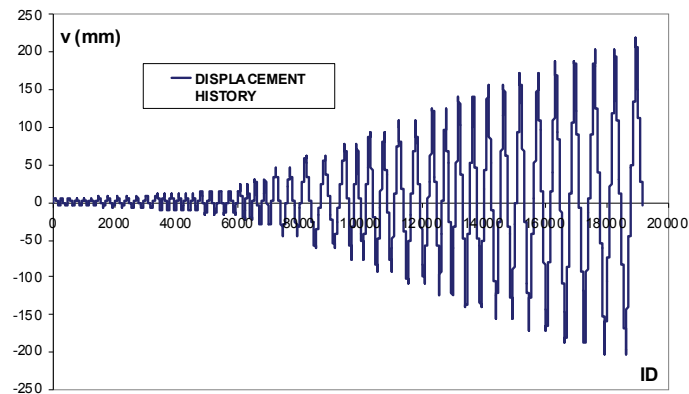
Fig. 97.   displacement history used for simulations

The selected data must be introduced in ABAQUS through the procedure:
Tools → Amplitude → tabular → (time span: step time)
Values of time/frequency became non-dimensional to 1 because the imposed time period is equal to 1.

6.3.3 Loads and boundary conditions

In the module Load the definition of load and boundary conditions is made. Several different situations may occur depending on the purpose of the FE-simulation. In this particular case the load condition is represented by the encastre at the base of the beam and by the time-history assigned to the set linea-carico:

1) BC →create → step: initial → symmetry/Antisimmetry/encastre → (after selecting the base of the beam) →U1=U2=U3=UR1=UR2=UR3=0

2) BC → create → step: step-1 → displacement/rotation → (after selecting the set linea-carico) →U1=0 (to avoid flexural-torsional instabilities); U2=1 with the amplitude defined in the previous module.

Module 7 (MESH), 8 (JOB), 9 (VISUALIZATION) and the calibration of the geometrical imperfections remain the same of the monotonic simulation.

6.3.4 Numerical-Experimental comparisons

As illustrated in the previous paragraph, the FE model realized has the following characteristics:

- model of the whole beam
- displacement control analysis using the time-history of the experimental tests
- true stress-true strain curve for the material using kinematic hardening
- geometrical imperfection (buckling modes)
- torsional constraint
- mesh composed of S4R element (shell with 4 nodes reduced integration)

The purpose of the numerical study has been the obtainment of a reliable model which correctly simulates the experimental behaviour of tested beams. In this way parametrical analyses can be carried out on members avoiding the great economic burden derived from an experimental campaign. Figure 88 compares F-v experimental and numerical responses of the specimens 150x100x5. As visible, the numerical simulation is in a good agreement with the experimental tests in terms of:

- stiffness
- strength
- ductility

For these reasons, the two parameters which are the object of the current study, overstrength and rotation capacity, are evaluated in a correct way.
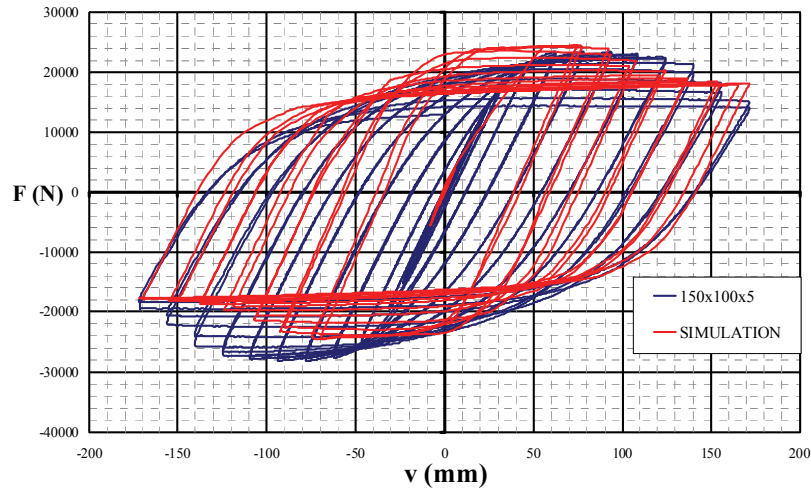
Fig. 98.   Numerical-experimental comparison

6.4 CONCLUSIONS

This chapter has described the finite element analysis of tested beams (I, RHS, SHS) using the FE program ABAQUS. The main aim of the analysis was to establish any trends in the plastic behaviour of beams. During the course of finite element study, a great number of analyses were performed, investigating the effects of many parameters because this typology of analyses provided a relatively cheap and rapid alternative to physical investigations.

With this purpose, two numerical models were realized to simulate monotonic and cyclic behaviour of steel members experimentally tested as illustrated in Chapter 5. First of all, a perfect specimen without imperfections was simulated, but it achieved rotation capacities much higher than those observed experimentally, so imperfections are introduced in the analyses. It was observed that the size of the imperfections had an unexpectedly large influence on the rotation capacity and on overstrength of the specimens.

Finally, both typology of simulations have shown a good agreement with actual behaviour of beams. In this way reliable models have been set up, useful to make parametric analyses which allow to take into account parameters that influences rotation capacity and overstrength such as: material properties, moment gradient, different slenderness of plates that constituted the section.

CHAPTER 7: NEW PROPOSAL OF "R" AND "s"

7.1 RECALIBRATION OF THE OVERSTRENGTH FACTOR "s" FOR I SECTIONS AND GENERALIZATION FOR RHS AND SHS

The determination of the overstrength factor "s" for members subjected to pure bending or bending and compression, requires the evaluation of the critical tension that brings local instability of compressed flange. The value of this tension is influenced by slenderness parameter of flange and web, by the degree of constraint that the web offers toward the flange, by the moment gradient and finally by the mechanical characteristics of the material [70]. Different authors provided theoretical formulations, without reaching reliable predictive models because of the complexity of this particular physical phenomenon [35], [58]. Other, instead, have provided expressions of the overstrength factor "s" using purely empirical models [30], [36], [53].

The expression of the overstrength factor "s" adopted by OPCM 3274 [68] represents a particularization, to the case of usual steels for carpentry, of the following generic expression:

$$1/s = C_1 + C_2 \lambda_f^2 + C_3 \lambda_w^2 + C_4 \frac{b_f}{L^*} + C_5 \frac{E}{E_h} + C_6 \frac{\varepsilon_h}{\varepsilon_y} \qquad (7.1)$$

In the equation (7.1) geometrical characteristics of section and of member and the mechanical properties of the material are taken into account, this last one described with an elastic-plastic-hardening model (Fig. 99). The influence of moment gradient is present in the term $\dfrac{b_f}{L^*}$. Coefficients C_i of the (7.1) have been determined starting from experimental results of three point bending tests made by different authors. In the specific case, the following experimentations are considered:

- 24 tests of Kuhlmann [41]
- 30 tests of Kato [36]
- 12 tests of Kemp [35]
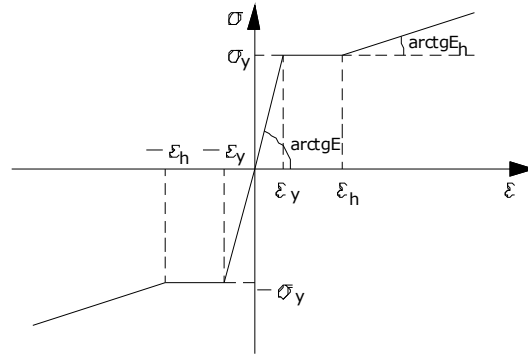
Fig. 99.   Elastic-plastic-hardening low of the material behaviour

Elaborating the results of experimental tests, through the multiple regression, the following expression of the overstrength factor "s" has been obtained [29]

$$1/s = 0.546 + 1.632\lambda_f^2 + 0.062\lambda_w^2 - 0.060\frac{b_f}{L^*} + 0.001\frac{E}{E_h} + 0.007\frac{\varepsilon_h}{\varepsilon_y} \qquad (7.2)$$

Subsequently the expression (7.2) has been particularized to the usual steels of carpentry combining the two terms concerning the inelastic properties of the material and the known term in an unique factor:

$$K = 0.546 + 0.001\frac{E}{E_h} + 0.007\frac{\varepsilon_h}{\varepsilon_y} \qquad (7.3)$$

At the second and the third terms of the equation (7.3) the following values have been assigned corresponding to different nominal steel properties:

$$\frac{E}{E_h} = 37.5 \,; \; \frac{\varepsilon_h}{\varepsilon_y} = 12.3 \qquad\qquad\qquad \text{steel S 235} \qquad (7.4)$$

$$\frac{E}{E_h} = 42.8 ; \frac{\varepsilon_h}{\varepsilon_y} = 11.0 \qquad\qquad\qquad \text{steel S 275} \qquad (7.5)$$

$$\frac{E}{E_h} = 48.2 ; \frac{\varepsilon_h}{\varepsilon_y} = 9.8 \qquad\qquad\qquad \text{steel S 355} \qquad (7.6)$$

In this way, three values of the parameter K have been obtained and consequently three expressions of the overstrength factor "s". At the end, an average of these three values has allowed to obtain the known term actually indicated into the OPCM 3274 [30].

Starting from these considerations, the first objective of this research was to propose a new expression of the overstrength factor "s" for I profiles, hot formed and welded, starting from the interpolation of a greater number of experimental results including the ones obtained by technical literature and the ones made by the experimental campaign. In fact, has illustrated in Chapter 5, the profiles are chosen as integration of experimental tests already made in technical literature.

- Members with I section

From the multiple regression of obtained data, the following expression has been formulated for members with I section:

$$1/s = 0.349 + 0.827\lambda_f^2 + 0.03\lambda_w^2 - 0.239\frac{b_f}{L^*} - 0.045\frac{E}{E_h} + 0.263\frac{\varepsilon_h}{\varepsilon_y} \qquad (7.7)$$

The equation (7.7) particularized to the usual steels for carpentry through the criterion already illustrated becomes:

$$1/s = 1.323 + 0.827\lambda_f^2 + 0.03\lambda_w^2 - 0.239\frac{b_f}{L^*} \qquad (7.8)$$

For the validation of the obtained expression of the overstrength factor the percentage errors EP[%] have been plotted for the considered tests (Figure 100). These errors are calculated by the introduction of the factor MSE (Mean Square Error) calculated applying the equations (7.2) and (7.7) to evaluate the

differences between the values obtained from experimental data and the ones numerically evaluated.

The MSE parameters are subsequently modified through the normalization of the i-mo error respect to the corresponding value, than extracting the square root, to obtain RMSEP. In this way the comparisons between errors evaluated on profiles with different cross-sections has been possible.

$$EP[\%] = \left(\frac{s_s - s_c}{s_s} \right) * 100 \tag{7.9}$$

$$RMSEP = \sqrt{\frac{\sum_{i=1}^{N} \left(\frac{s_s - s_c}{s_s} \right)^2}{N}} \tag{7.10}$$

where:

s_s is the value of the experimental overstrength factor s

s_c is the value of the calculated overstrength factor s

N is the total number of considered tests
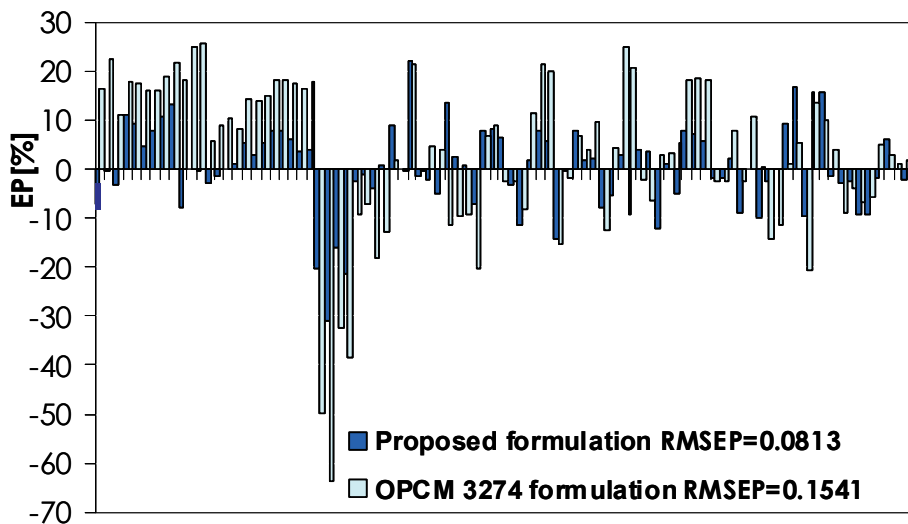
Fig. 100. Percentage Error for I profiles

The value of the RMSEP parameter has been 0.1541 applying the equation (7.2) and 0.0813 applying the equation (7.7). From the comparison of these

two values it is possible to understand that the expression (7.7) has a grater level of accuracy in the evaluation of the overstrength factor, because the RMSEP is about the half of the one obtained through the application of the equation (7.7). The dispersions between M_{max} and sM_{pl} evaluated applying these two formulations has been plotted in the following Figure 101:
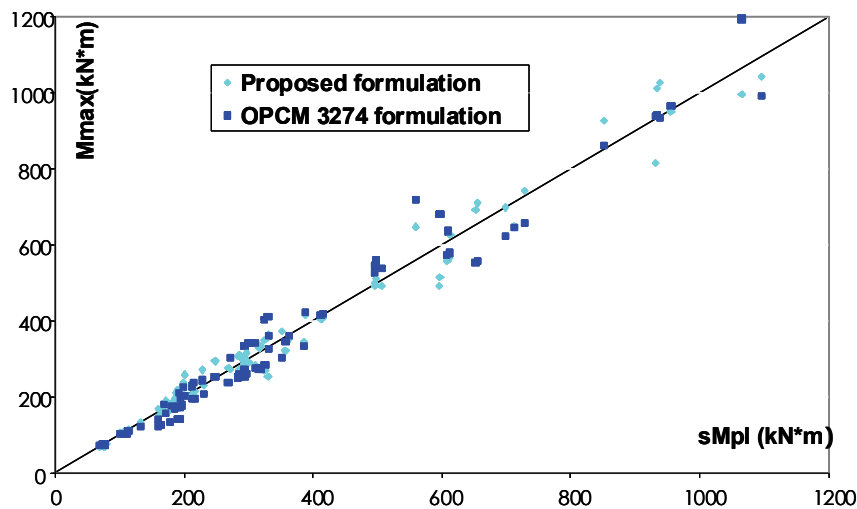
Fig. 101. Dispersion of results applying the proposed and the OPCM 3274 formulations

The second objective of the current research has to propose new expression of the overstrength factor "s" for members with different cross-sections. It is important to underline that the OPCM 3274 does not provide, till today, expressions of this parameter for members with cross-section different for I. Actually, for these sections, exists only the classification criterion proposed by EC3 and based on the evaluation of slenderness of plates which constitute the section. For this reason, in this Chapter, expressions of the overstrength factor for RHS and SHS are obtained:

- Members with Rectangular Hollow Section (RHS)

For the formulation of the expression of the overstrength factor for RHS, experimental tests made by Wilkinson on cold formed profiles are used as integration of experimental tests derived from the experimental campaign [80].

In this way the following expression of the overstrength factor has been obtained:

$$1/s = 0.97 + 0.62\lambda_f^2 + 0.0206\lambda_w^2 - 2.11\frac{b_f}{L^*} - 0.157\frac{E}{E_h} + 0.766\frac{\varepsilon_h}{\varepsilon_y} \qquad (7.11)$$

This expression particularized to the usual steels for carpentry becomes:

$$1/s = 2.7 + 0.62\lambda_f^2 + 0.0206\lambda_w^2 - 2.11\frac{b_f}{L^*} \qquad (7.12)$$

For the validation of the obtained expressions of the overstrength factor for RHS, the percentage errors EP[%] have been plotted (Figure 102). These errors are calculated by the introduction of the MSE (Mean Square Error) only at the obtained expression because there are not codified expressions of this one for making a comparison. The MSE parameter are subsequently modified through the normalization of the i-mo error respect to the corresponding value, than extracting the square root to obtain RMSEP.
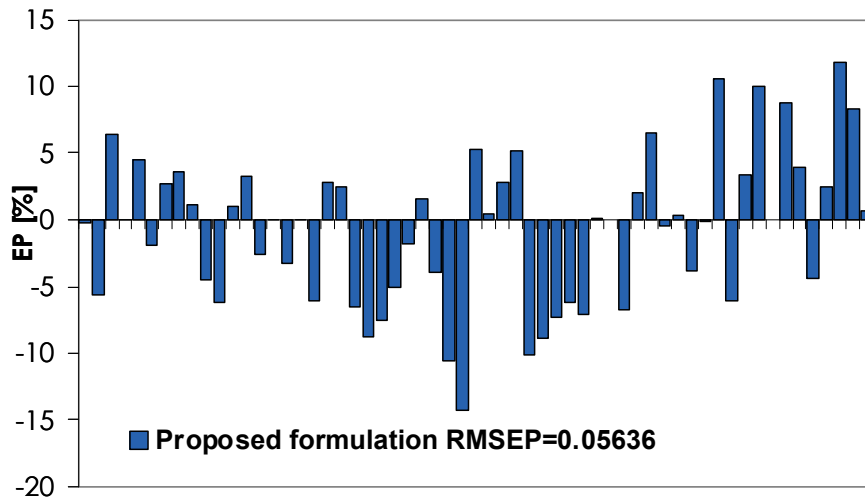
Fig. 102. Percentage error for RHS profiles

The value of the RMSEP parameter has been 0.05636, it means that the expression (7.12) predicts the overstrength factor with a great level of accuracy.

In the following Figure 103 the dispersion between M_{max} and sM_{pl} applying the formulation has been plotted:
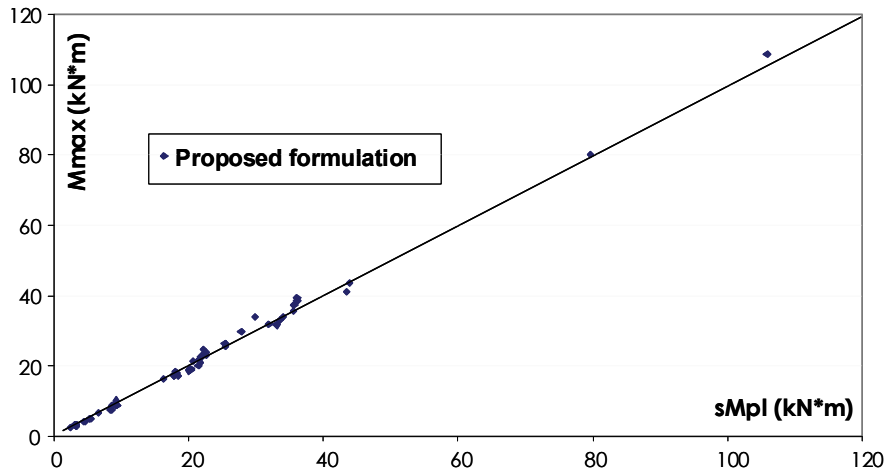
Fig. 103. Dispersion of results obtained applying the proposed formulation

- Members with Square Hollow Section (SHS)

For the formulation of the expression of the overstrength factor for SHS, experimental tests made by Wilkinson on cold formed profiles are used as integration of experimental tests derived from the experimental campaign [80]. In this way the following expression of the overstrength factor has been obtained:

$$1/s = 0.89 + 0.09\lambda_f^2 + 0.318\lambda_w^2 - 0.189\frac{b_f}{L^*} - 0.006\frac{E}{E_h} + 0.0071\frac{\varepsilon_h}{\varepsilon_y} \qquad (7.13)$$

This expression particularized to the usual steels for carpentry becomes:

$$1/s = 0.711 + 0.09\lambda_f^2 + 0.318\lambda_w^2 - 0.189\frac{b_f}{L^*} \qquad (7.14)$$

For the validation of the obtained expression of the overstrength factor for SHS, the percentage errors EP[%] have been plotted (Figure 104). These errors are calculated by the introduction of the MSE (Mean Square Error) only at the obtained expression because there are not codified expressions of this one for

making a comparison. The MSE parameter are subsequently modified through the normalization of the i-mo error respect to the corresponding value, than extracting the square root to obtain RMSEP:
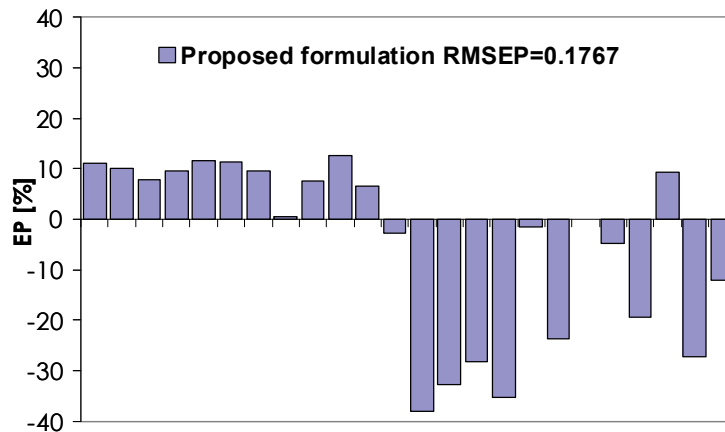
Fig. 104. Percentage errors for SHS profiles

The value of the RMSEP parameter has been 0.1767, it means that the expression (7.12) predicts the overstrength factor with an adequate level of accuracy [78].

7.2 EXPRESSIONS OF THE DUCTILITY FACTOR "R" FOR STEEL MEMBERS

Staring from the considerations made in Chapter 4 on the necessity of a classification criterion which takes into account simultaneously the overstrength and the ductility factors using the same procedures illustrated in the previous paragraph, expressions of rotation capacity have been obtained. As already said, in fact, the knowledge of the overstrength is necessary because it influences the capacity design criterion at global (overstrength of dissipative members) and at local (connection between dissipative and non-dissipative zones) levels; at the same time, the knowledge of the ductility is necessary because it is the rotation capacity and influences the behavioural factor q.

- Members with I section

In this section a new expression of the ductility factor "R" for I profiles, hot formed and welded, starting from the interpolation of a great number of experimental results including the ones obtained by technical literature and the ones made by the experimental campaign, are presented. In this way through the multiple regression of experimental data, the following expression of the ductility factor "R" has been formulated:

$$R = 6.5 + 0.877\lambda_f^2 - 0.962\lambda_w^2 + 30.77\frac{b_f}{L^*} - 0.26\frac{E}{E_h} + 1.035\frac{\varepsilon_h}{\varepsilon_y} \qquad (7.15)$$

The equation (7.15) particularized to the usual steels for carpentry applying the already illustrated the criterion becomes:

$$R = 16.8 + 0.877\lambda_f^2 - 0.962\lambda_w^2 + 30.77\frac{b_f}{L^*} \qquad (7.16)$$

In the following Figure 105 dispersions between R_{num} and R_{exp} obtained applying the formulation have been plotted:
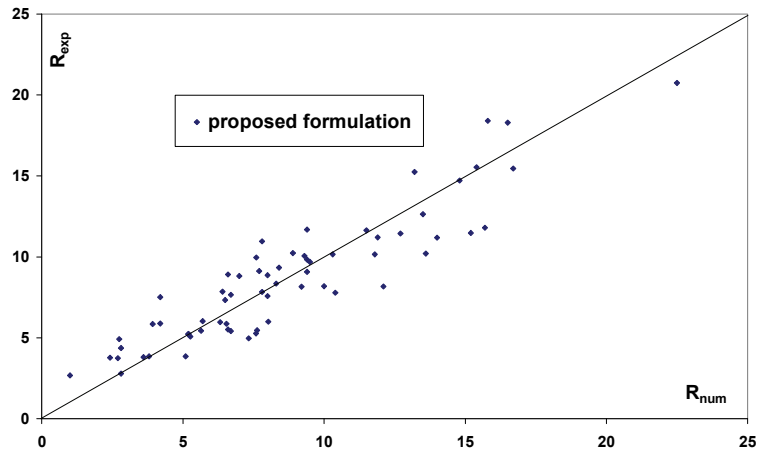
Fig. 105. Dispersion of results obtained applying the proposed formulation

For the validation of the obtained expression of the ductility factor "R" for I section, the percentage errors EP[%] have been plotted (Figure 106):
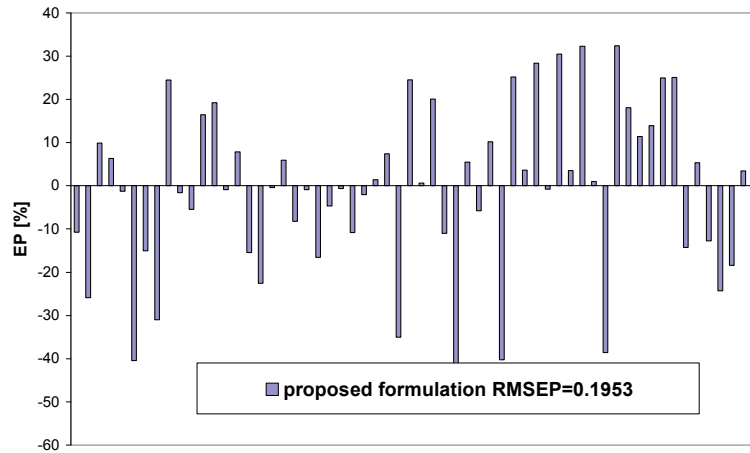
Fig. 106. Percentage errors for I profiles

The value of the RMSEP parameter has been 0.1953, it means that the expression (7.16) predicts the ductility factor with an adequate level of accuracy.

- Members with Rectangular Hollow Section (RHS)

For the formulation of the expression of the ductility factor "R" for RHS, experimental tests made by Wilkinson on cold formed profiles are used as integration of tests derived from the experimental campaign [80]. In this way the following expression of the ductility factor has been obtained:

$$R = 0.962 + 0.0015\lambda_f^2 - 0.0013\lambda_w^2 - 0.01032\frac{b_f}{L^*} - 0.047\frac{E}{E_h} + 0.999\frac{\varepsilon_h}{\varepsilon_y} \quad (7.17)$$

The equation (7.17) particularized to the usual steels for carpentry applying the criterion already illustrated becomes:

$$R = 9.97 + 0.0015\lambda_f^2 - 0.0013\lambda_w^2 - 0.01032\frac{b_f}{L^*} \quad (7.18)$$

In the following Figure 107 the dispersion between R_{num} and R_{exp} applying the formulation has been plotted:
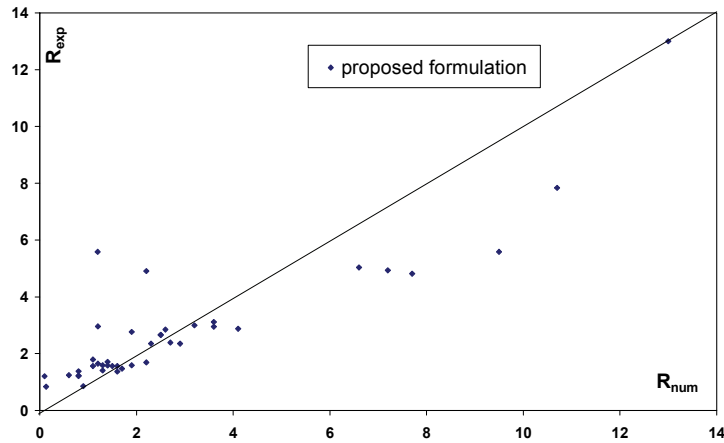
Fig. 107. Dispersion of results obtained applying the proposed formulation

For the validation of the obtained expression of the ductility factor for RHS, the percentage errors EP[%] have been plotted (Figure 108)
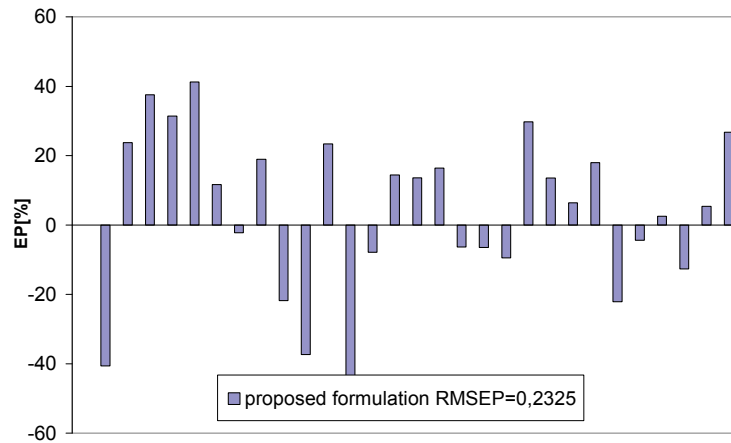
Fig. 108. Percentage errors for RHS profiles

The value of the RMSEP parameter has been 0.2325, it means that the expression (7.18) predicts the ductility factor with an adequate level of accuracy.

- Members with Square Hollow Section (SHS)

For the formulation of the expression of the ductility factor "R" for SHS, experimental tests made by Wilkinson on cold formed profiles are used as integration of tests derived from the experimental campaign [80]. In this way the following expression of the ductility factor has been obtained

$$R = 0.939 + 30.82\lambda_f^2 + 45.4\lambda_w^2 - 0.34\frac{b_f}{L^*} - 1.07\frac{E}{E_h} + 0.622\frac{\varepsilon_h}{\varepsilon_y} \qquad (7.19)$$

The equation (7.19) particularized to the usual steels for carpentry applying the criterion already illustrated becomes:

$$R = -38 + 30.82\lambda_f^2 + 45.4\lambda_w^2 - 0.34\frac{b_f}{L^*} \qquad (7.20)$$

In the following Figure 109 the dispersion between R_{num} and R_{exp} applying the formulation has been plotted:
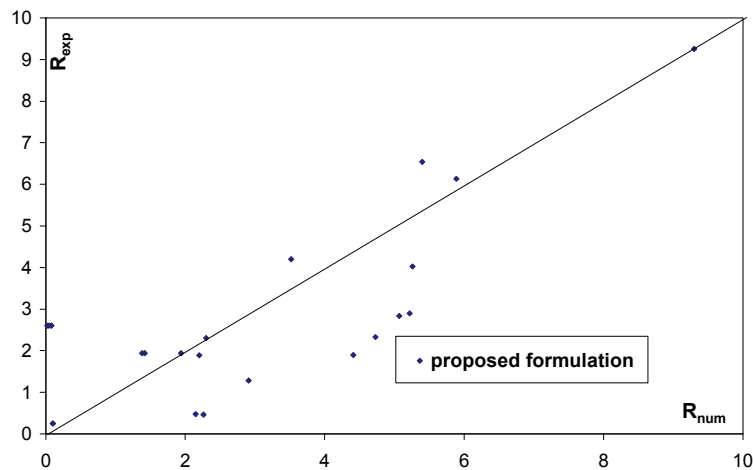
Fig. 109. Dispersion obtained applying the proposed formulation

For the validation of the obtained expression of the ductility factor "R" for SHS, the percentage errors EP[%] have been plotted (Figure 110)
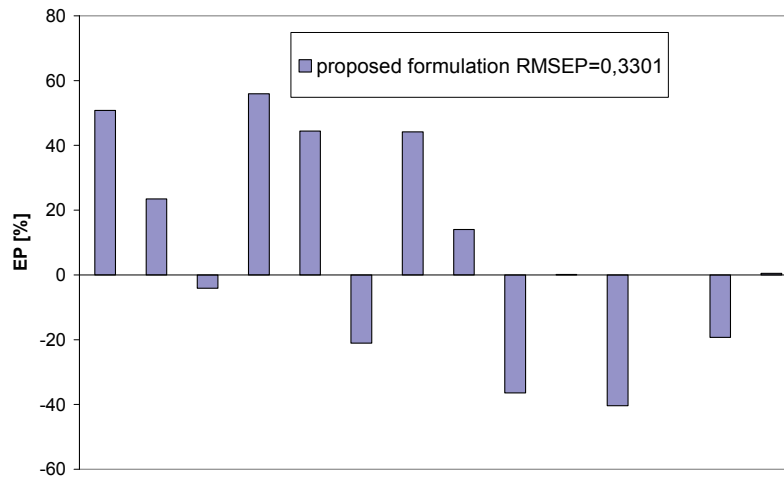
Fig. 110. Percentage errors for SHS profiles

The value of the RMSEP parameter has been 0.3301, it means that the expression (7.20) predicts the ductility factor with an adequate level of accuracy.

7.3 THE NEW PROPOSAL OF CLASSIFICATION CRITERION

In this work it is shown that the design of dissipative structural systems is based on the capacity of members to withstand deformations in elasto-plastic field without significant losses of resistance. Such structural systems dissipate the earthquake energy through inelastic excursions assuring the complete development of the collapse mechanism. For these reasons, it is necessary to ensure that dissipative zones have suitable ductility, while non dissipative ones have adequate overstrength to allow the inelastic strains of dissipative parts. So the concepts of ductility and ovestrength are fundamental. In the specific case of steel frame structures, modern codes for constructions in seismic zones adopt a design criterion which considers, during destructive seismic events, the possibility of developing plastic hinges at the end of the beams and at the base of the first floor columns. For frame structures the attainment of a globally ductile behaviour of the structure and of a locally ductile behaviour of the

members is required. A measure of local ductility is represented by rotation capacity of members which can be compromised by buckling phenomena that can interest both the section (local buckling) than the whole member (global buckling) in absence of torsional restraints. The proposed classification criterion is based on the evaluation, through the provided formulations, of the rotation capacity and overstrength parameters to be considered simultaneously for the classification of members.

7.4 CONCLUSIONS AND FURTHER DEVELOPMENTS

For MRF structures, designed applying the capacity design criterion, the attainment of a globally ductile behaviour of the structure, is possible only if, members have adequate local ductility which can be measured in terms of plastic rotation. The load bearing capacity of structural systems to withstand seismic actions in the non-linear range allows the design under actions lower than those corresponding to a purely linear elastic response of the structure. The force reduction is actually defined by a coefficient, namely behavioural factor, which is a measure of the structural ductility. The relationship between this factor and local ductility of members is stated in all current seismic codes. The local ductility of steel beams can be evaluated from their rotation capacity which can be measured in different ways [35], [36], [41].

This parameter can be compromised by the occurrence of local and global buckling phenomena that can affect the plates composing the section, and the whole member in absence of torsional restraints. The evaluation of the R parameter can be obtained through experimental tests, measuring and calculating the rotations or with Theoretical methods, Semi-empirical methods and Empirical methods.

In the seismic design of MRF, the available rotation capacity of beams is of primary importance. The subdivision of members into ductility classes is necessary because, as mentioned before, the rotation capacity influences the behavioural factor of the structure.

At the same time, the subdivision of the members into overstrength classes is necessary in order to apply the capacity design criteria both to local level (connections among dissipative and not dissipative zones), and to global level (overstrength of non-dissipative members).

The twice classification of the steel members in ductility and overstrength classes, based on relevant criteria, should be the most appropriate approach for the seismic applications. Unfortunately, current seismic codes adopt only one

classification criterion, from which both the consequences in terms of global ductility (behavioural factor) and in terms of capacity design are dependent.
The current work has been finalized to provide a contribution on the discussion about this topic, through a critical analysis of the classification criteria currently proposed by some European codes, the evaluation of their reliability starting from available experimental results and the proposal of a new classification criterion. In fact, Eurocode 3 [60] subdivides cross-sections starting from their geometrical characteristics, the steel type and the internal actions. The new Italian seismic code OPCM 3274 [68] classification is instead based on the evaluation of the overstrength factor s, which takes into account not only the slenderness of the different parts in the transversal section and the mechanical characteristics of the material, but also the moment gradient along the axis of the member. While the Technical Codes for Constructions (NTC '08)[69], following a performance approach, subdivide the steel sections in four classes according to the EC3 prescriptions but providing limit values of rotation capacity (R).

As visible, EC3 and NTC '08 define the concept of cross-section behavioural classes depending only on the width-to-thickness ratios of flanges and of web. These proposals contain some shortcomings [29]:

a) Independent limitations of these ratios are unreasonable, because, obviously, the flange is restrained by the web and the web is restrained by the flange.

b) The local ductility depends not only on the width-to-thickness ratios, but also on the ratio between width of flange and web, member length, moment gradient, level of axial load, eccentricity of axial load, steel quality, flexural-torsional buckling, etc. As a consequence of such additional factors, it seems that the concept of cross-section behavioural classes should be substituted by the concept of member behavioural classes [30].

c) As far as the values of b/t ratios in the different ductility classes are concerned, we can observe that this subdivision does not correspond to the actual behaviour of beam and beam-columns which are a continuous one and the given discrete values of b/t ratio seem to be very arbitrary. The local ductility is also influenced by the low-cycle fatigue, which reduces the ductility, causing premature failure.

In this context the more correct approach seems to be the adopted by OPCM 3274 which provides an expression of the overstrength factor "s" using a semi-empirical method. Starting from this assumption in this work, an empirical method has been used, based on multiple regressions of experimental data, to provide expressions of overstrength and ductility factors for I, RHS, SHS members. In this way it has been possible to propose a classification criterion based on both parameters, overstrength and ductility. In the future, push-over analyses must be carried to define the numerical upper and lower limits of the of variability ranges of these parameters.

REFERENCES

[1] Petroski H., (1985), To Engineer is Human. The Role of Failure in Successfull Design, Mac Millan, Londra.

[2] Osteraas J., Krawinkler H., (1989), The Mexico earthquake of September 19, 1985; Behaviour of steel structures. Earthquake Spectra, Vol. 5, No. 1, 51-88.

[3] De Buen O., (1996), Earthquake resistant design: A view from the practise, in 11th World Conference on Earthquake Engineering, Acapulco, 23-28 June 1996, CD-ROM 2002.

[4] Corsanegro A., (1995), Recent trend of earthquake damage interpretation, in 10th European Conference on Earthquake Engineering, (ed. G. Duma), Vienna, 28 August – 2 September 1994, Balkema, Rotterdam, Vol. 1, 763-771.

[5] Lew M., (1992), Characteristics of vertical ground motions recorded during recent California earthquakes, in the 10th European Conference on Earthquake Engineering, Madrid, 19-24 July 1992, Balkema, Rotterdam, 573-576

[6] Chouw N., (2000), Performance of structures during near-source earthquakes, in 12th World Conference on Earthquake Engineering, Auckland, 30 January-4 February 2000, CD-ROM 0368

[7] Trifunac M.D., Todorovska M.I., (1998), Nonlinear soil response as a natural passive isolation mechanism. The 1994 Northridge, California, earthquake. Soil Dynamic and earthquake Engineering, Vol. 17, 41-51.

[8] Mc Clure F.E., (1989), Lessons learned from recent moderate earthquake, in Earthquake Hazard and the Design of Constructed Facilities in the Eastern United States, (eds. K.H. Jacob, C.S. Turkstra), New York, 24-26 February 1988, Annuals of New York Academy of Science, Vol. 558, 251-258.

[9] CEN (European Communities for Standardization), Final Draft, EN 1998-1, (2004), Eurocode 8: Design of structures for earthquake resistance – Part 1: General rules, seismic actions and rules for buildings.

[10]   FEMA (Federal Emergency Management Agency) 222, (1992), NEHRP recommended provisions for the development of seismic regulation for new buildings, Washington D.C., USA.

[11]   SEAOC (Structural Engineers Association of California) Blue Book, (1990), Recommended lateral force requirements and commentary. Sacramento, California, USA.

[12]   Miranda E., Eeri M., Bertero V.V., (1994), Evaluation of strength reduction factors for earthquake-resistant design, in Earthquake Spectra, Vol. 10, No. 2, 357-379.

[13]   Miranda E., (1997), Strength reduction factors in Performance-Based design, in the EERC-CUREe Symposium in Honor of Vitelmo V. Bertero, Report UBC/EERC-97/05.

[14]   Santa-Ana P.R., Miranda E., (2000), Strength reduction factors for multi-degree of freedom systems, in Proceedings of the 12th World Conference on earthquake Engineering, Auckland, New Zeland.

[15]   Fajfar P., (2000), Design methodology, in Moment resistant connections of steel frames in seismic areas: design and reliability, Chapter 7.3, F.M. Mazzolani editor, E & FN Spon, London.

[16]   Mazzolani F.M., Piluso V., (1996), Theory and design of seismic resistant steel frames, London: E & FN Spon, an Imprint of Chapman & Hall.

[17]   Landolfo R., Mazzolani F.M., (1990), The consequences of the design criteria on the seismic behaviour of steel frames, in Proceedings of the 9th European Conference on Earthquake Engineering, Moskow, Vol. 2, 11-19.

[18]   Landolfo R. (2005), L'evoluzione della normative sismica, in Costruzioni Metalliche, No. 1, 54-66.

[19]   Mazzolani F.M., Piluso V., (1997), Plastic design of seismic resistant steel frames, Earthquake engineering and Structural Dynamics, Vol. 26, 167-191.

[20]   Faggiano B., (2000), Earthquake resistant steel frames: a new method for ductile design, Phd thesis in Structural Engineering, University of Naples "Federico II".

[21]   Della Corte G., D'Aniello M., Mazzolani F.M., (2006), Vibration mode vs collapse mechanism control for steel frames, in Proceedings of the International Conference "Behaviour of Steel Structures in Seismic Areas"

(STESSA), Yokohama, Japan, F.M. Mazzolani and A. Wada editors, published by E & FN Spon.

[22]   Gioncu V., Mazzolani F.M., (2002), Ductility of seismic resistant steel structures, Spon Press, London, Great Britain.

[23]   Bertero V.V., (1996), State of the art in design criteria, in 11th World Conference on Earthquake Engineering, Acapulco, 23-28 June 1996, CD-ROM 2005.

[24]   Bertero V.V., (1996), The need for multi-level seismic design criteria, in the 11th World Conference on Earthquake Engineering, Acapulco, 23-28 June 1996, CD-ROM 2120.

[25]   Bertero V.V., (1997), Codification, design, and application. General report, in Behaviour of Steel Structures in Seismic Areas, STESSA 97, (eds. F.M. Mazzolani, H. Akiyama), Kyoto, 2-8 August 1997, 10/17 Salerno, 189-206

[26]   Mazzolani F.M., Piluso V., (1997), A simple approach for evaluating performance levels of moment resisting steel frames. In seismic Design Methodologies for the Next Generation of Codes, (eds. P.Fajfar, H. Krawinkler), Bled, 24-27 June 1997, Balkema, Rotterdam, 241-252.

[27]   Tassios T.P., (1998), The seismic design: State of practice, in 11th European Conference on Earthquake Engineering, Paris, 6-11 September 1998, Balkema, Rotterdam, Invited Lectures, 255-267.

[28]   Bertero V.V., (1997), Performance based seismic engineering: a critical review of proposed guidelines, in Seismic Design Methodologies for the Next Generation of Codes (eds. P.Fajfar, H. Krawinkler), Bled, 24-27 June 1997, Balkema, Rotterdam, 1-31.

[29]   Mazzolani F.M., Piluso V., (1993), Design of steel Structures in Seismic Zones, ECCS Manual. TC13, Seismic Design Report

[30]   Mazzolani F.M., Piluso V., (1993), Member behavioural classes of steel beams and beam-columns, in XIV Congresso C.T.A., Viareggio, 24-27 October 1993, Ricerca Teorica e Sperimentale, 405-416.

[31]   Shape R.L., (1992), Acceptable earthquake damage on designed performance, in 10th World Conference on Earthquake Engineering, Madrid, 19-24 July 1992, 5891-5894.

[32]   Ghobarah A., Aly NM, El-Attar M., (1997), Performance level criteria and evaluation, in Fajfar P., Krawinkler H., editors, Seismic Design

Methodologies for the Next Generation of Codes, Rotterdam, AA Balkema, 207-215.

[33]   Poland CD, Derrik BH, (1997), Opportunities and pitfalls of performance based seismic engineering, in Fajfar P., Krawinkler H., editors, Seismic Design Methodologies for the Next Generation of Codes, Rotterdam, AA Balkema, 69-78.

[34]   Ghobarah A., (2001), Performance-based design in earthquake engineering: state of development, in Engineering Structures, Vol.23, 878-884.

[35]   Kemp A.R., (1985), Interaction of plastic local and lateral buckling, in Structural Engineering, Vol.111, n.10, 2181-2196.

[36]   Kato B., (1989), Rotation Capacity of H-section members as determined by local buckling, in Journal of Construction Steel Research, Vol.13, 95-109.

[37]   Kato B., (1990), deformation capacity of steel structures, in Journal of Construction Steel Reseach, Vol.17, 33-94.

[38]   Climenhaga J.J. Johnson R.P., (1972), Moment-rotation curves for locally buckling beams, in Journal of the Structural Division, Vol.98, ST6, 1239-1254.

[39]   Lukey A.F., Adams P.F. (1969), Rotation capacity of beams under moment gradient, in Journal of the Structural Division, Vol.95, ST6, 1173-1188.

[40]   Ivanyi M., (1979), Moment rotation characteristics of locally buckling beams, in Technical University Budapest, Vol.23, 217-230.

[41]   Kuhlman U., (1986), Rotations kapazitat biegebeanspruchter I-Profile unter Beriicksichtigung des plastichen Beulens, in Technical Reports Institute fur Konstruction Ingenieurbau Ruhr-Universitat Bochum, Mit. 86-5.

[42]   Kuhlman U., (1989), Definition of flange slenderness limits on the basis of rotation capacity values, in Journal of Construction Steel Research, Vol.14, 21-40.

[43]   Roik K., Kuhlman U., (1987), Rechnerische Ermittlung der Rotationskapazitat biegebeanspruchter I-profile, in Stahlbau, Heft 11, 321-327.

[44]   Spangemacher R., (1991), Zum Rotationsnachweis von Stahlkonstruktionen, die nachdemtraglastverfahren berechnet warden, Dissertation, Technischen Hochschule Aachen.

[45]   Giuncu V., Mateescu G., Iuhas A., (1994), contributions to the study of plastic rotational capacity of I steel sections in Proceedings of STESSA '94, Timisoara.

[46]   Vayas, I., Psycharis I.N., (1990), Behaviour of thin-walled steel elements under monotonic and cyclic loading, in Structural Dynamic, (eds Kratzig et al.), Balkema, Rotterdam, 579-583.

[47]   Mazzolani F.M., Piluso V., (1992), Evaluation of the rotation capacity of steel beams and beam-columns, in Proceedings of 1st State of the Art Workshop COST C1, Strasbourg.

[48]   Akiyama H., (1980), Earthquake Resistant Limit State Design for Buildings, University of Tokio Press.

[49]   Kato B., (1988), Rotation capacity of steel members subject to local buckling, 9th World Conference on Earthquake Engineering, Vol. 4, paper 6-2-3, Tokyo Kyoto.

[50]   Lay M.G., Galambos T.V., (1965), Inelastic Beams Under Uniform Moment, Journal of Structural Division ASCE, vol.91.

[51]   Southward R.E. (1969), Local Buckling in Universal Sections, Internal Report, University of Cambridge, Engineering Department.

[52]   Kato B., Akiyama H., (1981), Ductility of Members and Frames subject to Buckling, ASCE convention, May 11-15

[53]   Mitani I., Makino M., (1980), Post Local Buckling and Plastic Rotation Capacity of Steel Beam-Columns, 7th World Conference on Earthquake Engineering, Istanbul.

[54]   Nakamura T., (1988), Strength and Deformability of H Shaped Steel Beams and Lateral Bracing Requirements, Journal of Constructional Steel Research, N.9, 217-228.

[55]   Spangemacher R., Sedlacek G., (1992), On the Development of a Computer Simulator for Test of Steel Structures, in Proceedings of the First World Conference on Constructional Steel Design, Acapulco, Mexico, 6-9 december.

[56]   Massonnet C., Save M., (1980), Calcolo Plastico a Rottura delle Costruzioni, CLUP, Milano

[57]   Lay M.G., (1965), Flange Local Buckling in Wide Flange Shape, Journal of Structural Division ASCE, Vol. 91

[58]   Lay M.G., Galambos T.V., (1967), Inelastic Beams Under Uniform Moment, Journal of Structural Division ASCE, vol.93

[59]   Stowell E.Z. (1950), Compressive Strength of Flanges, Technical Note N. 2020, National Advisory Committee for Aeronautics.

[60]   CEN (European Communities for Standardization), Final draft, EN 1993-1: 2004. Eurocode 3: Design of steel structures-Part 1: General rules and rules for buildings.

[61]   Bjorhovde R., (1998), Deformation considerations for the design of steel structures. Festschrift J. Lindner, technishe Universitat Berlin, 21-31.

[62]   Szabo G., Ivanyi M., (1995), The influence of Luders-Hartmann lines on stability of steel members, in Stability of Steel structures (ed. M Ivanyi), Budapest, 21-23 september, Akademiai Kiado, 1057-1064.

[63]   Dodd L.L., Restrepo-Posada J.I. (1995), Model for predicting cyclic behaviour of reinforcing steel, Journal of Structural Engineering, Vol. 121, No. 3, 433-445.

[64]   Iwatsubo K., Koganemam T., Yamao T., Sakimoto T., (1997), Bending strength and ductility of H-section members made of high-strength steel with low-yield ratio, in Stability and Ductility of Steel Structures. SDSS 97 (ed. T. Usami), Nagoya, 29-31 July, 981-988

[65]   Kuwamura H., (1988), Effect of yield ratio on the ductility of high-strength steels under seismic loading, in 1988 Annual Technical Session of SSRC, Minneapolis, Minnesota, 26-27 April, 201-210.

[66]   Mazzolani F.M., 1974, Influence de l'effect Bauschinger sur le comportement des barres metalliques soumises a des cycles d'allongement. ECCS-Committee T16, Doc. 16-74-4.

[67]   De Martino A., Manfredi G., (1994), Experimental testing procedures for the analysis of the cyclic behaviour of structural elements: activity of RILEM Technical committee 134 MJP, in Danneggiamento Ciclico e Prove Pseudo-Dinamiche (ed. E. Cosenza), Napoli, 2-3 June 1994, Università degli Studi Federico II, 3-20.

[68]   OPCM 3274, (2003),First elements in the matter of general criteria for seismic classification of the national territory and of technical codes for structures in seismic zones, Official Gazette of the Italian Republic, Rome, and further modifications.

[69]   D.M. (2008), Nuove Norme Tecniche per le Costruzioni.

[70]   Piluso V., (1992), Il comportamento inelastico dei telai sismo resistenti in acciaio, Phd Thesis.

[71]   Boareave P., Lognard B., (1993), Elasto Plastic Behaviour of Steel Frame Works, in Journal of Construction Steel Research, 3-21.

[72]   Landolfo R., Brescia M., Mammana O., (2007), Capacità rotazionale e criteri di classificazione delle membrature di acciaio in zona sismica, in Proceedings of Anidis Conference, Pisa.

[73]   Brescia M., Mammana O., Landolfo R., (2007), On the classification of steel members in seismic areas, in Proceedings of CC2007 Conference, San Julian, Malta.

[74]   Brescia M., (2007), Rotation capacity and steel members classification criteria in seismic areas, in Pollack Periodica Vol. 2, No.2.

[75]   European Standard EN 10002, (1990), Metallic materials - Tensile testing – Method of tests (at ambient temperature).

[76]   Johansson B., Maquoi R., Sedlacek G., Muller C., Beg D., (2007), Commentary and worked examples to EN 1993-1-5, Plated Structural Elements, Joint Report, programme of CEN/TC 250.

[77]   Formisano A., (2003), Analisi Teorico-Sperimentale della fatica oligociclica di travi in acciaio in pareti sottili, Tesi di Laurea.

[78]   Brescia M., Mammana O., Landolfo R., (2007), Classificazione delle membrature in acciaio: ricalibrazione e generalizzazione del fattore di sovra resistenza s, in Proceedings of Materiali ed approcci innovativi per il progetto in zona sismica e la mitigazione della vulnerabilità delle strutture, Università degli Studi di Salerno

[79]   Hibbit, Karlsson, Soresen, (2004), Inc., ABAQUS/Standard version 6.7, Patwtucket, U.S.A.

[80]   Wilkinson T., (1999), The plastic behaviour of cold formed Rectangular Hollow Sections, Phd Thesis.

[81]   Yamawaki K., Kitamura H., Tsuneki Y., Mori N., Fukai S., (2000), Introduction of performance-based design, in the 12th World Conference on Earthquake Engineering, Auckland, 30 January- 4 February 2000, CD-ROM 1511

[82]   American Institute of Steel Construction inc., (2005), AISC 341/05, Seismic Provisions for Structural Steel Buildings, Chicago Illinois 60601-1802.

[83]   ATC, Applied Technology Council (1995), Guidelines and commentary for seismic rehabilitation of buildings, ATC report 33.03, Redwood City, California.

[84]   SEAOC Structural Engineers Association of California, (1995), Vision 2000, A framework for performance based design. Sacramento, California.

APPENDIX

Prospect
Scale 1:20

Section B-B
Scale 1:10

Section C-C
Scale 1:10

Particular of brace
Scale 1:10

Section A-A
Scale 1:10

TEST N.1   IPE 240   S275

LENGTH BEAM=3.7 m	WEIGHT BASE PLATE=35.32kg
WEIGHT BEAM=113.6 kg	NUMBER BOLTS M30 =8
SIZE BASE−PLATE=0.6x0.25x0.03 m	TYPE OF BOLTS=8.8

Prospect
Scale 1:20

Section B-B
Scale 1:10

Φ31

Section C-C
Scale 1:10

Particular of brace
Scala 1:10

Section A-A
Scale 1:10

TEST N.2   IPE 300   S275

LENGTH BEAM=3.7 m	WEIGHT BASE PLATE=35.32kg
WEIGHT BEAM=156.1 kg	NUMBER BOLTS M30 =8
SIZE BASE-PLATE=0.6x0.25x0.03 m	TYPE OF BOLTS=8.8

Prospect
Scale 1:20

Section B-B
Scale 1:10
Φ31

Section C-C
Scale 1:10

Particular of brace
Scale 1:10

Section A-A
Scale 1:10

TEST N.3   HEB240   S275

LENGTH BEAM=3.7 m	WEIGHT BASE PLATE=70.88kg
WEIGHT BEAM=307.8 kg	NUMBER BOLTS M30 =12
SIZE BASE-PLATE=0.6x0.43x0.035 m	TYPE OF BOLTS=8.8

Prospect
Scale 1:20

Section B-B
Scale 1:10

Φ31

400

45

90

160

90

45

20

205

430

205

49 151 151 49

3700

B B

C C

A A

Section C-C
Scale 1:10

9

R15

152

6

160

Particular of brace
Scale 1:10

146

190

118.46°

110

189

Section A-A
Scale 1:10

400

20

45

90

160

90

45

20

205

430

205

49 151 151 49

30

110

TEST N.4   HEA 160   S275

LENGTH BEAM=3.7 m	WEIGHT BASE PLATE=40.5kg
WEIGHT BEAM=112.5 kg	NUMBER BOLTS M30 =10
SIZE BASE-PLATE=0.4x0.4x0.03 m	TYPE OF BOLTS=8.8

Prospect
Scale 1:20

Section B-B
Scale 1:10

Φ31

45

600

90

160

90

45

20

205

205

151 151 151

73,5   73,5

B   B

3700

Section C-C
Scale 1:10

12

240

R21

7,5

230

Particular of brace
Scale 1:10

187

200

64,37°   15,63°

207

110

C   C

Section A-A
Scale 1:10

45

600

90

160

90

45

20

205

205

430

151 151 151

73,5   73,5

A   A

110

30

TEST N.5   HEA240   S275

LENGTH BEAM=3.7 m	WEIGHT BASE PLATE=60.77kg
WEIGHT BEAM=223.11 kg	NUMBER BOLTS M30 =12
SIZE BASE−PLATE=0.6x0.43x0.03 m	TYPE OF BOLTS=8.8

Prospect
Scale 1:20

Section B-B
Scale 1:10

Φ31

600
45
90
160
90
73,5
45
20
205
205
430
73,5
151 151 151

B   B

Section C-C
Scale 1:10

Particular of brace
Scale 1:10

23
R15
14
166
180

210
200
110
228

C   C

3700

Section A-A
Scale 1:10

600
45
20
90
160
90
73,5
20
205
205
430
73,5
151 151 151

A   A

30
110

TEST N.6   HEM160   S275

LENGTH BEAM=3.7 m	WEIGHT BASE PLATE=60.77kg
WEIGHT BEAM=282 kg	NUMBER BOLTS M30 =12
SIZE BASE−PLATE=0.6x0.43x0.03 m	TYPE OF BOLTS=8.8

Prospect
Scale 1:20

Section B-B
Scale 1:10

Φ31

600

45

115

115

250

160

20

73,5

73,5

45

151 151 151

Section C-C
Scale 1:10

150

100

4

Particular of brace
Scale 1:10

222

200

110

67,92°

112,08°

239

Section A-A
Scale 1:10

45

600

115

115

250

160

20

73,5

73,5

45

151 151 151

3700

110

30

TEST N.7   150x100x5   S275

LENGTH BEAM=3.7 m	WEIGHT BASE PLATE=35.32kg
WEIGHT BEAM=55.87 kg	NUMBER BOLTS M30 =8
SIZE BASE-PLATE=0.6x0.25x0.03 m	TYPE OF BOLTS=8.8

Prospect
Scale 1:20

Section B-B
Scale 1:10

Φ31

45
600
160
115
115
250
115
20
73,5
73,5
45
151 151 151

3700

B ⊢ ⊢ B

Section C-C
Scale 1:10

Particular of brace
Scale 1:10

160
80
5

216
200
67,58°
112,42°
110
234

C ⊢ ⊢ C

Section A-A
Scale 1:10

45
600
160
115
115
250
115
20
73,5
73,5
45
151 151 151

A ⊢ ⊢ A

110
30

TEST N.8   160x80x4   S275

LENGTH BEAM=3.7 m	WEIGHT BASE PLATE=35.32kg
WEIGHT BEAM=65.86 kg	NUMBER BOLTS M30 =8
SIZE BASE−PLATE=0.6x0.25x0.03 m	TYPE OF BOLTS=8.8

Prospect
Scale 1:20

Section B-B
Scale 1:10   Φ31

3700

B | B

C | C

A | A

30   110

Section C-C
Scale 1:10

200
100

Section A-A
Scale 1:10

Particular of brace
Scale 1:10

194
200   45,02°   114,92°   110
214

TEST N.9   200x100x8   S355

LENGTH BEAM=3.7 m	WEIGHT BASE PLATE=60.75kg
WEIGHT BEAM=129.89 kg	NUMBER BOLTS M30 =12
SIZE BASE-PLATE=0.6x0.43x0.03 m	TYPE OF BOLTS=8.8

Prospect
Scale 1:20

Section B-B
Scale 1:10
Φ31

45
600
20
147
90
205
160
90
205
20
430
73,5
45
151 151 151
73,5

B | B
3700

Section C-C
Scale 1:10

Particular of brace
Scale 1:10

250
100
10
167
200
110
61,66° 118,33°
190

C | C

Section A-A
Scale 1:10

A | A

45
600
20
147
90
160
205
90
20
205
430
73,5
45
151 151 151
73,5

110
30

TEST N.10   250x100x8   S275

LENGTH BEAM=3.7 m	WEIGHT BASE PLATE=60.75kg
WEIGHT BEAM=188.7 kg	NUMBER BOLTS M30 =12
SIZE BASE-PLATE=0.6x0.43x0.03 m	TYPE OF BOLTS=8.8

Prospect
Scale 1:20

Section B-B
Scale 1:10

Φ31

Section C-C
Scale 1:10

Particular of brace
Scale 1:10

Section A-A
Scale 1:10

TEST N.11   300x100x12.5   S275

LENGTH BEAM=3.7 m	WEIGHT BASE PLATE=60.77kg
WEIGHT BEAM=267.5 kg	NUMBER BOLTS M30 =12
SIZE BASE-PLATE=0.6x0.43x0.03 m	TYPE OF BOLTS=8.8

Prospect
Scale 1:20

Section B-B
Scale 1:10

Φ31

600

45
20
118.5

90
160
90

20
205
205
430

73,5
151 151 151
73,5

B   B

3700

Section C-C
Scale 1:10

300

200

14,2

Particular of brace
Scale 1:10

139

200
110

165

C   C

Section A-A
Scale 1:10

600

45
20
118.5

90
160
90

20
205
205
430

A   A

73,5
151 151 151
73,5

110

40

TEST N.12   300x200x14.2   S275

LENGTH BEAM=3.7 m	WEIGHT BASE PLATE=81.0kg
WEIGHT BEAM=381.1 kg	NUMBER BOLTS M30 =12
SIZE BASE−PLATE=0.6x0.43x0.04 m	TYPE OF BOLTS=8.8

Prospect
Scale 1:20

Section B-B
Scale 1:10   Φ31

Section C-C
Scale 1:10

Particular of brace
Scale 1:10

Section A-A
Scale 1:10

TEST N.13   150x150x5   S275

LENGTH BEAM=3.7 m	WEIGHT BASE PLATE=60.77kg
WEIGHT BEAM=83.6 kg	NUMBER BOLTS M30 =12
SIZE BASE−PLATE=0.6x0.43x0.03 m	TYPE OF BOLTS=8.8

Prospect
Scale 1:20

Section B-B
Scale 1:10 Φ31

B | B

C | C

A | A

3700

110

30

Section C-C
Scale 1:10

160

160   6,3

Particular of brace
Scale 1:10

220

200   67.48°   112.52°   110

235

Section A-A
Scale 1:10

600   45   125.5   20   90   160   90   45   73.5   205   205   20   430   151   151   151   73.5

600   45   125.5   20   90   160   90   45   73.5   205   205   20   430   151   151   151   73.5

TEST N.14   160x160x6.3   S355

LENGTH BEAM=3.7 m	WEIGHT BASE PLATE=60.77kg
WEIGHT BEAM=111.4 kg	NUMBER BOLTS M30 =12
SIZE BASE−PLATE=0.6x0.43x0.03 m	TYPE OF BOLTS=8.8

Prospect
Scale 1:20

Section B-B
Scale 1:10   Φ31

Section C-C
Scale 1:10

Particular of brace
Scale 1:10

Section A-A
Scale 1:10

TEST N.15   200x200x10   S355

LENGTH BEAM=3.7 m	WEIGHT BASE PLATE=60.77kg
WEIGHT BEAM=217.6 kg	NUMBER BOLTS M30 =12
SIZE BASE-PLATE=0.6x0.43x0.03 m	TYPE OF BOLTS=8.8

Prospect
Scale 1:20

Section B-B
Scale 1:10

Φ31

Section C-C
Scale 1:10

Particular of brace
Scale 1:10

Section A-A
Scale 1:10

TEST N.16   250x250x10   S355

LENGTH BEAM=3.7 m	WEIGHT BASE PLATE=60.77kg
WEIGHT BEAM=233.11 kg	NUMBER BOLTS M30 =12
SIZE BASE−PLATE=0.6x0.43x0.03 m	TYPE OF BOLTS=8.8

Prospect
Scale 1:20

Section B-B
Scale 1:10

Φ31

600

45
90
160
90
45

205
430
20
205

151   151   151

73.5   73.5

B   B

3700

Section C-C
Scale 1:10

250

250

5

Particular of brace
Scale 1:10

175

200   110

197

C   C

Section A-A
Scale 1:10

45
600

90
160
90
45

205
430
20
205

151   151   151

73.5   73.5

A   A

110

30

TEST N.17   250x250x5   S275

LENGTH BEAM=3.7 m	WEIGHT BASE PLATE=60.77kg
WEIGHT BEAM=141.7 kg	NUMBER BOLTS M30 =12
SIZE BASE-PLATE=0.6x0.43x0.03 m	TYPE OF BOLTS=8.8